Tracking traffic peaks in mobile networks and the impact of its imperfection on system performances

Aymen Jaziri

Enregistrée sous le n°
2016TELE0020

THÈSE DE DOCTORAT DE
Télécom SudParis - Institut Mines-Télécom
En co-accréditation avec l'Université Pierre et Marie Curie - Paris 6

Spécialité

Télécommunications

École doctorale Informatique, Télécommunications et Électronique (Paris)

EDITE - ED 130

Présentée et soutenue publiquement par

Aymen JAZIRI

Pour obtenir le grade de

DOCTEUR de Télécom SudParis - Institut Mines-Télécom
et de l'Université Pierre et Marie Curie - Paris 6

Sujet de la thèse :

Localisation des Hotspots de Trafic dans les Réseaux Mobiles et l'Impact de son Imperfection sur les Performances Système

soutenue le 20 octobre 2016

devant le jury composé de :

M. Tijani Chahed, Professeur, Telecom SudParis	Directeur de thèse
M. Ridha Nasri, Docteur, Orange Labs	Encadrant de thèse
M. Taieb Znati, Professeur, University of Pittsburgh - USA	Rapporteur
M. Erol Gelenbe, Professeur, Imperial College of London - Royaume Uni	Rapporteur
M. Guy Pujolle, Professeur, Université Pierre et Marie Curie - Paris 6	Examinateur
M. Nazim Agoulmine, Professeur, Université d'Evry Val d'Essonne	Examinateur

PhD thesis
Telecom Sudparis & UPMC
Department of Networks and Services

Tracking Traffic Peaks in Mobile Networks and the Impact of its Imperfection on System Performances.

AYMEN JAZIRI

Supervised by:

Prof. Tijani Chahed, Dr. Ridha Nasri

Committee

Prof. Erol Gelenbe, Prof. Taieb Znati

Prof. Nazim Agoulmine, Prof. Guy Pujolle

EDITE 130: Informatics, Telecommunications and Electronics

ORANGE LABS

October 2016

To My beloved parents
for your warmth and unfaltering patience, constant support, and unconditional love.
To My loving sibling
for your continuous guidance, neverending assistance, and true love.
To My sweetheart wife
for your encouraging words, optimistic influence on me, and generous honest love.

Acknowledgements

This research work was carried out at Orange Labs (France Telecom) in collaboration with Telecom SudParis. I would like to express my deepest gratitude to my industrial director, Dr Ridha Nasri and my academic director Prof. Dr. Tijani Chahed for guiding and supervising my research work with their unfaltering patience and involvement. Their genuine passion for research and guidance was evident throughout these years of my PhD. They were always there to comfort and reassure me in moments of doubt and kept believing in me until the very end. For these above reasons, in addition to their availability, their technical guidance for the collaborative work on the thesis and their contribution to supervising me so efficiently, I will remain eternally indebted to them. Thank you for providing me motivation and guidance with a lot of patience.

I would like to deeply thank Prof. Dr. Taieb Znati and Prof. Dr. Erol Gelenbe for their time and experience to review my thesis report and provide valuable comments.

I would like to pay my deepest gratitude to all the members of the former team, Radio Engineering for Mobile networks at Orange Labs for their excellent company and all the good times we have had. I would like to thank especially Sana Ben Jemaa, Zwi Altman, Emmanuel De Wailly, Salah Eddine El Ayoubi for the collaborations and discussions we had.

My heartful thanks goes out to Pierre Dubois and Hajer Khanfir of Radio Links Innovative Design team, who first took me within Orange Labs as an intern and gave me the opportunity to comfortably start and enjoy working in this great organization.

I would like also to thank my managers Laurent Marceron, Salah Eddine El Ayoubi and Benoit Badard, for helping me out with all the issues and making my stay in Orange a very pleasant one especially at the first half of these 3 years.

To my colleagues and friends at Orange Labs: Hajer Braham, Abdoulaye Tall, Yuting Lin, Ahlem Khlass, Ovidiu Iacoboaiea, Riad Habaz, Hind Zaaraoui, Aymen Anikaad, Abdenour Sahel, Yasir Khan, Nivine Abbas, Julien Floquet, Tony Daher, Maroua Temani, Fatma Salem and Yasser Azzouzi. Hang in there tight and enjoy the moment. Best of luck for all your future endeavors. It was great having all of us in the same boat and for all the interesting discussions over the lunches and cafees. Thanks for the great moments and the many jokes we shared together.

To my friends and all those names I missed to mention: I would like to thank you all for your moral support and constant motivation.

I would like to thank my dearly beloved parents who stood next to me throughout my life. My gratitude goes out to them for believing, trusting in me with unconditional support. Thanks for the support and love from my wife and my brother who are a true blessing one can ever ask for.

In retrospection, I have started to believe strongly that every soul on this earth has a remarkable story to say. A story of what made us whoever we have become, one which could have never been written alone had it not been the help, kindness and compassion of all those who have touched us at different moments in our lives.

Abstract

The continuous increasing traffic in existing cellular networks has forced the mobile operators to look for efficient and viable options to manage their networks so as to ensure operational efficiency over the network life cycle while also evolving with the implementation of new technologies and features. Traffic hotspot localization can help operators to identify the areas of capacity bottlenecks and also to deploy the appropriate solutions reducing the congestion in these areas. Small cell deployment represents one of the possible solutions allowing to reduce load and enhance service in high-dense areas. In fact, cellular operators are currently shifting towards Heterogeneous Networks as the most promising solution to meet user demands; by deploying small cells in a network of macrocells.

In this thesis, we firstly propose and assess a new traffic hotspot localization method based on the projection of O&M KPIs on the coverage map. Compared to probing methods using storage servers and trace analysis, the computational costs and the equipment expenditures are significantly reduced. In fact, all the exploited inputs are not large in terms of volume, they are already available at the operators' disposal and the way the KPIs are processed is not consuming in terms of computations. Moreover, the accuracy of localization is further improved as compared to actual operational methods leading to more efficient small cell deployments.

Next, in order to evaluate the impact of the limited accuracy of traffic localization tools on small cell deployment, we study the performances of three different scenarios. Namely, the first one considers a network of macrocells only and represents a benchmark to decide about the usefulness of small cells. The second one is based on a network of macrocells with a perfectly deployed small cell allowing to identify the limitations of small cell deployment and the last one is with an imperfectly deployed small cell. Static and dynamic level analysis are performed. First, we assess the distribution of the achievable data rates reflecting the distribution of radio conditions in the network. The results of the first part of the study are injected in the dynamic level analysis where the system presents dynamic arrivals and departures. The objectives of this study are i. to identify the areas where the small cell deployment brings capacity gains

and improve the radio conditions in the network and ii. to select the localization tools that can be efficient in the site planning process.

Realizing that a significant amount of cellular demand is generated on the go and suffers deteriorating quality, recent research efforts proposed deploying small cells on-board public transportation means to enhance cellular coverage and capacity. In this context, we investigate the potential performance gains of using moving small cells in the presence of stationary but temporary traffic hotspots. Deploying classic small cells is not efficient enough if they are installed for occasionally occurring traffic hotspots. So, we evaluate the possible capacity and quality of service gains that can be obtained when the hotspot is static. The major outcome is to understand if moving cells leverage the relative operators' investments or must be revised and enriched mainly in terms of mobility control to reach higher efficiency.

Finally, we propose a novel mobile data offloading mechanism which capitalizes on drone small cells to alleviate the data traffic load generated by traffic hotspots. Drones are activated after the detection of high load in their controlling macrocells. They are moved from a position to another thanks to the information provided by a traffic hotspot localization tool. The proposed mechanism is not energy-consuming since the drone will not fly when it starts to offload traffic. Better radio conditions with less interference, less handovers and better reactivity to congestion are the most important advantages of the proposed mechanism. Moreover, significant savings can be generated because less equipments are required, drones are not active all the time and no air conditioning is needed. At last, we realize a performance evaluation and comparison with classic small deployment and also with a network of macrocells only in order to estimate the additional capacity gains obtained from drone deployments.

Résumé

Introduction

Face à une augmentation importante du trafic de données et aux exigences des services en terme de débits élevés, les réseaux cellulaires ont évolué très rapidement avec l'introduction de nouvelles fonctionnalités de plus en plus avancées, ce qui a permis d'améliorer les services, leurs performances et leurs disponibilités.

Plusieurs idées innovatrices et très prometteuses ont émergé, que ce soit dans le domaine de la recherche ou de l'industrie. L'objectif commun est d'améliorer encore plus les performances des réseaux, l'expérience des utilisateurs et le business de l'opérateur. En effet, l'un des challenges le plus important pour les opérateurs des réseaux mobiles est de dimensionner le réseau de la manière la plus efficace possible, c'est-à-dire, bien planifier les ressources à mettre en œuvre pour fournir une bonne couverture et une meilleure capacité.

Résoudre le problème de croissance du trafic de données n'implique pas forcément une migration vers un nouveau système plus performant et donc plus coûteux, mais plutôt optimiser et mettre à niveau les systèmes actuels et aussi ajouter des fonctionnalités plus avancées qui ne requièrent que quelques changements mineurs sur l'infrastructure et la configuration déjà existantes.

Dans ce contexte, afin de mieux gérer le trafic généré dans le réseau, les opérateurs ont déployé des petites cellules pour aider les macro-cellules à délester (« offload » en anglais) les zones de la cellule où le trafic de données est significativement supérieur au trafic moyen dans la cellule; par souci de brièveté, on désignera ci-dessous une telle zone par le mot anglais « hotspot ». Cependant, le problème majeur de ces réseaux hétérogènes consiste à bien localiser ces hotspots et puis de mettre en place la meilleure solution pour les absorber.

Une mauvaise localisation de hotspot ne se répercute pas uniquement sur les utilisateurs qui vont avoir des débits très faibles suite à des conditions radio plus dégradées (à cause des interférences qui vont être reçu de la petite cellule qui est

supposée couvrir le hotspot mais elle est mal positionnée), mais aussi sur la capacité globale du réseau, du fait que ces utilisateurs (UE) vont consommer une proportion significative des ressources radio, affectant ainsi les performances globales du système.

Dans cette thèse, on traite le sujet de localisation de hotspot de trafic et on étudie l'impact de la mauvaise localisation sur les performances des solutions basées sur le déploiement des réseaux hétérogènes. Actuellement, ces deux sujets ont attiré beaucoup d'attention auprès des chercheurs, des industriels et de la communauté de standardisation.

On propose une nouvelle méthode de localisation de hotspot dans une première étape. L'objectif de cette méthode est de réduire les coûts de localisation, améliorer sa précision et réduire les calculs et les traitements faits sur les données de traffic remontées au niveau du réseau d'accès.

Dans une deuxième étape, on propose d'évaluer l'impact d'une mauvaise localisation de trafic sur le déploiement des petites cellules à travers une analyse de performances. Dans cette étude, on commence par établir les expressions de la distribution spatiale du débit pour trois différents scénarii et en présence d'une distribution spatiale de trafic non uniforme. Le premier scénario est basé sur un réseau de macro-cellules seulement permettant ainsi de déduire l'utilité des déploiements de petites cellules en le comparant avec les deux autres scenarii. Le deuxième suppose que la petite cellule couvre parfaitement le hotspot. Évaluer les performances de ce scénario permet de connaitre les limites des déploiements de petites cellules s'il en existe. Le troisième scénario prend en compte la mauvaise localisation de trafic. Le but est d'évaluer l'intervalle de précision qui peut être toléré si on déploie des petites cellules en exploitant les informations fournies par un outil de localisation de trafic. Les expressions obtenues de la distribution de débit sont injectées dans une étude basée sur des modèles de files d'attentes afin de mieux comprendre le comportement du système face à cette mauvaise localisation de trafic.

Sachant qu'une grande quantité de trafic de données dans le réseau mobile est générée par des utilisateurs qui sont en mouvement, on propose d'évaluer les performances des petites cellules mobiles, qui peuvent être déployés sur le toit d'un bus, d'un taxi ou un autre moyen qui circule dans des zones où on peut avoir plusieurs utilisateurs connectés au réseau. Dans cette troisième étape, le modèle de mobilité de Manhattan[1] est ainsi appliqué sur la petite cellule mobile puisque c'est un modèle qui s'approche de

[1]Le modèle de Manhattan est utilisé pour émuler le modèle de circulation des petites cellules mobiles dans des rues par des cartes. Ce modèle peut être utile dans la modélisation de circulation dans une zone urbaine dont la carte est composée d'un certain nombre de rues horizontales et verticales. Donc, la petite cellule mobile est autorisé à se déplacer selon la grille des rues.

la réalité surtout pour les zones urbaines. Cette étude est réalisée en deux parties; la première est le calcul de la distribution de débit en présence du hotspot et la deuxième se base sur l'exploitation de cette distribution de débit dans modèles de files d'attentes de plusieurs classes d'utilisateurs (chaque classe est caractérisée par un taux d'arrivé et un débit de service). L'objectif principal de cette étude est de décider de l'utilité des petites cellules mobiles et de voir si cet investissement est rentable ou non.

La quatrième étape consiste à améliorer encore la solution de déploiement de petites cellules en utilisant les drones. Initialement conçus à des fins militaires, les drones connaissent depuis quelques années un grand succès dans le domaine des services de surveillance et de contrôle. Or cette technologie pouvait également présenter un grand intérêt dans le domaine des télécommunications. En effet, des progrès significatifs ont été réalisés récemment sur le plan des coûts de déploiement et d'entretien, ainsi que sur le plan de la fiabilité du contrôle de vol des drones. C'est pourquoi une architecture réseau reposant sur une flotte de drones peut être utilisée avantageusement pour assurer le délestage du trafic dans une cellule d'un réseau mobile. L'objectif du mécanisme proposé est d'améliorer la mobilité de la petite cellule afin de bien couvrir les hotspots et améliorer les conditions radio avec des communications plus en ligne de mire.

Localisation des hotspots de trafic dans les réseaux cellulaires

Actuellement, la localisation de hotspot dans les réseaux cellulaires se fait principalement à l'aide des sondes. Après avoir récupéré les traces de communications capturées par les sondes et stockées dans des serveurs de stockage, des traitements sont exécutés sur ces traces selon une de plusieurs techniques (citons par exemple, la méthode de triangulation ou aussi la méthode de trilatération [19]). La localisation de trafic avec des sondes s'est avérée très coûteuse puisqu'elle nécessite une mise en place d'un outil d'acquisition de trace sur chaque interface du réseau. Puis, pas toutes les traces sont capturées et le mécanisme manque d'efficacité (précision de trafic de 100 à 150m en milieu dense urbain). De plus, cette solution est compliquée à gérer puisqu'elle nécessite des outils de traitement des sondes et des serveurs de stockage des traces avec une grande capacité mémoire.

Afin de remédier à ces derniers inconvénients, on propose une nouvelle solution de localisation de hotspot. Notre idée se base uniquement sur l'exploitation de certains compteurs et indicateurs de performance (KPI) que le réseau déjà fournit via le centre d'opération et de maintenance (OMC). En faisant quelques traitements de corrélation

avec les autres cellules voisines, nous pouvons estimer la localisation des hotspot de trafic à des précisions meilleures que celle des solutions des sondes (presque à la taille d'une petite cellule).

Principe

La solution proposée est basée sur 5 KPIs obtenus de l'OMC pendant les heures chargées de chaque cellule et moyennés sur un ensemble de jours. Ces KPIs sont:
1) La distribution du temps de propagation (« timing advance » en anglais) dans chaque cellule,
2) La distribution du angle d'arrivée (« Angle of arrival » en anglais) dans chaque cellule,
3) Le degré de voisinage de chaque cellule voisine à la cellule serveuse,
4) La corrélation entre les charges radio des cellules,
5) La moyenne arithmétique et harmonique de débit (notées AMT et HMT respectivement).

Ces KPIs sont correctement choisis en ce qui concerne deux critères importants: localiser les hotspots de trafic en termes de nombre d'utilisateurs connectés et aussi de quantité de trafic écoulé. En fait, l'AoA et le degré de voisinage des cellules peuvent être suffisants pour dériver la distribution spatiale des utilisateurs connectés. Cependant, un hotspot de trafic est mesuré non seulement par la haute densité d'utilisateurs connectés mais aussi par le volume de trafic. Ce dernier ne suit pas exactement la même évolution que le nombre d'utilisateurs. Par conséquent, la localisation du trafic est amélioré en ajoutant des KPIs directement liés au volume tel que la corrélation entre les charges des cellules voisines et la différence entre l'AMT et le HMT.

Selon chaque KPI, un poids de trafic est attribué à chaque maille (« pixel » en anglais) de la zone étudiée en exploitant les données de la carte de couverture[2] (principalement, l'identifiant de la meilleure cellule serveuse, l'identifiant de la meilleure cellule candidate pour le handover et le niveau de champs). La contribution de chacun de ces KPIs est pondérée par un facteur d'importance obtenu grâce à la résolution d'un problème d'optimisation minimisant la distance à la carte de lieux potentiels de trafic (cette carte se base sur des données commerciales et contient des informations sur les zones possibles d'apparition de hotspot comme les centres commerciaux, les zones industrielles, ...). Les facteurs d'importance sont assignés afin d'éviter un excès

[2]Carte de couverture (niveau de champs par pixel selon la résolution): cette carte est obtenue par un outil de prédiction de couverture ou par les techniques MDT. La carte contient aussi les coordonnées de chaque site et la zone de couverture de chaque cellule.

de confiance dans la localisation des hotspot de trafic dû à la corrélation entre les KPIs utilisés.

La méthode de localisation de trafic peut attribuer des poids importants à des pixels isolés ou à ceux qui sont en bordure d'un hotspot. Ainsi, le smoothing de la carte obtenue est une étape supplémentaire proposée dans ce travail, afin de rendre la distribution prévue du trafic plus précise. Cette étape permet principalement d'éliminer les faux hotspot.

L'exécution de la solution proposée n'exige pas des investissements et des coûts d'exploitation énormes puisqu'elle est basée sur les entrées qui sont déjà disponibles dans le réseau. Le seul coût de notre méthode est celui de l'exécution et du traitement des données des KPIs qui est raisonnable par rapport au coût des méthodes utilisées récemment comme celles basées sur les sondes.

Carte de couverture et KPIs: Définition et notation

Carte de couverture

La carte de couverture est une carte à granularité fine d'un secteur géographique exploitée dans des procédés de planification du réseau ainsi que d'autres utilisations. L'information extraite à partir des cartes de couverture couvrent les caractéristiques géographiques, les aspects radio, les services disponibles, les règlements spectraux, etc.

La taille de chaque pixel (appelée aussi résolution de la carte de couverture) est de l'ordre de 5 à 50 mètres dans la pratique. Cette carte est souvent prise des outils de prédiction de couverture ou de mesures terrains remontées grâce au techniques de minimisation des drivetests (MDT) [58].

Dans ce travail, la carte de couverture est dénotée par $\mathcal{L}$. Sans perte de généralité, nous supposons que $\mathcal{L}$ a la forme d'un carré et est discrétisé en m^2 pixels de même taille.

Pour $1 \leq i, j \leq m$, on note par $P_{i,j}$ les coordonnées de chaque pixel dans $\mathcal{L}$ et nous supposons que le pixel $P_{1,1}$ est situé au sommet en bas à gauche de la carte.

On note également, par $\mathcal{C} = \{C_1, C_2, \ldots, C_n\}$ l'ensemble des cellules situées dans la carte de couverture $\mathcal{L}$, où C_k est la zone géographique couverte par la cellule k et n est le nombre de cellules dans le réseau étudié. Il est clair que $\mathcal{C} \subseteq \mathcal{L}$ parce que le niveau de champs reçu dans quelques pixels ne permet pas d'avoir un minimum de qualité de service.

Soit $RSRP_{k,i,j}$ la puissance reçue de signal de référence (son équivalent dans UMTS est $RSCP$ et dans le GSM est $Rxlev$) [59] de la cellule k au pixel $P_{i,j}$. La couverture

de cette cellule, notée par C_k, est donnée, pour $1 \leq k \leq n$, par

$$C_k = \{P_{i,j} \in \mathcal{L} \text{ tel que } RSRP_{k,i,j} = \max_{1 \leq l \leq n} RSRP_{l,i,j}\} \tag{1}$$

Pour chaque pixel $P_{i,j}$ dans $\mathcal{L}$, on note par $c^*_{i,j}$ et $\hat{c}_{i,j}$ respectivement l'index la meilleure cellule serveuse et de la meilleure cellule candidate pour le handover.

$$c^*_{i,j} = arg \max_{1 \leq l \leq n} RSRP_{l,i,j} \tag{2}$$

$$\hat{c}_{i,j} = arg \max_{\substack{1 \leq l \leq n \\ l \neq c^*_{i,j}}} RSRP_{l,i,j} \tag{3}$$

KPIs

- Timing Advance: temps de propagation qui est une mesure de temps réalisée par une station de base (BS) entre sa propre transmission et celle reçue de l'UE [60]. La granularité de ce KPI dans les réseaux LTE est de l'ordre de 78.25 mètres[60]. En se basant sur cette granularité, le TA est discrétisé en 6 intervalles indexés par t de la forme $[78.25 \times t,\ 78.25 \times (t+1)]$, avec $0 \leq t \leq 4$, et $[391.25,\ +\infty)$ pour $t = 5$. Pour chaque cellule k, on note par $\tau_t(k)$ la valeur du TA KPI qui donne le pourcentage des UEs dans l'intervalle de TA t.

- Angle d'arrivée: l'angle que fait un UE par rapport une direction de référence, typiquement le nord géographique [61]. Généralement, n'importe quel signal de la liaison montante (UL) de l'UE peut être employé pour estimer l'AoA, mais typiquement, on utilise les signaux de référence comme le SRS ou le DMRS [62]. La BS détermine la direction de l'arrivée en mesurant le timing advance à différents éléments du réseau d'antennes. En conséquence, l'AoA est estimé à l'aide de ces délais différents. Selon ce KPI, la cellule est divisée en trois zones géographiques. Pour chaque cellule k, on note par $\phi_t(k)$ la valeur de AoA KPI qui donne le pourcentage des UEs dans la zone de AoA t (Fig. 1).

- Degré de voisinage: Dans différents événements de la connexion des UEs au réseau tel que le processus de handover, chaque UE mesure les signaux des cellules détectées et envoie un rapport de ces mesures à sa cellule serveuse. Le compteur dans la base de données de O&M représentant le niveau voisinage d'une cellule voisine est incrémenté à chaque fois que cette cellule est remontée (dans un rapport de mesure) comme cellule éligible de candidat pour la passation (fig. 2).

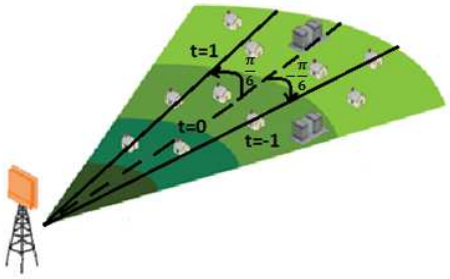

Fig. 1 Division de la zone couverte par la station de base selon l'AoA.

Afin d'obtenir ce KPI comme une distribution, le niveau voisinage de chaque cellule est définit par le nombre de remontée rapportant cette cellule comme meilleure candidate pour le handover divisé par le nombre total de remontée. Pour chaque voisine l d'une cellule serveuse k, on note par $\vartheta_l(k)$ le nombre de fois où la cellule l est rapportée comme la meilleure cellule pour le handover.

- La charge de la cellule: la charge est définie comme le rapport entre les ressources occupées et les ressources disponibles dans la cellule durant une période d'observation. Ce KPI est calculé par heure et est donné durant les heures chargées ou pour la journée, la semaine ou aussi le mois. On note par $\rho(k)$ la charge dans la cellule k.

- La moyenne arithmétique (AMT) et harmonique (HMT) des débits: AMT représente le débit utilisateur et HMT représente le débit cellule. Le HMT diffère de l'AMT par le fait qu'il donne plus d'importance aux UEs avec de mauvaises conditions radio. Sachant que la différence entre ces deux mesures de débits est plus grande lorsque le trafic est au centre de la cellule, on peut ainsi déduire la localisation du trafic dans la cellule si c'est au centre ou en bordure. Pour chaque cellule k, on note par $\mu_a(k)$ et $\mu_h(k)$, respectivement, les KPIs AMT et HMT obtenus de la base de données O&M.

Carte des lieux potentiels de trafic

Une carte des lieux potentiels de trafic est une couche supplémentaire obtenue à partir des données commerciales afin d'améliorer la localisation des hotspot. Dans ce cas, la distribution spatiale du trafic est calculée prenant en compte la connaissance apriori de l'emplacement des secteurs industriels et commerciaux ou l'emplacement des résidences. Cette carte contient également des informations sur l'emplacement des rivières, des

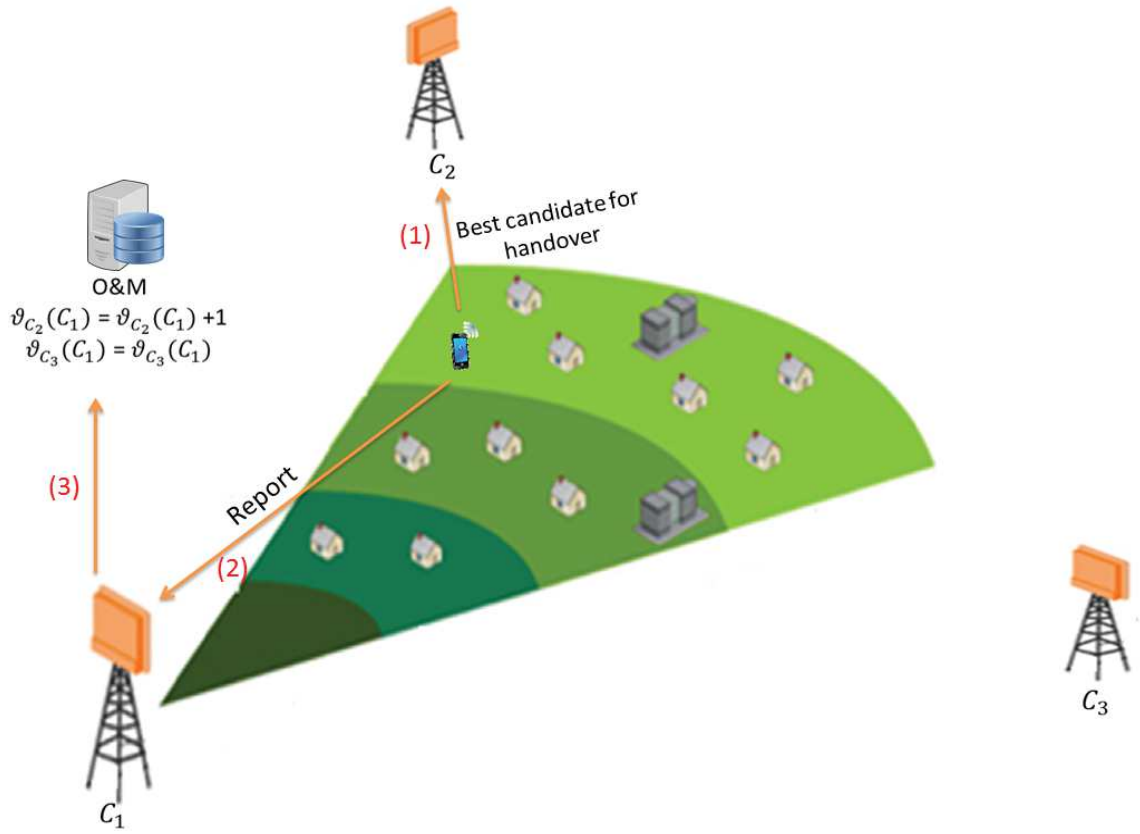

Fig. 2 Mise à jour du degré de voisinage.

forêts, des événements de masse etc. Une telle carte peut être une carte de référence pour définir la contribution de chaque KPI dans la localisation du trafic.

On note par $\hat{Q} = (\hat{q}_{i,j})_{1 \leq i,j \leq m}$ la carte (ou la matrice) représentant les lieux potentiels de trafic.

$$\hat{q}_{i,j} = \begin{cases} \omega_{i,j} & \text{si } P_{i,j} \text{ est dans un hotspot potentiel} \\ 0 & \text{sinon} \end{cases} \tag{4}$$

où $\omega_{i,j}$ est une valeur définissant l'intensité possible du hotspot.

Algorithme: Conception et optimisation

Étape 1: calcul de la carte de trafic selon TA

Chaque pixel prend un poids de trafic égal au pourcentage des UEs dans l'intervalle de TA correspondant à ce pixel.

$$q_{i,j}^{(1)} = \sum_{t=0}^{5} \tau_t(c_{i,j}^*) \times \chi_{1,t}(P_{i,j}) \tag{5}$$

où $\chi_{1,t}(P_{i,j})$ est la fonction indicatrice du la zone de TA t dans la cellule $c_{i,j}^*$ et $\chi_{1,t}(P_{i,j})$ prend la valeur 1 si le pixel appartient à la zone de TA t et 0 sinon.

Étape 2: calcul de la carte de trafic selon AoA

Chaque pixel prend un poids de trafic égal au pourcentage des UEs dans l'intervalle de TA correspondant à ce pixel.

$$q_{i,j}^{(2)} = \sum_{t=-1}^{1} \phi_t(c_{i,j}^*) \times \chi_{2,t}(P_{i,j}) \tag{6}$$

où $\phi_t(c_{i,j}^*)$ représente la valeur du KPI AoA qui donne le pourcentage des UEs la zone de AoA t et $\chi_{2,t}(P_{i,j})$ est donnée par

$$\chi_{2,t}(P_{i,j}) = \begin{cases} 1 & \text{si } Angle(P_{i,j}, c_{i,j}^*) - \theta(c_{i,j}^*) \in I_t \\ 0 & \text{sinon} \end{cases} \tag{7}$$

avec

$$I_t = \begin{cases} [-\frac{\pi}{6},\ \frac{\pi}{6}] & \text{si t=0} \\ [\frac{\pi}{6},\ \pi] & \text{si t=1} \\ [-\pi,\ -\frac{\pi}{6}] & \text{si t=-1} \end{cases} \tag{8}$$

$Angle(P_{i,j}, c_{i,j}^*))$ est l'angle entre le pixel $P_{i,j}$ et sa cellule serveuse $c_{i,j}^*$ par rapport au nord géographique de la carte de couverture. $\theta(c_{i,j}^*)$ est l'azimuth de l'antenne couvrant la cellule $c_{i,j}^*$.

Étape 3: calcul de la carte de trafic selon le degré de voisinage

En exploitant le degré de voisinage, on attribut les poids de trafic comme illustré dans la figure 3.

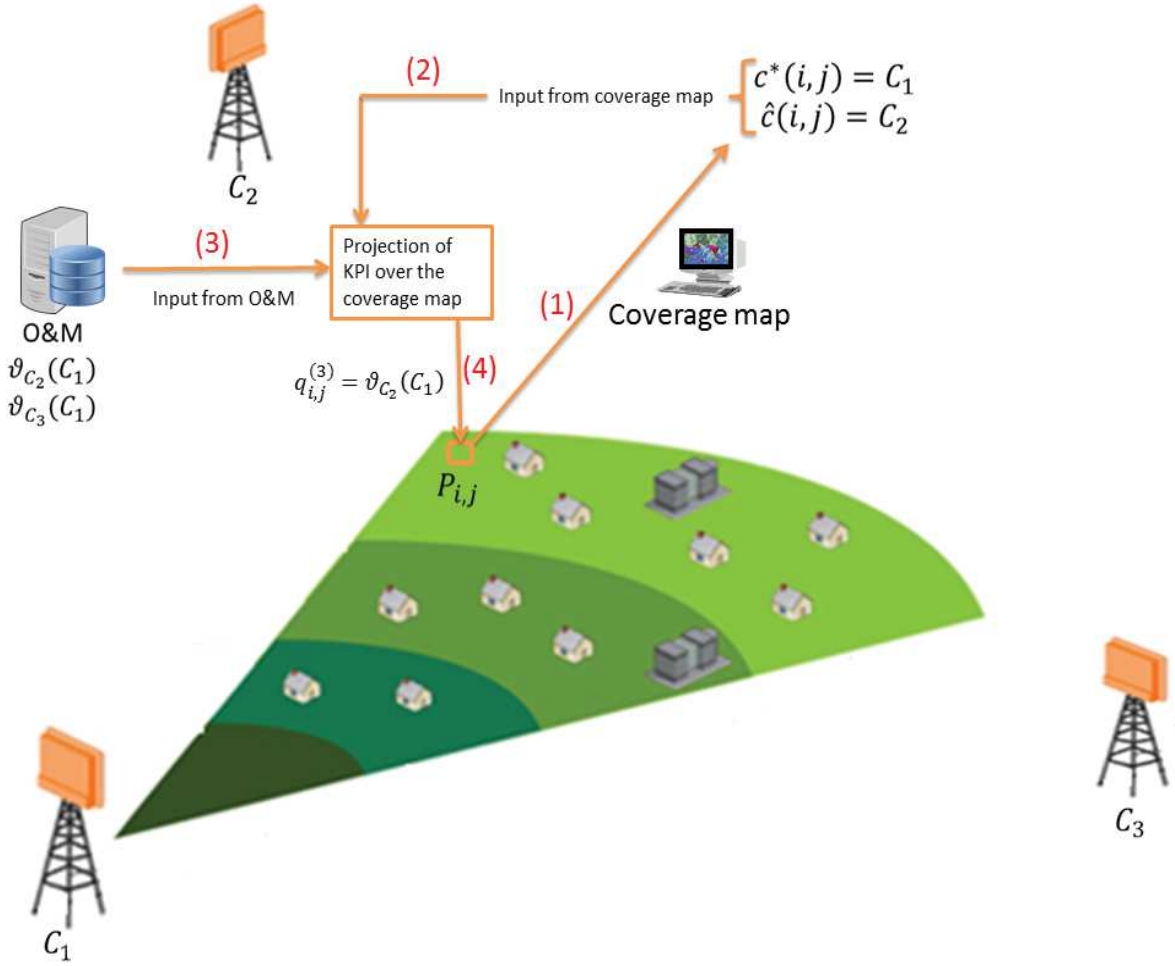

Fig. 3 Attribution des poids de trafic selon le degré de voisinage.

On attribut à chaque pixel $P_{i,j}$ le poids $q_{i,j}^{(3)}$ égale à $\vartheta_{\hat{c}_{i,j}}(c^*_{i,j})$

Étape 4: calcul de la carte de trafic selon la corrélation des charges radio

On note par $\psi_{c^*_{i,j}}$ l'ensemble des cellules voisines ayant le même niveau de charge que la cellule $c^*_{i,j}$ et qui sont éligible pour un handover pour des UEs au pixel $P_{i,j}$. Le poids attribué est donné par

$$\psi_{c^*_{i,j}} = \{k \in \mathcal{C} \text{ tel que } |\rho(c^*_{i,j}) - \rho(k)| < \epsilon \text{ et } |RSRP_{c^*_{i,j},i,j} - RSRP_{k,i,j}| < \gamma\} \qquad (9)$$

où γ est une paramètre permettant d'identifier les cellules éligibles pour un possible handover et ϵ est utilisé pour identifier les cellules ayant le même comportement que la cellule étudiée en terme de charge radio.

$$q_{i,j}^{(4)} = \begin{cases} \frac{1}{n(\psi_{c_{i,j}^*})} \sum\limits_{k \in \psi_{c_{i,j}^*}} \rho(k) & \text{si } \rho(c_{i,j}^*) > \tilde{\rho} \\ 0 & \text{sinon} \end{cases} \tag{10}$$

où $n(\psi)$ est le nombre d'éléments de ψ et $\tilde{\rho}$ est le seuil utilisé pour identifier les cellules chargées.

Étape 5: calcul de la carte de trafic selon AMT versus HMT

Dans cette étape, le poids de trafic attribué est la différence entre ces deux moyennes divisée par une constante μ_0 (μ_0 peut être définit comme le débit maximum qu'un utilisateur peut atteindre et elle permet d'avoir toujours une valeur dans $[0,\ 1]$).

Le poids de trafic $q_{i,j}^{(5)}$ attribué à chaque pixel est formulé comme suivant:

$$q_{i,j}^{(5)} = \begin{cases} \frac{\mu_a(c_{i,j}^*) - \mu_h(c_{i,j}^*)}{\mu_0} & \text{si } RSRP_{c_{i,j}^*,i,j} > RSRP_0 \\ 1 - \frac{\mu_a(c_{i,j}^*) - \mu_h(c_{i,j}^*)}{\mu_0} & \text{si } RSRP_{c_{i,j}^*,i,j} < RSRP_0 \end{cases} \tag{11}$$

où $RSRP_0$ est le niveau de champs seuil qui permet de différencier entre les utilisateurs qui sont en bordure de cell et les utilisateurs qui sont au centre.

Étape 6: combinaison de tous les KPIs dans une métrique globale

On note par $Q = (q_{i,j})_{1 \leq i,j \leq m}$ la carte de trafic qui en résulte de la combinaison de tous les KPIs. La carte $Q^{(s)} = (q_{i,j}^{(s)})_{1 \leq i,j \leq m}$, $1 \leq s \leq 5$, avec un facteur d'importance donné par $\mathbf{x} = (x_1, x_2, x_3, x_4, x_5)^T$ est définie par

$$Q = \sum_{s=1}^{5} x_s Q^{(s)} \tag{12}$$

Étape 7: smoothing de la carte de trafic estimée

Dans cette étape, afin d'éliminer les faux hotspots, on fait comme suit

$$q^*_{i,j} = \frac{\sum_{P_{i',j'} \in \mathcal{L}} G(P_{i,j}, P_{i',j'}) q_{i',j'}}{\sum_{P_{i',j'} \in \mathcal{L}} G(P_{i,j}, P_{i',j'})} \tag{13}$$

où

$$G(P_{i,j}, P_{i',j'}) = \frac{1}{2\pi h} e^{-\frac{|P_{i,j} - P_{i',j'}|^2}{2h}} \tag{14}$$

avec $|P_{i,j} - P_{i',j'}|$ la distance euclidienne entre les pixels $P_{i,j}$ et $P_{i',j'}$ et h un paramètre lié au nombre de pixels voisins inclus dans le smoothing de l'estimation au pixel $P_{i,j}$. Les $q_{i,j}$s sont les poids de trafic obtenus après l'exécution de l'étape 6 et les $q^*_{i,j}$s sont les poids de trafic obtenus après l'exécution de l'étape 7.

Optimisation de l'algorithme de localisation de hotspot

Obtenir le meilleur vecteur des facteurs d'importance lié au KPIs $\mathbf{x}$ est le résultat d'un problème d'optimisation qui réduit la distance entre les poids de trafic obtenus dans l'étape 6 et les poids de trafic donnés par la carte des lieux potentiels de trafic $\hat{Q}$. Ce problème d'optimisation est donné par

$$\begin{cases} \underset{\mathbf{x} \in \mathbb{R}^5}{minimise} \sum_{i,j=1}^{m} (q_{i,j} - \hat{q}_{i,j})^2 = \sum_{i,j=1}^{m} \left(\sum_{s=1}^{5} x_s q^{(s)}_{i,j} - \hat{q}_{i,j} \right)^2 \\ \qquad x_s \geq 0, \ s = 1..5 \end{cases} \tag{15}$$

Tout d'abord, on reformule le problème comme suivant:

$$A^T = \begin{bmatrix} q^{(1)}_{1,1} & \cdots & q^{(1)}_{1,m} & \cdots & q^{(1)}_{2,1} & \cdots & q^{(1)}_{m,m} \\ \cdot & \cdot\cdot & \cdot & \cdot\cdot & \cdot & \cdot\cdot & \cdot \\ q^{(5)}_{1,1} & \cdots & q^{(5)}_{1,m} & \cdots & q^{(5)}_{2,1} & \cdots & q^{(5)}_{m,m} \end{bmatrix}$$

et

$$\mathbf{b} = [\hat{q}_{1,1} ... \hat{q}_{1,m} ... \hat{q}_{2,1} ... \hat{q}_{m,m}]^T$$

La forme du problème initiale devient

$$\begin{cases} \underset{\mathbf{x} \in \mathbb{R}^5}{minimise} \| A\mathbf{x} - \mathbf{b} \|_2 \\ \quad x_s \geq 0 \ , \ 1 \leq s \leq 5 \end{cases} \tag{16}$$

La solution de cette dernière forme est donnée par la méthode des moindres carrées qui est simplement obtenue avec Gauss Newton [70].

Résultats

On prend un réseau LTE tri-sectoriel avec une distribution de station de base obtenue d'un réseau réel ainsi que sa configuration. On génère un trafic non uniforme avec des hotspots dans la carte et on essaye de les trouver. Avec notre algorithme, les hotspots sont bien localisés avec une bonne précision.

Fig. 4 représente la CDF des poids trafic calculée en se basant sur l'algorithme proposé. Pour localiser les hotspots, on s'intéresse à la partie encerclé en bleu dans la figure 4 qui représente les poids élevés.

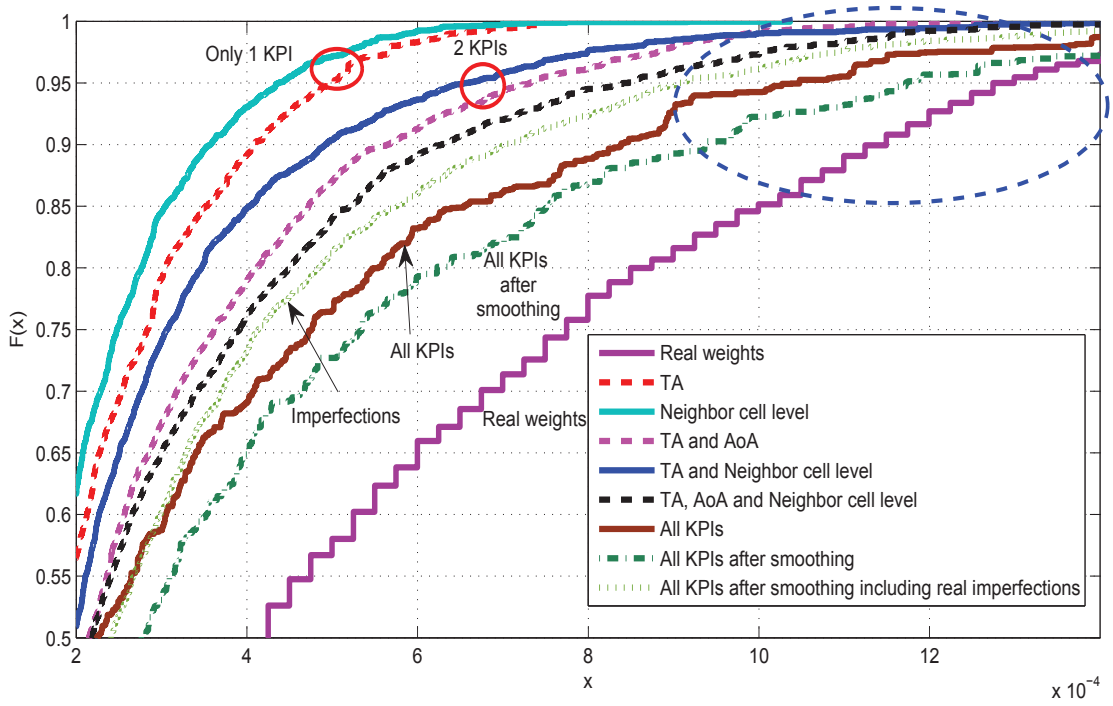

Fig. 4 CDF du trafic généré et estimé.

Selon les résultats de la Fig. 4, l'exploitation des 5 KPIs donne une meilleure estimation de la distribution spatiale de trafic comparée à l'utilisation de quelques KPIs. L'estimation est encore amélioré lorsque on exécute toutes les étapes de l'algorithme proposé.

Conclusion

Dans cette étude, on a proposé une solution de localisation de hotspot de trafic qui réduit les coûts et améliore en même temps la précision avec moins de calculs. Les résultats de simulations ont confirmé l'efficacité de la solution et a montré qu'on peut se débarrasser de l'utilisation des sondes à cause de leur coût important et leur précision faible.

Impact de la localisation parfaite et imparfaite des hotspots sur le déploiement des petites cellules

Les zones urbaines denses sont des environnements où le spectre est une ressource rare et le besoin de grande capacité est urgent pour assurer une bonne qualité de service. En conséquence, un déploiement de réseau dense est nécessaire avec une topologie adaptée à l'environnement de la zone étudiée afin d'assurer une meilleure couverture dans la cellule entière. La compréhension de l'efficacité du déploiement des petites cellules en présence des hotspots de trafic est un sujet qui attire l'attention des opérateurs.

En ce chapitre, on évalue l'impact du mauvais positionnement d'une petite cellule sur les performances du réseau. On décrit tout d'abord, le modèle de système qu'on étudie avec une focalisation spéciale sur les aspects radio. Puis, on calcule la distribution du débit et sa moyenne après une analyse au niveau statique, qui se réfère dans notre contexte, à un ensemble de snapshots de réseau décorrélés où la distribution d'emplacement des utilisateurs varie seulement dans l'espace. Trois scénarios différents sont étudiés : i. avec des macro cellules seulement, ii. avec une petite cellule déployée exactement au centre du hotspot de trafic et à iii. avec une petite cellule pas parfaitement déployée près du hotspot de trafic (sa position est différente de celle du hotspot).

On considère deuxièmement la dynamique du système (largement appelé analyse flow level), avec des utilisateurs arrivant à des temps aléatoires au système et restant pour une durée finie de temps correspondant à la fin de leurs services. Le modèle de files d'attente étudié est basé sur le multi-classe processor sharing couplé. Le couplage entre la macro cellule et la petite cellule est la conséquence de l'interférence produite par chacune des cellules sur les utilisateurs de l'autre. On établie des expressions analytiques pour plusieurs métriques de performance réseau prenant en compte le niveau de précision des outils de localisation des hotspots de trafic [20].

D'après les résultats obtenus, si on considère les analyses au niveau statique seulement, on peut dire que l'efficacité du déploiement de petites cellules pour offloader le trafic de la macro cellule congestionnée dépend principalement de la précision du procédé de localisation de hotspot utilisé, de la position du hotspot dans la cellule et aussi de la position de la petite cellule par rapport à l'emplacement de la macro cellule.

D'ailleurs, on observe que quand le hotspot est en bordure de cellule, les imperfections de la localisation du hotspot sont plus tolérées et les performances système peuvent être améliorées en déployant de petites cellules comparé à un réseau composé de macro cellules seulement. Par contre, quand le hotspot est au centre de la macro cellule, même un positionnement parfait de la petite cellule n'est pas bénéfique pour les performances globales du système et n'apporte pas des gains.

L'analyse de niveau dynamique nous a permis de conclure que le positionnement parfait de la petite cellule par rapport à la position du hotspot est suffisante pour obtenir de meilleurs résultats mais il n'est pas suffisant pour obtenir le gain maximal. Ce dernier dépend de plusieurs autres paramètres tels que la portée radio de la petite cellule (s'il couvre tout le hotspot ou une partie de lui quand ce ce dernier est plus large), la capacité de la petite cellule et la quantité de trafic qu'elle doit offloader.

Analyse de performance des déploiements de petites cellules mobiles dans les réseaux cellulaires en présence des hotspots

Le concept de déplacement des petites cellules dans les réseaux mobiles est présenté et évalué en considérant la dynamique du système. Une petite cellule se déplace selon un modèle de mobilité de Manhattan qui est le cas quand la petite cellule est déployée sur le dessus d'un autobus suivant une trajectoire prédéfinie dans les secteurs où il y a généralement pleins de gens connectés. On étudie au niveau dynamique du système un modèle de files d'attente basé sur un système multi-classe processor sharing couplé. Le couplage est dû à l'interférence mutuelle produite par chaque cellule sur l'autre (puisqu'elles fonctionnent dans le même spectre de fréquence).

Les résultats numériques obtenus des analyses réalisées prouvent que déployer les petites cellules mobiles pour absorber le trafic dans la macro cellule congestionnée peut être une solution efficace quand la petite cellule se déplace près du hotspot et couvre une part importante de ce dernier. Cependant, quand la petite cellule se déplace loin du hotspot de trafic, les performances système sont dégradées comparées à un réseau

composé de macro cellules seulement. Ceci est dû à l'interférence mutuelle élevée entre la macro cellule et la petite cellule.

Procédé de délestage de trafic utilisant les drones au sein du réseau mobile

Description du mécanisme proposé

Les états du drone et de la macro cellule

Le drone peut être soit en mode:

- Idle: le drone est en état d'arrêt ou il recharge ses batteries,
- Stand-by: le drone active quelques composants électronique afin de se préparer pour une congestion possible dans la cellule.
- Active: Le drone active tous ces composants lui permettant de voler et se déplace à côté du hotspot.
- Ready: Le drone désactive les composants lui permettant de voler, active ses composants RF et commence à servir les utilisateurs du hotspot.

Les états de charge de la macro cellule sont donnés par la figure 5.

La couleur verte représente un état de charge normal. Le jaune est un signe de congestion possible en bordure de la cellule. Le rouge confirme l'apparition du hotspot. Le bleu est la région où le drone peut se retourner en état d'inactivité après avoir éliminé complètement le hotspot de trafic.

Dans la figure 5, $Cell\_Load$ représente la charge de la cellule et $Hotspot\_position$ représente la position du hotspot de trafic par rapport au centre de la cellule.

On définit par $\{TP_i, i = 1.n\}$ l'ensemble d'emplacements où le drone peut s'installer afin de bien couvrir toutes la macro cellule. En outre, SEL_offset, HO_hys et HO_offset sont trois paramètres supplémentaires utilisés pour le processus de la sélection et du handover des UEs. N_{UE} est le nombre d'utilisateurs servis par le drone.

Dans la figure 6, les différentes étapes exécutées et les scénarios possibles de ce mécanisme sont présentés.

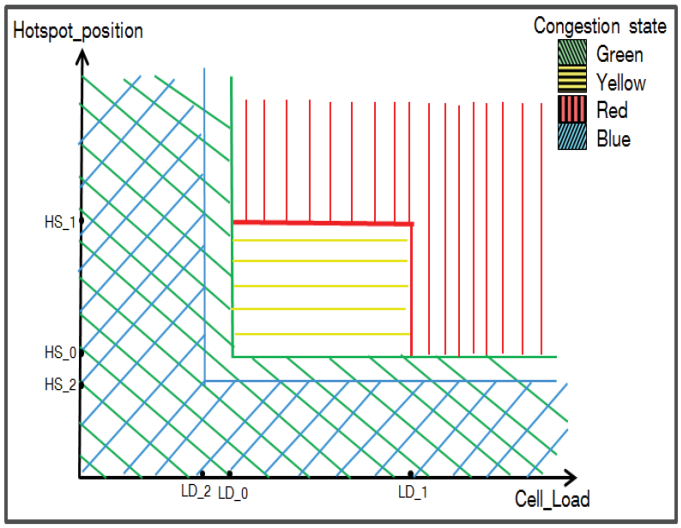

Fig. 5 State Diagram controlling the drone.

Spécification du mode d'accès

Un drone peut communiquer avec la station de base de la cellule via un lien filaire ou non-filaire. Dans le cas d'un lien non-filaire, la station de base et le drone communiqueront entre eux, de préférence, dans une bande de fréquences basses en FDD (initiales des mots anglais « Frequency Division Duplexing » signifiant « Duplexage en Fréquence »), ce qui est rendu possible par la portée étendue du drone en ligne de mire. Ce principe permet d'avoir une faible congestion dans le spectre licencié, et peu d'interférences avec d'autres applications dans le domaine radio ou avec des communications par satellite.

Quant aux communications entre le drone et les terminaux, elles utilisent de préférence le spectre licencié si les ressources nécessaires sont disponibles, et le spectre non-licencié dans le cas contraire. Concernant le spectre non-licencié, l'utilisation du WiFi, qui est de fait une technologie disponible dans la plupart des smartphones commercialisés ainsi que dans d'autres dispositifs, permet aux opérateurs d'obtenir un revenu supplémentaire de la part des dispositifs compatibles seulement avec le WiFi. Cependant, la facturation et la sécurité exigent des mises à jour matérielles et logicielles liées au module WiFi du drone. Les mises à jour doivent être faites au niveau du réseau cœur pour le système de facturation, et au niveau du drone pour assurer la sécurisation des communications. De plus, les interférences dans la bande WiFi ne peuvent pas être contrôlées en raison de la large utilisation de cette bande non-licenciée dans d'autres domaines, tels que les domaines médicaux, scientifiques et industriels. De préférence, on n'utilisera donc le WiFi qu'en cas d'insuffisance de ressources dans le spectre licencié. Concernant justement le spectre licencié, on utilisera de préférence

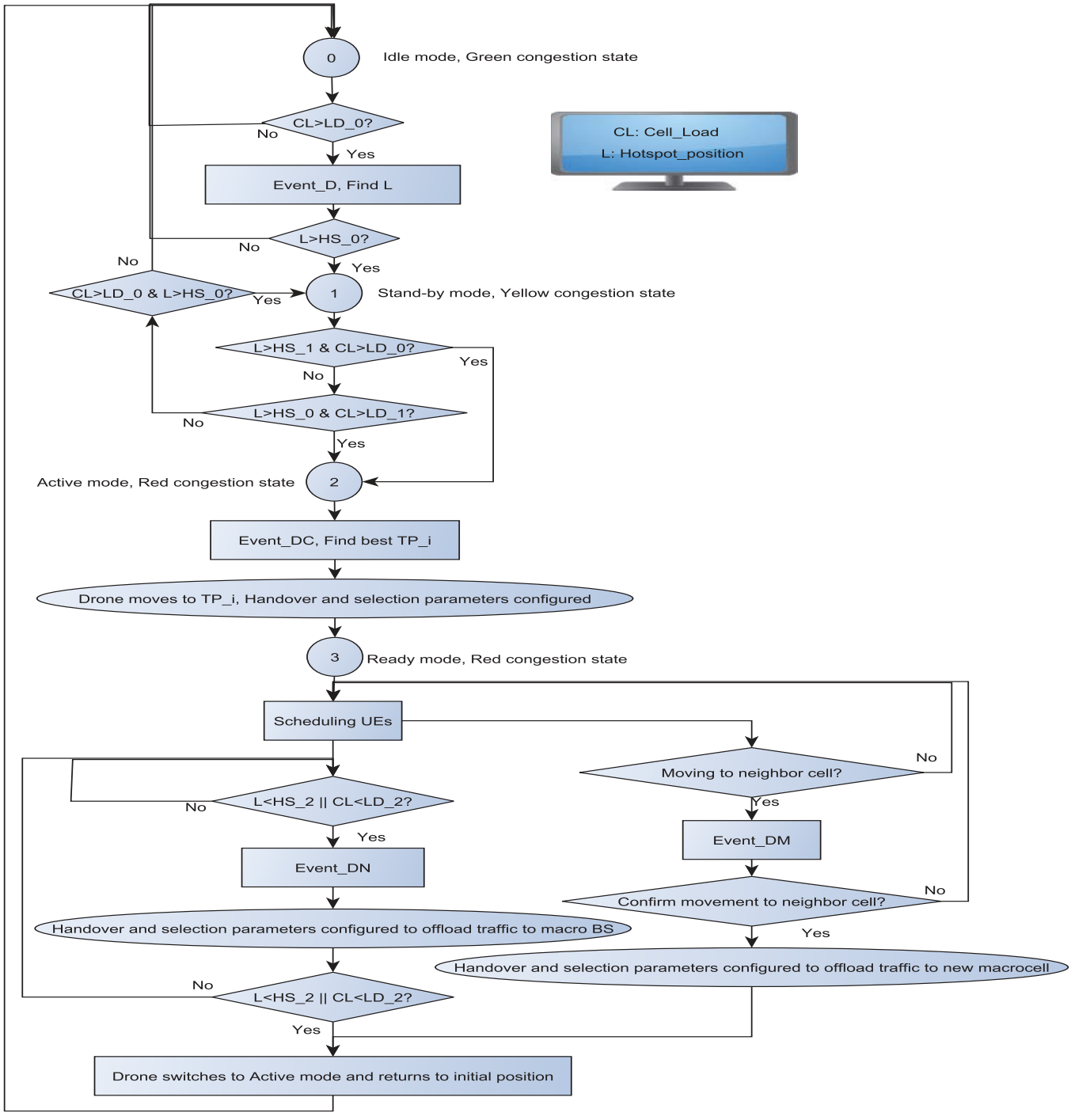

Fig. 6 Mécanisme de décongestion du réseau.

le TDD (initiales des mots anglais « Time Division Duplexing » signifiant « Duplexage en Temps ») pour les communications entre le drone et les terminaux mobiles, car (comme il est connu de l'Homme du Métier) le TDD fonctionne efficacement pour les communications sur de petites distances, d'autant que la plupart des opérateurs ont investi dans l'achat d'une bande de fréquences licenciée en TDD, même si toutes ces bandes ne sont pas exploitées (d'où un gaspillage de ressources). Grâce à l'utilisation de ces bandes, on aura moins d'interférences dans les bandes FDD, les performances globales du système seront améliorées, et l'on fera un usage efficace des ressources radio disponibles.

Points forts et points à explorer

La solution proposée présente de nombreux avantages. Ainsi :

- les drones peuvent être déployés très rapidement aux endroits souhaités ;

- les drones peuvent se poser de manière stable près des hotspots, par exemple en des points d'attachement prédéterminés (tels qu'un réverbère ou un bâtiment), et même suivre les terminaux mobiles concernés (par exemple, une foule en marche) dans leur déplacements au sein de la cellule, en « sautant » d'un point d'attache à un autre ;

- les communications entre, d'une part, un drone et les terminaux mobiles qu'il dessert, et d'autre part ce drone et la station de base qu'il aide, sont en ligne de mire ;

- chaque drone possède, durant son déplacement, une base de données où tous les trajets entre les points d'attachement sont définis ; le drone donc peut donc circuler à basse altitude sans risque d'accident ;

- une fois le drone posé, il peut aisément établir un lien filaire ou non-filaire stable avec la station de base ;

- la distance entre un drone et un terminal mobile étant courte, la puissance d'émission requise aussi bien pour le terminal mobile que pour le drone est faible ;

- dès qu'un drone se pose, il active les composants RF et désactive les composants qui lui permettent de voler ; la consommation électrique d'un drone est donc faible, surtout s'il est alimenté par l'énergie solaire (comme on peut l'envisager si la surface des ailes du drone est assez grande) ;

- le ravitaillement du drone est aisé puisqu'il peut se poser directement sur une aire de ravitaillement pour recharger ses batteries ; on peut par exemple installer des équipements de ravitaillement au sommet de quelques réverbères répartis dans la cellule.

Les points qui ne sont pas encore abordés dans le monde de la recherche et de l'industrie sont:

- De nos jours, les drones sont à la crête de leur développement et beaucoup de constructeurs investissent dans la recherche afin de produire des modèles commercialement viables et qui sont efficaces, autonomes, stables et qui ne consomment pas beaucoup d'énergie. Néanmoins, l'exploitation des drones pour usage professionnel manque toujours dans les réglementations gouvernementales. Ce sujet a besoin des investigations approfondies au sujet de leur contrôle pour créer de nouvelles règles principalement liées à la sécurité nationale et également à l'interférence avec d'autres applications.

- Un autre point à investiguer est la coexistence avec les autres dispositifs et d'autres applications et les possibilités d'interférence et de collision.

Conclusion

On a proposé un nouveau mécanisme utilisant les drones pour réduire la congestion dans les réseaux cellulaires. Les drones réagissent immédiatement en réponse à l'apparition des hotspot de trafic et commence à offloader le trafic efficacement. La disparition et le mouvement du hotspot de trafic sont également adressés afin de faire un mécanisme de décongestion complet, fiable et faisable. De plus, le mode d'accès des utilisateurs et la communication du drone avec la station de base de la macro cellule sont aussi

adressés. Enfin, les avantages et les points à explorer pour déployer ce mécanisme dans le réseau réel sont abordés.

Conclusion

Dans cette thèse, et d'après les études menées, les scénarios évalués et les mécanismes développés, nous pouvons conclure ce qui suit :

- La précision des outils opérationnels de localisation de hotspot doit toujours être améliorée si des ingénieurs radio sont tentés en exploitant la production de ces outils dans le processus de déploiement des HetNets. Autrement, la petite cellule déployée en se basant sur ces outils sera toujours risquée et peut mener aux pertes possibles en termes de dépenses et également de la capacité.

- L'O&M KPIs et la carte de couverture représentent des entrées intéressants pour développer des méthodes de localisation plus sophistiqués afin d'améliorer encore la précision.

- Le déploiement petites des cellules classiques au centre de la macro cellule dégrade les performances globales du réseau. En effet, l'interférence de la macro cellule sur les utilisateurs de la petite cellule sera ainsi très élevée conduisant à des débits dégradés pour ces utilisateurs.

- Le déploiement petites des cellules en bordure de cellule est souvent une solution bénéfique même avec des erreurs dans la localisation du trafic. Ceci est expliqué par le fait que les conditions radio seront toujours améliorées dans ces secteurs.

- Les petites cellules mobiles peuvent être une solution efficace en termes d'efficacité et également de coût. Néanmoins, l'incapacité pour contrôler la mobilité de ces cellules est toujours un souci important et constitue une question ouverte afin que cette solution atteigne le stade de maturité.

- Les petites cellules drone est une nouvelle alternative prometteuse pour absorber le trafic dans les réseaux cellulaires. C'est un sujet de recherche ouvert pour les déploiements des technologies futures.

Author communications

During the studies realized in the scope of the thesis, we were able to submit four Journal papers in journals with excellent reputations, five conference papers in well-known conferences. Our productions include also three new inventions where only one is submitted as a patent, the second one is under the juridic redaction in order to cover and protect most of the invention use cases. The third one in supposed to be exploited in internal tasks which is a decision made by the staff in charge of patenting new inventions.

Journal papers

1. A. Jaziri, R. Nasri and T. Chahed, *Tracking traffic peaks in mobile networks using statistics of performance metrics*, accepted with major revisions in International Journal of Wireless Information Networks.

2. A. Jaziri, R. Nasri and T. Chahed, *System level analysis of heterogeneous networks under imperfect traffic hotspot localization*, in IEEE Transactions on Vehicular Technology 2016.

3. R. Nasri and A. Jaziri, *On the Analytical Tractability of Hexagonal Network Model with Random User Location*, in IEEE Transactions on Wireless Communications 2016, vol. 15, no 5, p. 3768-3780.

4. A. Jaziri, R. Nasri and T. Chahed, *Offloading moving traffic hotspots with drone cells in future wireless networks*, submitted to IEEE Transactions on Vehicular Technology.

Conference Proceedings

1. A. Jaziri, R. Nasri and T. Chahed, *Traffic Hotspot localization in 3G and 4G wireless networks using OMC metrics*, in Proc. IEEE PIMRC, p. 270-274, September 2014, Fundamentals and PHY symposium.

2. A. Jaziri, R. Nasri and T. Chahed, *Performance Analysis of Small Cells' Deployment under Imperfect Traffic Hotspot Localization*, in IEEE Globecom 2015, p. 1-6, Wireless Networks symposium.

3. R. Nasri and A. Jaziri, *Tractable Approach for Hexagonal Cellular Network Model and its Comparison to Poisson Point Process*, in IEEE Globecom 2015, p. 1-6, Wireless Communications symposium.

4. A. Jaziri, R. Nasri and T. Chahed, *Offloading traffic hotspots using moving small cells*, in IEEE ICC 2016, p. 1-6, Wireless Networks symposium.

5. A. Jaziri, R. Nasri and T. Chahed, *Congestion Mitigation in 5G Networks using Drone relays*, in International Wireless Communications & Mobile Computing Conference (IWCMC 2016), 5G Communications Techniques symposium.

Patents

1. PROCEDE DE DELESTAGE DE TRAFIC AU SEIN D'UNE CELLULE D'UN RESEAU MOBILE.

2. PROCEDE ET SYSTEME POUR EFFECTUER DES MESURES RADIO DANS UN RESEAU MOBILE.

Table of contents

List of figures

List of tables

List of acronyms

Acronyms / Abbreviations

3GPP 3rd Generation Partnership Project

5G 5th generation mobile networks

AMT Arithmetic Mean Throughput

AoA Angle of Arrival

BS Base Station

CAPEX Capital Expenditure

CCDF Complementary Cumulative Distribution Function

CDF Cumulative Distribution Function

CQI Channel Quality Indicator

D2D Device to Device communications

FDD Frequency Division Duplexing

GSM, 2G Global System for Mobile Communications

HetNet Heterogeneous Network

HMT Harmonic Mean Throughput

KPI Key Performance Indicator

LTE or 3.9G Long Term Evolution

LTE-A, 4G LTE-Advanced

MDT Minimizing Drive Tests

O&M Operation & Maintenance

OPEX Operational Expenditure

PS Processor Sharing

QoS Quality of Service

RSRP Reference Signal Received Power

SINR Signal to Interference plus Noise Ratio

SNR Signal to Noise Ratio

TA Timing Advance

TDD Time Division Duplexing

UE User Equipment

UMTS, WCDMA, 3G Universal Mobile Telecommunications System

Chapter 1

Introduction

1.1 Background and general context

Over the last few years, the demand for higher data rates in cellular networks has been unceasingly increasing making from cellular services an undeniable success story. Cellular networks were initially installed to ensure voice communications and to fulfill wide area voice coverage. Nowadays, it has become a vital part of our everyday life with a strong need for "everywhere and seamless" connectivity. In fact, many day-to-day activities have been shifted to our online presence thanks to the widespread use of smartphones, tablets etc.. and the development of several services (such as Internet downloading, E-mail, web browsing, high definition video streaming, social networking, file sharing, etc..). Facing this traffic increase represents a big challenge for operators. So, they are always eager to implement new technologies such as 5G technology to meet these rising capacity and quality of service demands. Meanwhile, operators have to maintain the current network operational, reliable and efficient into absorbing the existing traffic demands. The common goal is to improve network performance, users' experience, and operators' business as well.

Actually, cellular networks are facing an explosive increase in data traffic and a frequent appearance of areas of capacity bottlenecks, which creates a fundamental challenge for cellular operators. Dealing with this challenge can be ensured by an efficient use of the available capacity with advanced features that only require few modifications to the existing network infrastructure and configuration. Consequently, during the planning and optimization process, radio engineers have to find the best solution allowing the network to reach higher capacity and better quality of experience without moving urgently to a new technology. This task can be further enhanced if

they exploit most of the available informations about the treated traffic scenario, in an accurate way.

In this context, several studies have been realized to find the best answers appropriate to these issues. While awaiting the outcomes of the new technologies proposed and tested by the scientific community, Heterogeneous Networks (HetNet) deployment remains one of the existing solutions that can be further enhanced allowing the network to reach its capacity limits and to reduce the congestion in it. This kind of deployments ranges from the installation of additional small cell sites and relay stations, as well as signal boosters to the deployment of Wireless Fidelity (WiFi) networks for dual mode devices to complement existing macrocell infrastructure. HetNets have been considered as one of the main aspects to be investigated in 3rd Generation Partnership Project (3GPP) Long Term Evolution (LTE)/Long Term Evolution-Advanced (LTE-A) deployments [1]. This trend is encouraged by different factors: i. a fast and efficient coverage and capacity expansion, ii. its ability to offload the mobile data traffic and more specifically traffic hotspots, iii. its ability to improve poor radio conditions, iv. its significant increase in spectral reuse efficiency per area, v. its reduced CAPEX and OPEX costs and the expected performance results making from it a cost-effective solution. Due to these relevant benefits, small cell deployments have garnered more interest in the industrial and research communities which led to its consideration as an integral part of 5G cellular network architecture [2].

1.2 Problem definition and challenges

In 4G networks, the tangible application of HetNet deployments did not reach yet the maturity stage for different reasons. First, the uniform traffic scenario is always considered in the capacity and coverage planning process. However, small cells are deployed, in several cases, at targeted high-demand areas (traffic hotspots). Consequently, the estimation of network performances must be based on the characteristics of the studied traffic scenario in order to be near to the really obtained results. From this first challenge, we notice the importance of the accuracy of the collected informations about the traffic distribution in each area. So, the second challenge is to make the data collected more informative and precise through the definition of new algorithms and processes. On the one hand, an accurate traffic hotspot localization will lead to a better network design and planning. On the other hand, including the imperfect small cell positioning (due to the limited accuracy of the used traffic localization method) in performance analysis of HetNet deployments is also of great importance. Indeed, this evaluation

allows to assess the gain that can be generated from the deployment of a small cell considering an error in hotspot localization. It allows also to identify the threshold of localization accuracy that can be tolerated in operational tasks of HetNet deployments. Next, the traffic mobility inside each cell is generally neglected in the network design which results in unexpected performances. So, mobility of traffic hotspots must be involved in the performance analysis and prediction in cellular networks. Moreover, developing new intelligent, realizable and energy-efficient mechanisms to offload the moving hotspots represents also a major concern in operators' roadmaps. Next, improving the mobility of the existing offloading mechanisms to follow the trajectory of traffic hotspots is also a relevant topic to investigate. In addition to the aforementioned challenges, operators always seek to reduce the costs without impacting the global performances of the network or even with expecting more improvements.

1.3 Original contributions

This thesis includes four major contributions:

1. Development of a new traffic hotspot localization method using O&M KPIs projected over the coverage map:

   Nowadays, most of the connected devices are equipped with a GPS module leading to a very good precision of traffic localization. However, due to the considerable battery consumption related to the activation of this module, most of mobile users prefer to put off their installed applications related to GPS. Therefore, mobile operators are actively testing new solutions to localize traffic based on their own data measurements. Probing and trace analysis is the actual operational method used by operators in localizing traffic. Based on the stored call traces, measurements analysis are performed to optimize the network configuration and deploy new small cells or switch on/off some cells in areas with low traffic intensity. As an alternative to probing based methods, it is possible to identify the heavy traffic areas in the network using KPIs directly taken from the O&M. It is true that key performance indicators can give an idea about the hotspot zones with very low accuracy (with about a granularity of the cell radius). However, the combination of many KPIs would significantly increase the precision of traffic localization. The exploited KPIs are firstly projected over the coverage map and then combined in a weighted sum. The weights are optimized using additional information about potential hotspot areas obtained from commercial

data. Furthermore, mobile equipment and field imperfections are considered in the numerical results in order to meet with the real imperfections. Mobile equipment imperfections consist mainly in the difference between the signal level measured by the UE (User Equipment) and the signal level available in the coverage map. This difference is typically due to the shadowing effect, the category and the speed of the UE. On the other hand, field imperfections mean that some KPIs present sporadic errors which are observed in real data measurements performed in the context of individual UE localization. These errors do not really impact the localization in the presence of a traffic hotspot since these errors are sporadic and it is not common to have significant proportion of UEs with wrong measurements, otherwise, the implementation of these KPIs becomes worthless. Using the proposed localization method, a sufficient localization performance is achieved along with significant savings on the expenditures as well as in the computation complexity.

2. Performance analysis of small cell deployment under perfect and imperfect traffic hotspot localization:

   In the second line of contribution, system level analysis are realized for small cell deployment and the impact of the imperfect traffic hotspot localization is evaluated. So, three different scenarios are studied: i. with macrocells only, ii. with a small cell deployed exactly at the center of the traffic hotspot and iii. with a small cell not perfectly deployed near the traffic hotspot (its position is different from the hotspot one). The derivation of the system performances is realized through two main analysis levels: static and dynamic. In the static level, we evaluate the distribution of the achievable data rates reflecting the distribution of radio conditions in the network in the presence of the traffic hotspot. Then, the results of the first part are injected in the dynamic level analysis where the system presents dynamic arrivals and departures. Besides, the dynamic system model presents a coupling between the macrocell and the small cell. In fact, the interference generated from the one cell on the users of the other cell is counted only when there is at least one user served by the interfering cell.

   The objectives of this study are, firstly, to identify the areas where the small cell deployment is accompanied with capacity gains and improve the radio conditions in the network. Second, with involving the accuracy of traffic localization tools in the analysis and considering the impact of imperfect small cell positioning, radio engineers can be able to select the localization methods whose implementation in

the planning process is followed by potential performance winnings. Moreover, the predicted performance results will match better with the real ones helping thus to optimize efficiently the network design.

3. Performance analysis of moving small cells in cellular networks under the presence of mass events:

   In the third line of contribution, the performances of moving small cells are evaluated in the presence of a stationary but temporary traffic hotspot (reflecting a mass event such as a street show). Deploying classic small cells is not efficient enough if they are installed for occasionally occurring traffic hotspots. So, we evaluate the possible capacity and quality of service gains that can be obtained when the hotspot is static or is following a different trajectory compared to the small cell one. The major outcome is to understand if moving cells leverage relative operators investments or must be revised and enriched mainly in terms of mobility control to reach higher efficiency.

   Deploying moving cells is a topic already investigated in literature but with considering in general, uniform traffic distribution. Moreover, to the best of our knowledge, the previous studies were based on observed simulation results and no mathematical expressions are derived from the initial definitions of the evaluated performance metrics.

4. Development and performance analysis of a new mechanism for congestion mitigation in cellular networks using drone small cells:

   In the fourth line of contribution, we propose a new mechanism for congestion mitigation in cellular networks using drones. Based on a traffic hotspot localization tool, the drone can be activated and placed in areas of capacity bottlenecks until regaining a normal situation without congestion. A drone cell is supposed to replace the deployment of many classic small cells inside the coverage area of each macrocell. So, significant savings can be generated because less equipments are required, they are not active all the time and no air conditioning is needed. The advantages and the limitations of the proposed mechanism are discussed. A performance analysis and comparison with classic small cell deployments is carried out in order to show the importance of deploying drones in cellular networks.

1.4 Thesis outline

The structure of the thesis is as follows:

- In Chapter 2, an extensive state of the art on traffic hotspot localization in mobile networks is provided. This is followed by a review of the different studies made on HetNet deployments in 4G and 5G networks including moving small cells and drone small cells.
- Chapter 3 starts with a description of a new proposed traffic localization method. This is followed by details on the used inputs, the steps to be executed and how the localization can be much more accurate. The performances of the proposed method are investigated and are further compared to those of other methods based on probing.
- Chapter 4 presents a static and dynamic level analysis for small cell deployment under perfect and imperfect traffic hotspot localization. Performance expressions are derived and numerically evaluated for three scenarios of deployments: i. with macrocells only, ii. with a perfectly deployed small cell and iii. with an imperfectly deployed small cell.
- Chapter 5 is devoted to investigating the performance of moving small cells deployment under the presence of traffic hotspots in cellular networks. The performances of the moving small cell scenario is compared to those of a network composed of macrocells only.
- Chapter 6 proposes a new mechanism for congestion mitigation in cellular networks using drone small cells. Performance analysis of the proposed solution and a comparison to other classic small cell solutions is also provided.
- Chapter 7 summarizes and concludes the work outlining the challenges and limitations while providing directions for potential future work.

Chapter 2

Related works and state of the art

In this chapter, we review the contributions of related works and the state-of-the-art on the subject of traffic localization in cellular networks and performance analysis of HetNet deployments. This chapter includes also a bibliographic overview about moving cells and drones deployments and their respective efficiencies in offloading congesting traffic in cellular wireless networks.

2.1 Traffic hotspot localization in cellular networks

With the exponential growth of data traffic in modern mobile networks and the emergence of a wide variety of connected devices, tracking mass events and localizing traffic hotspots have become one of the major concerns in the operators roadmaps for several planning and design processes such as deploying small cells or optimizing the tilt[1] or the azimuth[2] of antennas. Indeed, radio engineering tasks must be based on a precise and valid performance evaluation of any network configuration which emphasizes the need of having accurate spatial traffic localization. Besides, the trend of tracking traffic peaks is also driven by dominant themes for wireless evolution towards 5G networks [3] such as the problem of hotspot offloading solutions, the emergence of HetNets [4, 5] with small cells' deployment and the development of Green Networks' concept [6].

Several traffic modeling and tracking techniques have been proposed in the literature [7–19]. For traffic modeling, a temporal analysis of the traffic distribution has been carried out in [7] based on the downloaded volume in all the Base Stations (BSs) of a

[1]The tilt represents the inclination or angle of the antenna to its horizontal axis.

[2]The azimuth is the angle between the direction of maximum antenna radiation with respect to the geographical North.

3G network. In [8], a spatio-temporal study has been conducted in order to analyze the stationarity of traffic hotspots. Moreover, the spatial traffic distribution has been well investigated in [9] for 4G HetNets through the analysis of traffic statistics. A parameterized statistical model is proposed to characterize the correlation between user and BS locations. In [10], authors proposed to extract the data volume downloaded of each cell and then these measurements are distributed over the Voronoi cells constructed through the BSs' locations because of the complexity of projecting this measure on the real coverage map (not following the Voronoi model). Results of [10] showed that the traffic is log-normally distributed over the entire studied coverage area and Weibull distributed across the cells. Obviously, the obtained results are very interesting relatively to the ease of generating traffic maps mainly used for network performance prediction. Nevertheless, the accuracy of the analysis is inappropriate for most of the radio environments especially in urban zones (where shadowing effect significantly impacts the Voronoi geometry) and also in rural zones (where BSs are deployed more sparsely). And so, the relative precision is low. In reference [11], the analysis is much more improved since authors proposed to use a spatial discretization technique which allows to enhance the granularity of the traffic map.

For operational hotspot localization techniques, they are mostly based on probing supporting trace analysis and protocol decoding [12–14]. The most important information extracted from traces is the received power level and the timing advance, defined respectively as the duration between the BS transmission and the first signal received from the UE. Authors in [12] provided a test transmitter playing the role of a neighboring cell at first and then the role of a serving BS. Tests are realized within the existing cells in the network in order to assess the traffic density within the vicinity of the transmitting equipment. This solution requires to configure the test transmitter and realize measurements in each subarea separately. So, it may take a long time to assess the traffic distribution in the entire area covered by a BS. In the same context, patent [13] disclosed a method where UEs send periodically their radio measurements related to signals received from both the serving cell and the neighboring cells. A recording unit is installed at the interface between the BS and the studied Base Station Controller (BSC), termed A-bis, to examine the messages exchanged on this interface. Then, based on these measurements, the traffic distribution is derived. It was shown that the obtained precision does not fit with the small cell dimensions. Another method was presented in patent [14] and proposed to localize traffic hotspots in GSM networks using statistical analysis of timing advance and neighboring cell measurements extracted from call traces. Authors in [15] proposed to exploit the predictability of

human mobility patterns in localizing performance measurements in UMTS networks. They used a snapshot of network signaling events at the Radio Network Controller (RNC) to accurately assign performance measurements to fine-grained geographic regions with the execution of clustering algorithms. Results in [15] show that the accuracy of localization is improved compared to other methods elaborated in the literature. Nevertheless, since the traffic localization is mainly extracted from handover reports, the precision of localization is still not sufficient enough especially when most of the traffic is located in the cell center. Proximity location is another method of localization based on the detection of close Wi-Fi Access Points (Wi-Fi APs). This helps to calculate the position of the UE knowing the location of the AP [18, 19]. RF-Fingerprinting [16, 19], cell-ID (LTE Rel 8) and Assisted-Global Positioning System (A-GPS) (LTE Rel 9) [19] are also well-known techniques for locating individual UEs with different accuracy levels.

Despite its wide use in the industrial field, probing-based methods suffer from some shortcomings. First, not all the traces are captured by probes, some of them are lost. Second, they require high capacity storage servers that cannot be provided by the existing O&M databases. Third, using call traces, the position of each UE is calculated separately leading to a heavy tracking process. Eventually, the tools needed for probing, storing traces and processing them are expensive and do not improve sufficiently the localization accuracy.

Another family of localization methods makes use of Key Performance Indicators (KPIs) in order to infer the level of traffic in each area of the cell. In [17], authors proposed to divide each cell of the network into several subareas, and to calculate a traffic value for each subarea from O&M measurements in the network. The indicators used to compute traffic values are the load of the cell, the call attempts and the number of handovers. This method is very simple and does not require additional tests or equipments. However, it is not efficient enough because of its important computational cost. Moreover, for high data rate networks, such as LTE-A networks and beyond, it only localizes traffic hotspots in terms of number of UEs and not in terms of data volume.

In order to improve the method used in [17] with increased accuracy and fast computations, we propose, in Chapter 3, a new method for tracking peaks of traffic generated by permanent activity such as in industrial areas or temporary activity related to mass events. This method consists in the exploitation of 5 KPIs directly extracted from the O&M database in each cell of the network and projected over the coverage map. These performance metrics are: Timing Advance (TA), Angle of

Arrival (AoA), neighboring cell level, cell load and two mean throughputs: arithmetic (AMT) and harmonic (HMT). Chapter 3 gives a definition of each of these KPIs and a detailed description of the new proposed localization method in addition to its performance evaluation. All the provided description and results are published in our papers referenced by [20, 21].

2.2 Small cell deployment under perfect and imperfect traffic hotspot localization

Traffic hotspot localization is always accompanied with errors resulting in imperfect traffic localization. Therefore, it is important to evaluate the impact of this limited accuracy on the performance of the network especially when this information is included in the deployment of a solution allowing to offload this congesting traffic. In particular, performance analysis of small cell deployment under the presence of traffic hotspots is a relevant issue to investigate and also to include in network planning process, as it allows to evaluate the efficiency of HetNet deployments. In fact, cellular operators are currently shifting towards HetNets as the most promising solution to meet user demands; by using a mix of Macro BSs and Small ones. Therefore, considering the impact of imperfect small cell positioning provides important results in terms of hotspot localization accuracy beyond which it is worthless to perform network optimization based on the information provided by the applied traffic localization technique. This study falls in the area of network densification representing thus a relevant subject in the performance analysis of wireless networks.

The efficiency of small cell deployment was the subject matter of many works using different network topology models which yield either optimistic or pessimistic results. An excellent survey on heterogeneous cellular networks is elaborated in reference [22]. In [23–25], authors considered a network with different tiers to evaluate performance metrics such as the coverage probability, the average achievable rate and the average load per tier. The network structure in each tier is based on a spatial Poisson Point Process (PPP). Using PPP model allows simple and tractable analytical expressions but it remains quite different from the real network layout, especially for macro tier which is close to the hexagonal grid with imperfections [26, 27]. Moreover, the deployment of small cells should be made based on the traffic distribution as well. Considering small cell distribution as a PPP model implies that the traffic hotspot - in case it is the reason for deploying small cells - follows also a PPP model with a constant traffic value in each hotspot which is not the case, as shown in [10, 11]. It is important to recall that

radio engineering tasks must be based on a precise and definite performance evaluation of any network configuration leading thus to the need to include more accurate data traffic profiles.

A different approach was used in [28] where the authors used a fluid model in order to study the impact of small cell location on the performance and QoS in HetNets. Non-uniform spatial traffic distribution and user dynamics were however not considered in the analysis. In general, it is recommended to perform analysis in a hexagonal network layout because of the fact that radio engineers start the design of the network based on a hexagonal model. The deviation of the real network structure from the hexagonal model is basically linked to the constraints imposed by engineering rules, field imperfections and government charters. Then, according to these deviations, some interfering sites will be closer to the UE resulting in high received interference and some of the other sites will be farther from the UE resulting in less received interference. In sum, the total experienced interference in any position of the network will be approximately the same as the interference calculated in a regular hexagonal network. More details are further discussed in [29] showing the importance of using hexagonal model and the limitations of PPP model.

Performance of cellular networks incorporating sophisticated queuing models have been well investigated in [30–35]. In the context of LTE-A HetNets, Ge et al. evaluated the efficiency of deploying femtocells with partially open channels in [33]. The blocking probability and the spectrum and energy efficiencies were derived based on a Markov chain model including important parameters used in planning and network design processes such as the number of femtocells, the average number of users and the number of open channels. In references [34, 35], Saker et al. studied a network of Processor Sharing (PS) queues to model the evolution of the system and how flows are served by either macrocells or small cells. Under the stability condition, capacity, energy consumption and outage rate in the network were evaluated. Authors showed that the densification of the network with small cells is globally a good solution to offload traffic and reduce the energy consumption. However, the spatial traffic distribution was assumed to be uniform all over the covered area and the studied scenario did not take into account the presence of traffic hotspots. Moreover, the small cell could be even deployed near the macro BS, contrary to what had been recommended in [28]. In fact, it was shown in [28, 36] that deploying small cells in already well-covered areas does not generate capacity gains and even degrades the performances of the network either in the presence of traffic hotspots or with a uniform spatial traffic distribution (this observation is also verified in the numerical results of Chapter 4).

The problem of the impact of bad traffic localization on small cell deployment is investigated in Chapter 4 with a static and dynamic level analysis. From a practical point of view, this study allows to evaluate the gain that can be generated from the deployment of small cells for its own sake and more specifically the performance of realistic and imperfect small cell positioning, due to errors generated by traffic hotspot localization tools. It allows also to identify the tolerated margins of errors in hotspot localization techniques exploited in operational tasks of HetNet design. Most of the analysis given in Chapter 4 is published in our articles [36, 37].

2.3 Moving small cells in 5G networks in the presence of mass events

Contrary to the deployment of classic HetNets, the idea of moving small cells is a fresh topic not exhaustively investigated in the literature. This new trend is motivated by the fact that static small cells cannot be flexibly placed to fulfill time/space-varying traffic. Mobility of small cells is the most advantageous feature allowing to efficiently offload moving and/or unpredictable congesting traffic leading thus to improve the network performance. Moreover, if the small cell is deployed on the top of public transportation means (a bus or a taxi for instance) circulating in very crowded streets, it will offload the traffic generated by its own passengers in addition to the one coming from UEs in its vicinity. Consequently, the data rate of each user in the coverage area of this moving cell will be improved since the Line-Of-Sight (LOS) signal is enhanced and the effect of slow fading is reduced. So, moving small cells are supposed to serve more users for longer periods of time maximizing thus the service time of the small cell without wasting the available radio and energy resources.

In [38], authors presented the benefits and the challenges of using moving relay nodes and applied a simulation approach in order to evaluate the capacity gains generated from deploying this technology. Reference [38] showed that the performance of vehicular users at cell edge are significantly improved with the new deployment concept. This is explained by the fact that moving relay nodes can provide better propagation conditions compared to the direct links to macro cells. Authors in [39] stated that deploying mobile cells is among the promising key 5G wireless technologies allowing to accommodate high-mobility users. In that regard, it has been shown in [40] that using mobile femtocells makes high-data-rate services easily accessible with reduced signaling overhead. In [41], a probabilistic approach is followed to allocate the radio resources in the network containing moving small cells. Moreover, authors of [41]

proposed to exploit the headway characteristics of city buses to study the interference relationship between different moving small cells. Numerical results showed that with moving cells, the usage rate of resource blocks is significantly reduced which boosts more the consideration of this new technology in real deployments. The signaling overhead for channel feedback is also investigated for a network of mobile small cells and authors in [42] proposed a user-centric downlink scheduling scheme. Results confirmed that the developed scheme is able to realize an appreciable increase in sum-rate and throughput and also an important decrease of the signaling overhead.

Some of the research communities are trying to boost the combination of moving cells' concept with other new developing solutions such as the use of millimeter Wave technology [43, 44] or the aggregation with Wi-Fi [45] or even with the implementation of Multiple Input Multiple Output (MIMO) systems in order to reduce interferences and improve coverage and capacity of the network.

Parallel to studies related to moving cells, a competing technology based on three dimensional beamforming [46] is under study. Nevertheless, this feature remains not very practical in real environments because of the complexity of the system and the heavy signaling overhead related to the channel state information allowing to focus the beam in a precise direction. So, from the vendors and operators point of view, moving cells is one of the upcoming solutions which is expected to upgrade the network performance.

Chapter 5 is dedicated to study a scenario where the small cell is moving according to Manhattan mobility model (it models a movement in city streets environment such as the classic bus trajectory using grid road topology) and we consider a stationary traffic hotspot. In such traffic scenario, it is clear that operators do not need moving small cells. Nevertheless, if this traffic hotspot is temporary, then deploying classic small cells would be costly and inefficient (even with the cell shutdown concept because not all the energy-consuming components in the BS are turned off in case of small load.) and it turns out credible to replace them by smaller number of moving small cells. Consequently, studying the scenario of moving small cells allows to evaluate the possible capacity and QoS gains in case the traffic hotspot is not moving or is following a different trajectory compared to the small cell one. The results allow operators to understand if this solution can leverage the relative investments or must be revised and enriched mainly in terms of mobility control to reach higher efficiency. The results of Chapter 5 are published in our article [47].

2.4 Offloading traffic hotspots using drones in 5G Networks

As indicated in the previous sections, the occurrence of mass events or the existence of areas of capacity bottlenecks have become among the important scenarios to be taken into consideration in operators' roadmaps to reach their objectives in terms of capacity, coverage and quality of service. To deal with this issue, several features are proposed in the literature to be implemented in real networks such as Device-To-Device (D2D) communications [48], HetNet deployments and mmWave technology [49]. Obviously, in the context of HetNet deployment, small cells do not represent an entirely new concept in cellular networks but enhancing this offloading solution with more efficient mechanisms is still a fresh topic to investigate. As a matter of fact, research and industrial communities continue to develop and evaluate new approaches allowing to realize the expansion of small cell-based technologies. Moreover, using drone cells have come to prominence very recently with the study of 5G scenarios related to mass events and the mobility of the traffic. Actually, using drones is still theoretic and not feasible since no efficient and energy-saving drone-based mechanism has been developed until today.

Small cell deployment is a concept well-investigated in the literature and different categories of small cells have been developed with sophisticated mechanisms [22, 39, 5, 50–53]. The main advantages of small cells are the coverage expansion and the capacity enhancement. Furthermore, previous studies cited many other advantages in deploying small cells. First, the cost of small cells is very low compared to macrocell equipments. The price is reduced because no heavy air-conditioning is needed with small cells, the transmitting power is low (harmless to human and less CO_2 emission) and the cost of the hardware is also reduced. Second, small cells allow to achieve more homogeneous user experience and more fair spread of the capacity between users. Third, it is clear that small cell technology is a solution to combat the shadowing, the penetration loss and even fast fading since the channel behaves more in a correlated manner when users are near the small cell. Fourth, since small cells are close to UEs, a green aspect of prolonged UE battery life can have also a positive impact to boost studies of this technology even if operators do not generate direct revenues from this advantage. Nevertheless, each reference between [22, 50–52] presents some limitations making its provided solution not very encouraging to deploy. Some of these reasons can be summarized in the lack of efficiency in terms of capacity improvement when the traffic is not static and also in the additional costs of the installation and of the

connection to the backhaul. In fact, deploying small cells might be an inappropriate solution if the area where they are installed does not generate high traffic anymore. Moreover, if the connexion to the backhaul is wireless, additional interferences will be experienced in the macrocell and if this connexion is wire-lined, the cost of the infrastructure will be increased. The different drawbacks of the existing studies on HetNet deployments, principally those related to mobility (time-variability of traffic), quality of service and network planning efficiency, have stressed the need to find new alternatives to these ideas.

In contrast with the deployment of classic small cells, the concept of using low altitude drone cells in cellular networks is still a fresh topic not actively discussed in research and industrial communities [54, 55] because until recently, they are trying to boost network performance with lower operational costs. It is true that costs of deploying drones are quite high, but recently, many advances have been realized to produce more efficient drones with good performance in terms of energy consumption and stability control. The question is to find a mechanism allowing drones to efficiently consume energy and react rapidly to congestion situations.

Performance of cellular networks is supposed to be improved with the deployment of drones. This can be explained by the fact that drone cells can provide better propagation conditions compared to the direct links to macrocells. They allow to reduce interferences, handover rates, service times and power used in downlink transmissions. Compared to classic small cells, the Line-Of-Sight from both sides (from the UE and the macrocell) is always guaranteed with drone cells and they are still operational in periods of natural disasters. Nevertheless, deploying drones in cellular networks is still not an encouraging solution and requires quite important operational expenditures in the way it is supposed to be exploited until recently. So, incorporating some improvements are absolutely essential to encourage the deployment of new mechanism based on drones.

In Chapter 6, we propose and evaluate the performance of a new mechanism for congestion mitigation in 5G networks using drone cells. Based on a traffic hotspot localization tool [20], the drone can be activated and placed in areas of capacity bottlenecks until regaining a normal situation without congestion. The proposed mechanism is not energy consuming since the drone will not fly when it starts to offload traffic. This advantage boosts more the feasibility of the drone-based solution from a green point of view. Moreover, the proposed mechanism allows to improve the network performance by providing better radio conditions with less interference, less handovers and better reactivity to congestion. A drone small cell is supposed to replace the deployment of many classic small cells inside the coverage area of each macrocell. So,

significant savings can be generated because less equipments are required, they are not active all the time and no air conditioning is needed. Chapter 6 is elaborated based on our published papers [56, 57].

Chapter 3

Traffic Hotspot tracking in LTE networks

One of the most important tasks that a telecommunication professional has is network planning and optimization especially with the new technologies proposed in 3GPP standards like HetNet deployments [4] and the features of Green Networks [6]. These tasks can be improved by providing additional informations about heavy loaded areas [14]. Besides, if we do not localize these areas of capacity bottlenecks properly - like choosing wrong areas - the worst consequences range from an overall bad system performance (compared to what it could be) to cases where we need more equipment to meet the same requirements in the studied area. In other words, it implies losses of CAPEX and OPEX and poor network quality.

In this chapter, we propose a new traffic hotspot localization technique allowing to improve the localization accuracy with low operational costs. A detailed description of the proposed process is given with several simulation results including imperfections in coverage prediction and mobile equipment capabilities in handling measurements.

3.1 Principle

The proposed algorithm of tracking traffic hotspots is depicted in Fig. 3.1. As stated earlier in Section 2.1, five KPIs define the first main inputs of the algorithm: TA, AoA, neighboring cell level, correlation between traffic loads and the difference between the mean throughputs AMT and HMT. Extracting information from these 5 KPIs and projecting them over the coverage map, as will be explained later in Section 3.3, allow to obtain the traffic level in each pixel of the coverage map.

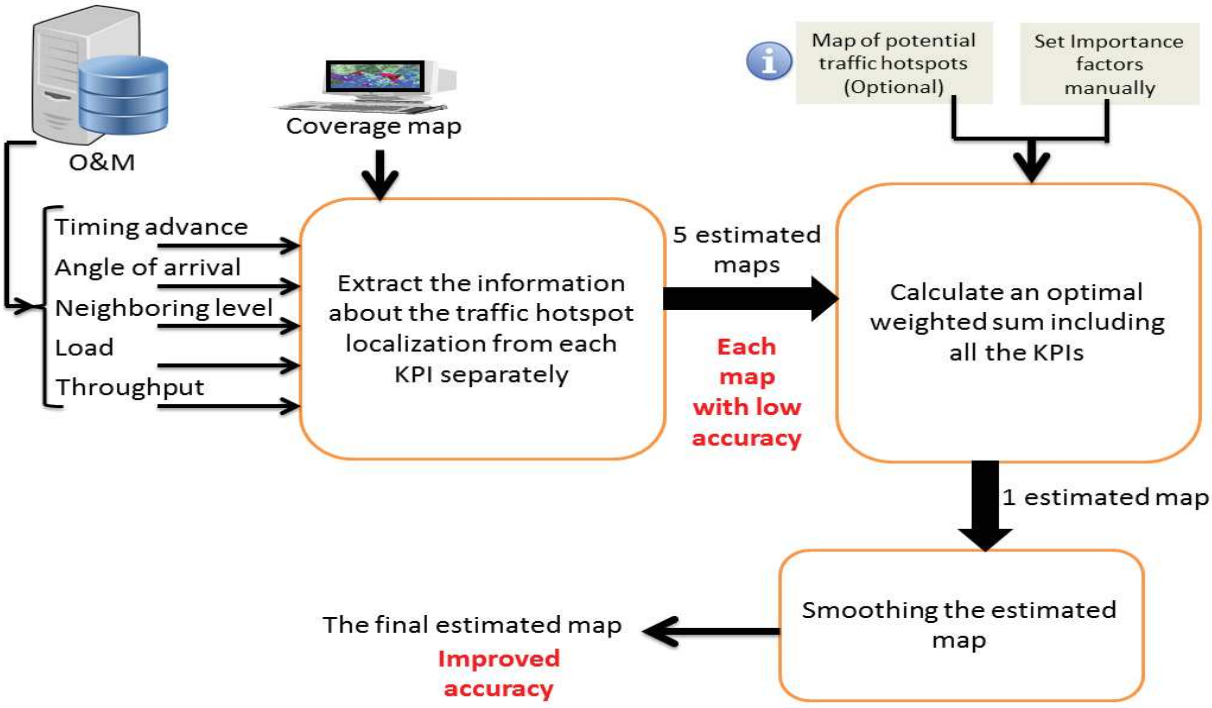

Fig. 3.1 General process of tracking traffic hotspots.

The 5 KPIs are properly chosen with respect to two important criteria: locating hotspots in terms of number of connected UEs and traffic volume. In fact, TA, AoA and neighboring cell level can be sufficient for deriving the spatial distribution of connected UEs. However, in practice, a hotspot is measured not only by the high density of connected UEs but also by the traffic volume. Actually, this latter does not follow exactly the same evolution as the number of connected UEs. Therefore, the traffic hotspot tracking is improved by adding directly data-volume related KPIs such as the correlation between the cells' traffic loads and the difference between the AMT and HMT.

The contribution of each KPI is measured and an importance factor is assigned to it in order to avoid the over-confidence in the localization of traffic hotspots due to the correlation between KPIs. Optimal importance factors are found by solving a least square problem minimizing the distance between subareas of the estimated map (based on the weighted sum of the obtained maps corresponding to each KPI) and the relative map of potential traffic hotspots if this latter is available. The map of potential hotspots represents additional and optional informations about potential hotspot areas obtained from commercial data (if this information is not available, it is

possible to set importance factors intuitively). Next, a global metric combining all the five KPIs and using the optimal importance factors is defined.

The localization of traffic hotspot areas can give significant weights to isolated areas, or pixels, as well as pixels in the edge of a hotspot. And so, smoothing the estimated map is an additional step proposed in this work, in order to make the estimated traffic distribution more accurate.

The implementation of the proposed solution does not require important investments and operational costs since it is based on inputs that are already available in the network. Hence, the only relative cost is the one of the execution of the proposed localization method which is reasonable compared to the cost of the recently used methods such as those based on probing.

Eventually, more KPIs such as the call block rate, the interference level or the Channel Quality Indicator (CQI) distribution are also analyzed and can give insights about the location of hotspots. Nevertheless, these KPIs, when combined with the proposed ones, do not improve the localization accuracy since they are highly correlated with them. For example, the call block rate and the cell traffic load practically carry the same information about the location of traffic which leads to an over-confidence in the estimation.

3.2 Traffic tracking inputs

3.2.1 Coverage map: Definition and notation

The coverage map is theoretically an abstraction of real-world radio scenarios. It is a fine-grained map of a bounded geographical area where environmental information and prior knowledge for cognitive radios are given in each pixel of the network map. The length of each pixel is called the resolution of the coverage map (often from 5 to 50 meters in practice). This map is often taken from coverage prediction tools or from real measurements such as coverage provided by the Minimization of Drive Tests (MDT) techniques [58] and it can be exploited in network planning processes and for decision support. The information extracted from coverage maps cover geographical features, radio aspects, available services, spectral regulations, activity profile of radio devices and past experiences.

In this work, the coverage map is denoted by $\mathcal{L}$ and constitutes a bounded part of $\mathbb{R}^2$. Without loss of generality, we assume that $\mathcal{L}$ has the form of a square and is discretized into equally m^2 pixels.

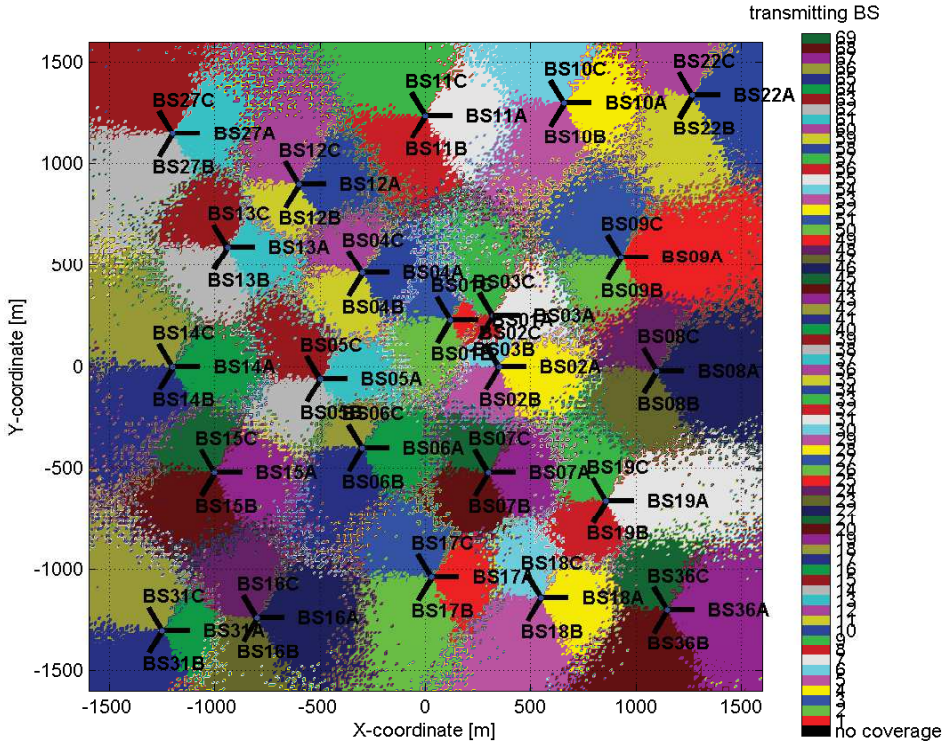

Fig. 3.2 Best server map in the covered area.

For $1 \leq i, j \leq m$, we designate by $P_{i,j}$ the coordinates of each pixel in $\mathcal{L}$ and we assume that the pixel $P_{1,1}$ is located at the lower left corner of the map.

We denote by $\mathcal{C} = \{C_1, C_2, ..., C_n\}$ the set of the cells located in the coverage map $\mathcal{L}$, where C_k is the geographical area covered by cell k and n is the number of cells. It is clear that $\mathcal{C} \subseteq \mathcal{L}$ because some pixels may be not covered by any cell.

Let $RSRP_{k,i,j}$ be the Reference Signal Received Power (its equivalent in UMTS is $RSCP$ and in GSM is $Rxlev$) [59] from cell k in pixel $P_{i,j}$, then the cell coverage C_k is given, for $1 \leq k \leq n$, by

$$C_k = \{P_{i,j} \in \mathcal{L} \text{ such that } RSRP_{k,i,j} = \max_{1 \leq l \leq n} RSRP_{l,i,j}\} \tag{3.1}$$

For every pixel $P_{i,j}$ in $\mathcal{L}$, we denote by $c^*_{i,j}$ and $\hat{c}_{i,j}$ respectively the index of the first and second best serving cells.

$$c^*_{i,j} = arg \max_{1 \leq l \leq n} RSRP_{l,i,j} \tag{3.2}$$

$$\hat{c}_{i,j} = arg \max_{\substack{1 \leq l \leq n \\ l \neq c^*_{i,j}}} RSRP_{l,i,j} \tag{3.3}$$

Fig. 3.2 illustrates an example of the coverage map with the best serving cell in each pixel. Colors illustrate the area covered by each sector in the network. Each site has an identifier (BS01, BS02..) and sector's identifier in each site is either A, B or C since we are working in a tri-sectorized network.

Note that in practice even if each pixel has a best serving cell, a UE located indeed in this pixel is accepted in the network only if the signal level received from its serving cell is higher than a certain threshold, called $Q_{rxlevmin}$ in 3GPP LTE standard.

3.2.2 Definition of the extracted performance metrics (KPIs)

Traffic measurements or performance metrics (called also KPIs, the short of key performance indicators) are expressed by sum or average values in a granularity period and include all aspects related to paging, network access, congestion and handover. They are collected from network entities called O&M centers or from drivetests and they provide data characterizing the behavior of the system in addition to call traces intercepted by probes. KPIs are reliable information that can be incorporated in operational tasks such as network planning, network monitoring, and network maintenance.

We now detail the 5 KPIs we use in our work.

Timing Advance

Timing Advance (TA) (in GSM, LTE and LTE-A) or propagation delay (in UMTS) is a time offset realized by the BS between its own transmission and the transmission received from the UE. According to the calculated offset, the serving BS determines the suitable TA [60] for the UE. Then, from this TA, the BS calculates the distance traveled by the radio signal. Depending on the resolution (or granularity) of TA, a specific distance range where the UE is located will be calculated.

In practice, TA is used as a KPI for network supervision and analysis, with a granularity of 78.25 meters in LTE networks [60]. Based on this granularity, TA is discretized into 6 intervals indexed by t of the form $[78.25 \times t,\ 78.25 \times (t+1)]$, with $0 \leq t \leq 4$, and $[391.25,\ +\infty)$ for $t = 5$.

As illustrated in Fig. 3.3, each cell is divided into several intervals according to the defined ranges of distances. The TA KPI that we obtain from the O&M database is the distribution of the distance from the BS to the UEs in the cell. For example, 30% of the UEs are in the range of $t = 0$, 20% in the range of $t = 1$, 40% in the range of $t = 2$, 10% in the range of $t = 3$ and 0% in the range of $t = 4$ and $t = 5$.

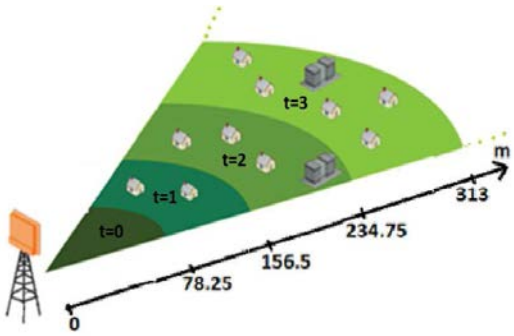

Fig. 3.3 The division of the covered area based on TA.

For each cell k, we denote by $\tau_t(k)$ the value of the TA KPI that gives the percentage of UE in the TA interval t.

Angle of Arrival

Angle of Arrival (AoA) is defined as the estimated angle of a UE with respect to a reference direction, typically the geographical North. The value of AoA is positive in an anticlockwise direction [61]. In general, any uplink signal from the UE can be used to estimate the AoA, but typically a known signal such as the Sounding Reference Signals[1] (SRS) or DeModulation Reference Signals[2] (DMRS) would be used [62]. The serving BS determines the direction of arrival by measuring the timing advance at individual elements of the antenna array. Consequently, the AoA is predicted from these delays.

In order to construct the shape of the downlink beam, direction of arrival estimation already exists and is supported in UMTS but it is not standardized [63]. Experiments in [64–66] showed that the accuracy of AoA estimation depends mainly on the number of antenna elements and also on the separation distance between them. It varies from small deviations (around 2° to 5°) to significant deviations (about $30° = \frac{\pi}{6}$) [64–66].

Based on the possible AoA deviations provided in [64–66], we assume that the cell is divided into 3 areas, as depicted in Fig. 3.4, relative to the angle between the UE, the BS and the geographical North. Likewise the TA, we denote by $t = -1, 0$ or 1 the index of each AoA area.

For each cell k, we denote by $\phi_t(k)$ the value of the AoA KPI that gives the percentage of UE in the AoA area t. Therefore, the percentage of UEs connected to

[1]The Sounding Reference Signal is a reference signal transmitted by the UE in the uplink direction which is used by the BS to estimate the uplink channel quality over a wider bandwidth.

[2]DeModulation Reference Signals are used to enable coherent signal demodulation at the eNodeB.

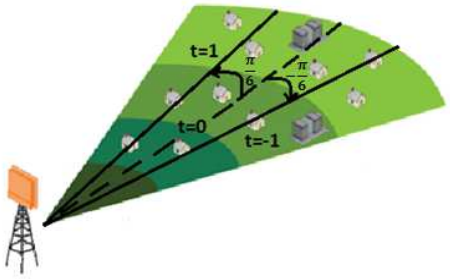

Fig. 3.4 The division of the covered area based on AoA.

cell k and which are in the range of $[-\frac{\pi}{6}, \frac{\pi}{6}]$ is denoted by $\phi_0(k)$. $\phi_1(k)$ represents the percentage of UEs connected to cell k and which are with an angle of arrival higher than $\frac{\pi}{6}$. $\phi_{-1}(k)$ represents the percentage of UEs connected to cell k and that are with an angle of arrival smaller than $-\frac{\pi}{6}$. In this sectorization, we consider that the angle of arrival is equal to zero when pixel $P_{i,j}$ has the same angle as the azimuth of its serving sector.

Neighboring cell level

In different events of UEs connection to the network such as handover process, every UE measures the signals of the detected cells and sends a report of these measurements to its serving cell. In GSM, the detected neighboring cells list is reported periodically by the UE to the BS. However, in 3G and 4G networks, it is reported to the BS only when a special event is triggered. The counter in the O&M database representing the neighboring cell level of a given neighboring cell is incremented whenever that cell is received (in a measurement report) as an eligible candidate cell for handover (Fig. 3.5). In order to get the KPI as a distribution, the neighboring cell level of each neighboring cell is calculated with respect to the total number of reported neighboring cells.

For each neighboring cell l of the serving cell k, we denote by $\vartheta_l(k)$ the relative number of times where cell l is reported as eligible candidate cell for handover in a measurement report to the serving cell k.

Normalizing with the total number of reported neighboring cells makes $\vartheta_l(k)$ a density distribution KPI, i.e.,

$$\sum_{l \in S_k} \vartheta_l(k) = 1 \tag{3.4}$$

where S_k is the set of the neighboring cells to cell k.

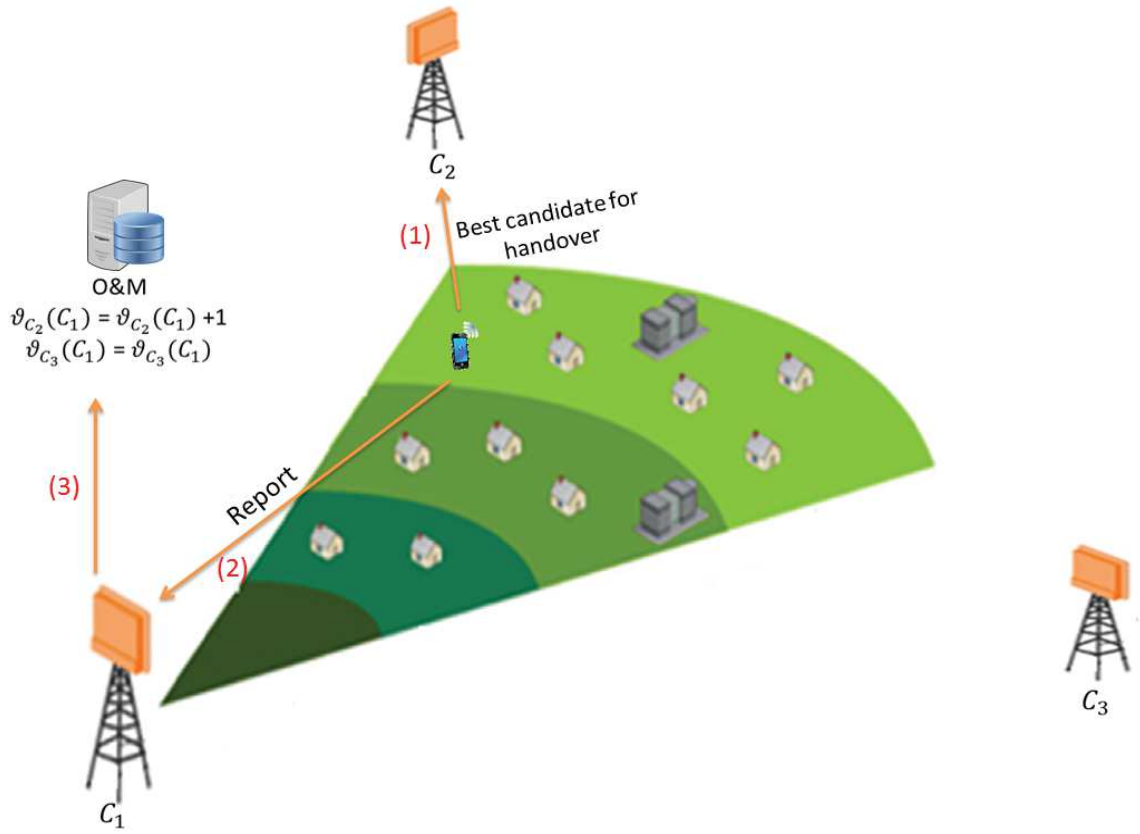

Fig. 3.5 Updating the neighboring cell level KPI.

Cell load

For each cell, the load is defined as the amount of occupied resources with respect to the available ones in the cell during an observation period. The load value grows with the cell's traffic demand and the co-channel interference received from neighboring cells. Intuitively, low load means that the network has sufficient capacity to meet the demand and most of its radio resources are not occupied, whilst high load indicates poor performance in terms of potential service outage. In the latter case, the network design and the parameters' settings should be revised and adapted to the real conditions in the covered area in order to reduce the congestion in the studied cell.

This KPI is already defined and provided by all O&M vendors. It is calculated per hour and can be given for the busy hours, for the day, the week or the month. We denote by $\rho(k)$ the load of cell k.

Arithmetic and Harmonic Mean throughputs

The Arithmetic Mean Throughput (AMT) is the classic mean of the throughputs of all connected UEs. On the other side, the Harmonic Mean Throughput (HMT) is the inverse of the average of the reciprocals of the throughputs[3]. The HMT differs from the AMT by the fact that it gives more importance to throughputs of UEs in bad radio conditions so that the HMT is more influenced by the throughput of cell edge UEs. Based on the formula of the cell throughput defined in the O&M database by most equipment vendors, it is important to notice that the cell throughput has almost the same value as the HMT.

The utility of these KPIs comes from the following possible scenarios: if most of the users are at cell edge, the HMT becomes more significant and the AMT is decreased and gets close to the HMT. However, if most of the users are in good radio conditions, the difference between the HMT and the AMT becomes significant. So, the location of the traffic in the cell can be deduced from the difference between the AMT and HMT.

To better understand this idea, we consider the following example. First, we divide UEs into two clusters depending on the throughput of each one and we calculate the ratio and the difference between HMT and AMT. Then, in numerical results, we notice that the behavior of the difference between HMT and AMT changes according to the proportion of UEs in each cluster as shown in Fig. 3.6a. However, in Fig. 3.6b, the ratio between HMT and AMT is almost symmetric giving only an idea about the uniformity of the UEs' spatial distribution.

In Fig. 3.6a, we show that when most of the UEs are in the center of the cell, the difference between AMT and HMT is very important and this is due to the fact that the AMT is high and the HMT is low. However, in the opposite case, the AMT is very low and the HMT is decreased a little but remains near the AMT. In summary, we conclude that exploiting the difference between the AMT and HMT brings additional information about the traffic distribution in the network and it is more informative than the ratio between these two metrics.

Note that this proposition is true only under certain conditions; in the case where there is a high proportion of UEs in the center or in the edge, the AMT is practically equal to the HMT. In reality and with statistics provided by a tool of network supervision, we were able to extract the Channel Quality Indicator (CQI) distribution and we found that it is divided in a percentage of 85% of UEs in the center (with good $CQI > 9$) and 15% in the edge (with bad $CQI < 9$)(see Fig. 3.7). So, the real

[3]HMT is always lower than AMT according to the mathematical definition of the harmonic mean and the arithmetic mean.

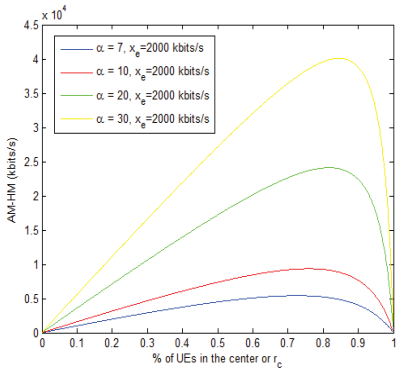

(a) The difference between AMT and HMT.

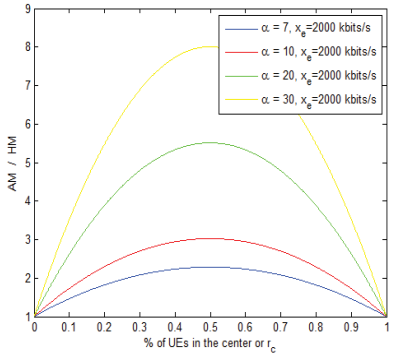

(b) The ratio between AMT and HMT.

Fig. 3.6 AMT vs HMT for 2 clusters of mobile users (r_c is the ratio of UEs close to the serving cell, x_e is the AMT for UEs in the edge of the cell, α is the number of times the throughput for UEs close to the serving cell is higher compared to the UEs at cell edge).

scenarios can exploit the information extracted from the difference of arithmetic and harmonic throughputs.

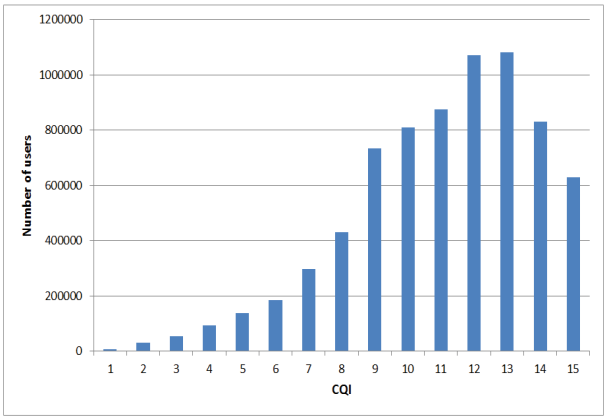

Fig. 3.7 Example of field CQI distribution.

Fig. 3.7 represents an example of field CQI distribution in the week six of the year 2014 taken in the cell E1 of Agency Orange Bastille. This measurement reflects the signal to noise plus interference ratio reported by the UE to its serving BS. In reality, the scheduled UEs are in most of the cases located in the cell center as observed in Fig. 3.7, because during the planning process, radio engineers always work on ensuring good coverage and capacity, especially in very crowded areas. Consequently, most of the users will experience acceptable radio conditions in most of the covered area.

For each cell k, we denote by $\mu_a(k)$ and $\mu_h(k)$, respectively, the AMT and the HMT KPIs taken from O&M database.

3.2.3 Map of potential traffic hotspots

A map of potential traffic hotspots is an additional layer obtained from commercial data so as to improve the hotspot localization. In this case, the spatial traffic distribution is calculated taking into consideration the apriori knowledge of the location of industrial and commercial areas or the location of residences. This map includes also information about the location of rivers, forests, etc. Mass events such as a protest march or a concert can be further a useful information than can be projected in the map of potential hotspots. Such a map can be a reference map to define the contribution of each KPI in the estimation of the spatial traffic distribution as described in Subsection 3.3.2.

We define $\hat{Q} = (\hat{q}_{i,j})_{1 \leq i,j \leq m}$ as the matrix representing the potential hotspots.

$$\hat{q}_{i,j} = \begin{cases} \omega_{i,j} & \text{if } P_{i,j} \text{ is in a potential hotspot} \\ 0 & \text{otherwise} \end{cases} \tag{3.5}$$

where $\omega_{i,j}$ represents the importance of the potential hotspot. In fact, the weight assigned to each hotspot is evaluated according to the heaviness of the traffic that can be carried inside it. For example, a residence cannot take the same weight as a commercial area.

3.3 Hotspot Tracking Algorithm: Design and Optimization

3.3.1 Description of the algorithm

Before running the localization algorithm, the O&M reports the statistics of each KPI corresponding to the cells in its controlled area. Then, the following steps are executed.

Step 1: calculate the map of traffic weights according to TA

Based on TA KPI, we attribute to each pixel $P_{i,j}$ a traffic weight $q^{(1)}_{i,j}$. To do this, each cell in the coverage map is divided into 6 areas depending on the distance from the BS

as illustrated in Fig. 3.3. Then, each pixel takes a weight equal to the percentage of UEs in its range of TA.

$$q_{i,j}^{(1)} = \sum_{t=0}^{5} \tau_t(c_{i,j}^*) \times \chi_{1,t}(P_{i,j}) \tag{3.6}$$

where $\chi_{1,t}(P_{i,j})$ is the indicator function of TA area t in serving cell $c_{i,j}^*$ and $\chi_{1,t}(P_{i,j})$ takes the value 1 if the pixel belongs to TA area t of its serving cell $c_{i,j}^*$ and 0 otherwise.

Step 2: calculate the map of traffic weights according to AoA

In this step, each cell in the coverage map is divided into 3 areas as illustrated in Fig. 3.4. So, each pixel in the same range of AoA takes a traffic weight $q_{i,j}^{(2)}$ equal to the percentage of connected UEs in this range of AoA.

$$q_{i,j}^{(2)} = \sum_{t=-1}^{1} \phi_t(c_{i,j}^*) \times \chi_{2,t}(P_{i,j}) \tag{3.7}$$

where $\phi_t(c_{i,j}^*)$ is the value of the AoA KPI that gives the percentage of UEs in the AoA area t of the cell $c_{i,j}^*$, $\chi_{2,t}(P_{i,j})$ is the indicator function of AoA area t in cell $c_{i,j}^*$ and $\chi_{2,t}(P_{i,j})$ is given by

$$\chi_{2,t}(P_{i,j}) = \begin{cases} 1 & \text{if } Angle(P_{i,j}, c_{i,j}^*) - \theta(c_{i,j}^*) \in I_t \\ 0 & \text{otherwise} \end{cases} \tag{3.8}$$

with

$$I_t = \begin{cases} [-\frac{\pi}{6},\ \frac{\pi}{6}] & \text{if t=0} \\ [\frac{\pi}{6},\ \pi] & \text{if t=1} \\ [-\pi,\ -\frac{\pi}{6}] & \text{if t=-1} \end{cases} \tag{3.9}$$

$Angle(P_{i,j}, c_{i,j}^*))$ is the angle between pixel $P_{i,j}$ and its serving cell $c_{i,j}^*$ with respect to the geographical North of the coverage map. $\theta(c_{i,j}^*)$ is the azimuth of the antenna covering the cell $c_{i,j}^*$.

Step 3: calculate the map of traffic weights according to the neighboring cell level

Exploiting the neighboring cell level is motivated by the fact that when a neighboring cell is reported many times rather than others, the pixels having this cell as the second best serving cell contain probably most of the traffic.

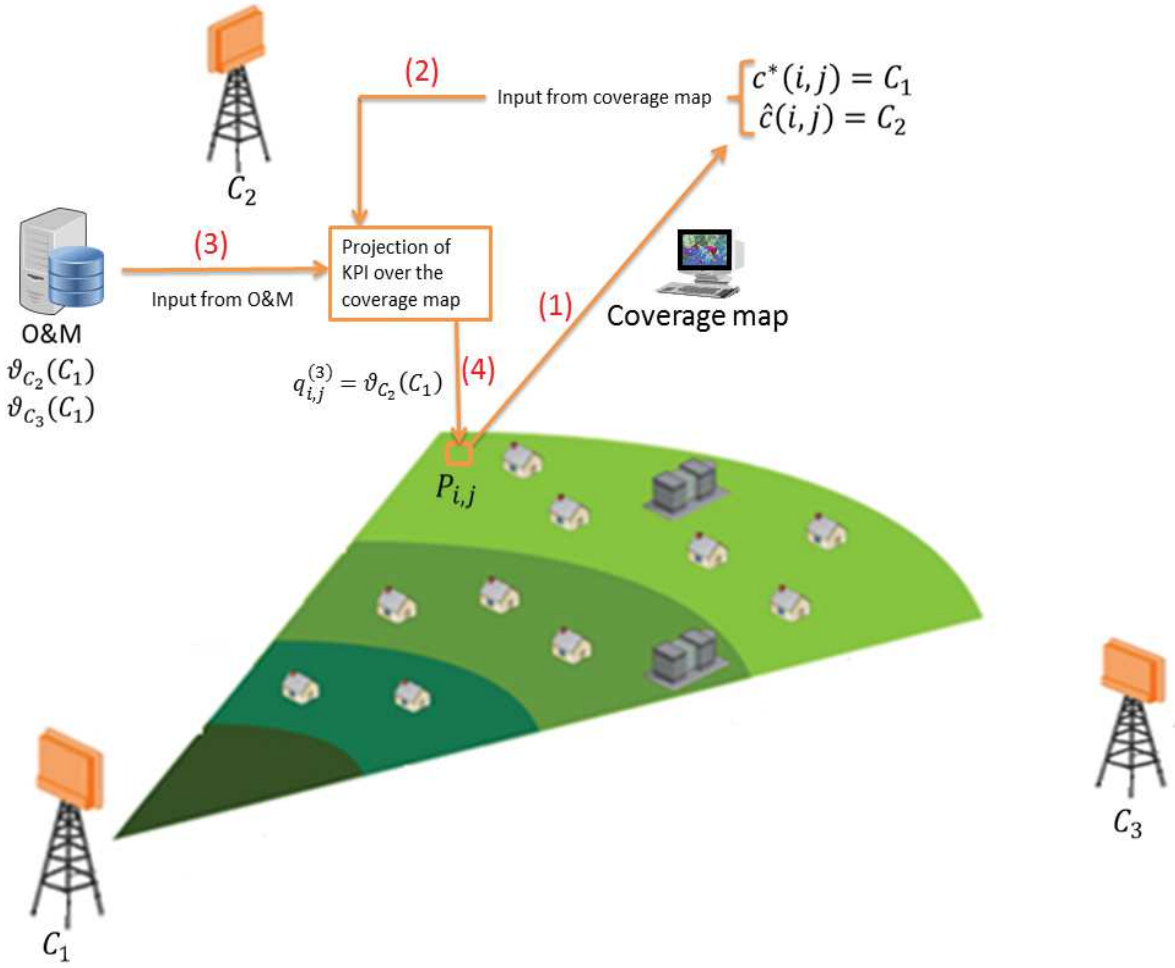

Fig. 3.8 Traffic weights attribution with Neighboring cell level.

We attribute to each pixel a traffic weight $q_{i,j}^{(3)}$ equal to the value of the neighboring cell level of its second best serving cell, as shown in Fig. 3.8.

$$q_{i,j}^{(3)} = \vartheta_{\hat{c}_{i,j}}(c_{i,j}^*) \tag{3.10}$$

Step 4: calculate the map of traffic weights according to cell loads

In hotspot areas, the traffic evolution has almost the same behavior in the neighboring cells due to the load balancing [67, 68] and also the users' mobility. As a consequence, if a cell is congested and one of its neighbors is congested too, it is likely that most of the traffic is located in the edge between the two cells and if there is no correlation with any of the neighboring cells, then traffic is most probably generated from users close to the serving cell. Furthermore, if two cells are congested but the heavy traffic is not located between them, the attributed traffic weight in the region between these two cells will be significant. The next step provides corrections to this step since it allows to identify if the traffic hotspot is at the cell edge or not.

We denote by $\psi_{c^*_{i,j}}$ the set of neighboring cells having the same behavior in terms of load as the serving cell $c^*_{i,j}$ and are eligible for RSRP-based handover in $P_{i,j}$. It is given by

$$\psi_{c^*_{i,j}} = \{k \in \mathcal{C} \text{ such that } |\rho(c^*_{i,j}) - \rho(k)| < \epsilon \text{ and } |RSRP_{c^*_{i,j},i,j} - RSRP_{k,i,j}| < \gamma\} \quad (3.11)$$

where γ is a parameter used to identify the set of candidate cells for a possible handover (by default, it is equal to the handover margin) and ϵ is used in order to get only the cells having the same behavior as the serving cell (ϵ is set to 0.1 in the localization exercise shown, next, in the simulation results).

The traffic weight $q^{(4)}_{i,j}$ attributed to each pixel based on the load KPI is then given as follows

$$q^{(4)}_{i,j} = \begin{cases} \frac{1}{n(\psi_{c^*_{i,j}})} \sum\limits_{k \in \psi_{c^*_{i,j}}} \rho(k) & \text{if } \rho(c^*_{i,j}) > \tilde{\rho} \\ 0 & \text{otherwise} \end{cases} \quad (3.12)$$

where $n(\psi)$ is the number of elements in the set ψ and $\tilde{\rho}$ is a threshold used to identify the very loaded serving cells (in practice the congestion threshold is set to 70%). Thus, only pixels belonging to congested cells get traffic weights according to this KPI.

Step 5: calculate the map of traffic weights according to AMT versus HMT

According to this step, the attributed traffic weights are the difference between the AMT of the cell and the HMT divided by a constant μ_0 in order to have all the calculated weights in the range [0, 1]. The constant μ_0 is the maximum achievable throughput. The weight in each pixel depends on its position relative to the position

of its best serving cell and also on the value of the difference between the two mean throughputs. So, the weights for pixels in the cell center take the value of the difference between the HMT and the AMT divided by μ_0. The rest of the pixels in the cell takes a traffic weight as given in equation (3.13).

The traffic weight $q_{i,j}^{(5)}$ attributed to each pixel is then formulated as follows:

$$q_{i,j}^{(5)} = \begin{cases} \frac{\mu_a(c_{i,j}^*) - \mu_h(c_{i,j}^*)}{\mu_0} & \text{if } RSRP_{c_{i,j}^*,i,j} > RSRP_0 \\ 1 - \frac{\mu_a(c_{i,j}^*) - \mu_h(c_{i,j}^*)}{\mu_0} & \text{if } RSRP_{c_{i,j}^*,i,j} < RSRP_0 \end{cases} \tag{3.13}$$

where $RSRP_0$ is a RSRP threshold used to differentiate between the cell edge versus cell center UEs.

Step 6: combine all KPIs in a global metric and estimate peaks of traffic in the coverage area

After analyzing all the KPIs and extracting information about hotspots from them, this step defines the way to transpose all the outputs from the previous steps into a unique map of traffic weights $Q = (q_{i,j})_{1 \leq i,j \leq m}$. The simplest way to get the matrix Q is by making a weighted sum of the matrices $Q^{(s)} = (q_{i,j}^{(s)})_{1 \leq i,j \leq m}$, $1 \leq s \leq 5$, with an importance factor $\mathbf{x} = (x_1, x_2, x_3, x_4, x_5)^T$ depending on the quantity of information extracted from each KPI. So, we have that

$$Q = \sum_{s=1}^{5} x_s Q^{(s)} \tag{3.14}$$

The trivial value of $\mathbf{x}$ is $(\frac{1}{5}, \frac{1}{5}, \frac{1}{5}, \frac{1}{5}, \frac{1}{5})^T$. In this case, $\mathbf{x}$ is not optimal because some KPIs provide more precision than others and some KPIs are correlated, as stated earlier. For these reasons, we define the optimal value of $\mathbf{x}$ as the result of an optimization problem which reduces the distance between the map of potential hotspots and the matrix Q. This optimization is detailed in subsection 3.3.2.

Step 7: smoothing of the estimated spatial distribution of the traffic

The estimated spatial traffic distribution is further enhanced with a smoothing step which consists in combining the values estimated in each pixel with the values estimated in the neighboring pixels. The main advantage of smoothing [69] is to delete isolated pixels with significant weights (wrong estimated hotspots). On the other hand, this

step allows to ensure more the existing hotspots in the network once they are not eliminated.

It was shown in [10] that the spatial traffic distribution is very heterogeneous. Therefore, we choose the function of the smoother to be as follows

$$q^*_{i,j} = \frac{\sum_{P_{i',j'} \in \mathcal{L}} G(P_{i,j}, P_{i',j'}) q_{i',j'}}{\sum_{P_{i',j'} \in \mathcal{L}} G(P_{i,j}, P_{i',j'})} \tag{3.15}$$

where

$$G(P_{i,j}, P_{i',j'}) = \frac{1}{2\pi h} e^{-\frac{|P_{i,j} - P_{i',j'}|^2}{2h}} \tag{3.16}$$

with $|P_{i,j} - P_{i',j'}|$ the euclidean distance between the pixels $P_{i,j}$ and $P_{i',j'}$ and h a parameter related to the number of the neighboring pixels that are involved in the smoothing of the value in pixel $P_{i,j}$ (in simulations, we take $h = 10^{-3}m^2$). The $q_{i,j}$s are the elements of the traffic weight matrix obtained from the previous step and the $q^*_{i,j}$s are the elements of the traffic weight matrix estimated after smoothing.

3.3.2 Optimization of the traffic tracking algorithm

It is possible to manually set the importance factors but the relative performance of the traffic tracking process may result in inaccurate localization precision compared to existing solutions. For instance, KPIs holding small information should not be heavily considered in the aggregated traffic weight Q because they bias the results. So, in order to improve the accuracy of the proposed traffic tracking method, the importance factors, as defined in step 6, need to be optimized so that the contribution of each KPI in the weighted sum can be justified.

Finding the optimal vector $\mathbf{x}$ is the result of an optimization problem that reduces the distance between the available map of potential hotspots $\hat{Q}$ and the estimated traffic map Q found in Step 6 of the algorithm. The optimization is performed only one time for an area where the map of potential hotspots is already available. The obtained optimal importance factors might be used later for any similar environment (urban, suburban, rural etc.) without any knowledge of its potential hotspots because the contribution of each KPI mostly depends on the type of environment. For instance, TA and AoA are more efficient and have more contribution in rural areas, however in urban areas, measuring the TA or the AoA presents more errors due to obstacles (resulting thus in more reflections and diffractions).

The optimization of $\mathbf{x}$ can be formulated as follows:

$$\begin{cases} \underset{\mathbf{x}\in\mathbb{R}^5}{minimize} \sum_{i,j=1}^{m}(q_{i,j}-\hat{q}_{i,j})^2 = \sum_{i,j=1}^{m}\left(\sum_{s=1}^{5} x_s q_{i,j}^{(s)} - \hat{q}_{i,j}\right)^2 \\ \quad x_s \geq 0,\ s = 1..5 \end{cases} \tag{3.17}$$

where m^2 is the number of pixels in the coverage map.

In order to put the optimization problem in a known and solvable form, we consider

$$A^T = \begin{bmatrix} q_{1,1}^{(1)} & \dots & q_{1,m}^{(1)} & \dots & q_{2,1}^{(1)} & \dots & q_{m,m}^{(1)} \\ \cdot & \cdot\cdot & \cdot & \cdot\cdot & \cdot & \cdot\cdot & \cdot \\ q_{1,1}^{(5)} & \dots & q_{1,m}^{(5)} & \dots & q_{2,1}^{(5)} & \dots & q_{m,m}^{(5)} \end{bmatrix}$$

and

$$\mathbf{b} = [\hat{q}_{1,1}...\hat{q}_{1,m}...\hat{q}_{2,1}...\hat{q}_{m,m}]^T$$

A is a matrix of m^2 lines and 5 columns and $\mathbf{b}$ is a vector of length m^2.

Using matrix notation, the optimization problem of equation (3.17) becomes a minimization of the distance between the vectors $A\mathbf{x}$ and $\mathbf{b}$ in the space $\mathbb{R}^{m^2}$:

$$\begin{cases} \underset{\mathbf{x}\in\mathbb{R}^5}{minimize} \|A\mathbf{x}-\mathbf{b}\|_2 \\ \quad x_s \geq 0\ ,\ 1 \leq s \leq 5 \end{cases} \tag{3.18}$$

where $\|.\|_2$ is the standard 2-norm (the Euclidian norm) in the space $\mathbb{R}^{m^2}$.

This formulation represents a least square optimization problem and can be simply solved using the Gauss Newton method [70].

3.4 Numerical results

3.4.1 Parameters' setting

In order to evaluate and validate the proposed algorithm, we use an LTE simulator that allows dynamic users' arrivals and departures after being served.

At each time step of the simulator, equal to $1s$, the number of call attempts are generated according to a Poisson distribution with intensity $\lambda = 200$ UEs/s. UE positions are generated depending on the traffic weight in each pixel of the coverage map. UEs are accepted in the network only when there are available resources and

when their RSRP is higher than the threshold $Q_{rxlevmin}$ (set to $-115dBm$ in this work). We suppose that each UE has a file of size $1Mb$ to download. Each UE quits the network after downloading the entire file. Moreover, we consider that a part of UEs (20%) are moving during their transmission with a speed of $8.33km/h$. This means that the simulation supports also handover events with a handover margin set to $6dB$. UEs are scheduled according to the round robin model. At the end of the simulation, which lasts 1 hour, all KPIs (including the previously cited ones) are calculated and stored in a file.

The simulated network is shown in Fig. 3.2 and composed of 23 tri-sectorized BS (called also eNodeB) covering an area of $3 \times 3km^2$. eNodeB positions and physical characteristics are taken from a real network. Each sector in each eNodeB is equipped with a directive antenna of type Kathrein K742-234 having a beamwidth equal to 65^o. The used antenna mask is drawn in Fig. 3.9 with $G(\theta)$ representing the antenna gain depending on the angle deviation from the direction of the maximum antenna radiation. Moreover, each sector has an available capacity equivalent to $20MHz$ of spectrum bandwidth operating in the band $2.6GHz$. Because of the network heterogeneity, the list of parameters (e.g., BS transmitter noise figure, cable loss, maximum transmit power, etc), involved in this simulation depends on each site. Hence, it is worthless to cite all these parameters.

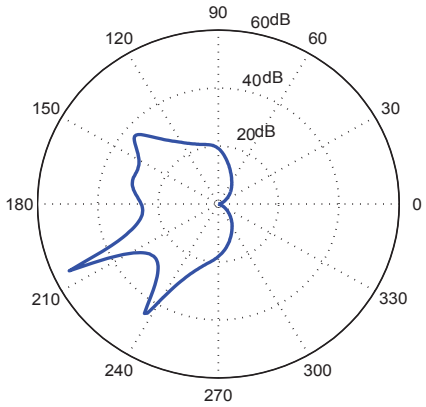

Fig. 3.9 Representation of $-10log(G(\theta))$ of the antenna mask.

The coverage map (RSRP from each cell in each pixel), provided by a planning tool, has a resolution equal to 20 meters. According to this map, the first and the second best serving cell are identified in each pixel.

Before starting the simulation, we attribute the traffic weight in each pixel of the coverage map based on a mixture of Log-normal distributions [10]. As shown in Fig. 3.10, each peak of a Log-normal density represents a traffic hotspot.

For the potential traffic map, we attribute arbitrary weights in some pixels according to our knowledge about some hotspot areas in the chosen map. The exploitation of this map improves the precision of hotspot localization but is not a key element in the proposed algorithm.

The validation of the algorithm consists in finding the traffic weight in each pixel (following the steps of the algorithm) and comparing it with the original traffic weights generated at the beginning of the simulation.

In order to have a better understanding of the efficiency of the proposed method in real networks, we further consider real imperfections due to errors in the reported measurements by UEs or due to errors in the coverage prediction tools of network operators. The considered mobile equipment and field imperfections are as follows:

- The signal level received at the UE is equal to the signal level in its position taken from the coverage map plus a normal random variable with zero mean and a standard deviation equal to $10dB = \sqrt{8^2 + 6^2 + 2^2}$. These three values correspond, respectively, to the impact of shadowing effect on mobile measurements plus the incertitude of the coverage measurement in addition to the possible errors generated by the mobile equipment when realizing measurements.
- The TA measurements are altered by adding a normal random variable with zero mean and standard deviation equal to 75.25 meters in terms of distance.
- The AoA measurements are also altered by adding a normal random variable with zero mean and standard deviation equal to $\frac{\pi}{6}$.

3.4.2 Results

Running the traffic tracking algorithm and performing the optimization, as described in Subsection 3.3.2, we get the importance factor as follows

$$\mathbf{x} = [0.418 \quad 0.2689 \quad 0.2281 \quad 0.0358 \quad 0.0491]^T \tag{3.19}$$

In simulations, we were able to test other values for the importance factors and the relative results are further improved after the optimization step. These optimal importance factors are directly used in the performance evaluation of the present traffic tracking process.

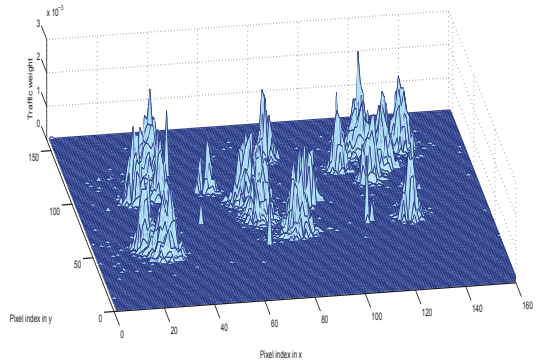

Fig. 3.10 Original traffic distribution.

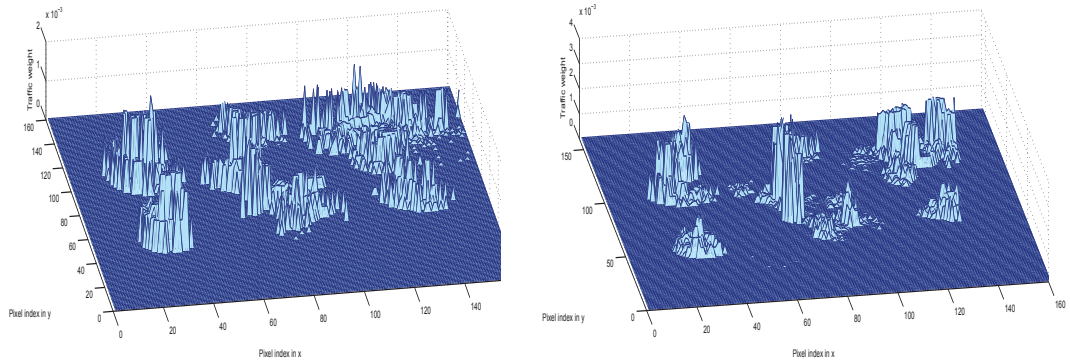

(a) Estimated traffic distribution in step 6.

(b) Estimated traffic distribution in step 7.

Fig. 3.11 Spatial traffic distribution.

In Fig. 3.10, the original traffic distribution generated at the beginning of the simulation is drawn. In Fig. 3.11a, the estimated traffic distribution is depicted based on the proposed algorithm without including the smoothing process. Fig. 3.11b represents the spatial traffic distribution after smoothing the calculated distribution. Then, Fig. 3.12 represents the estimated spatial traffic distribution with introducing imperfections impacting both the coverage map and the mobile measurement reports.

Regarding the identification of the hotspot areas, we observe that most of the hotspot areas are found in the entire network map even when the estimation takes into account the mobile and field imperfections detailed above. Nevertheless, we observe that the precision of localization is somewhat affected by the consideration of these imperfections.

In Table 3.1, the coordinates of the generated hotspots and those estimated in steps 6 and 7 and after taking into account mobile and field imperfections are extracted

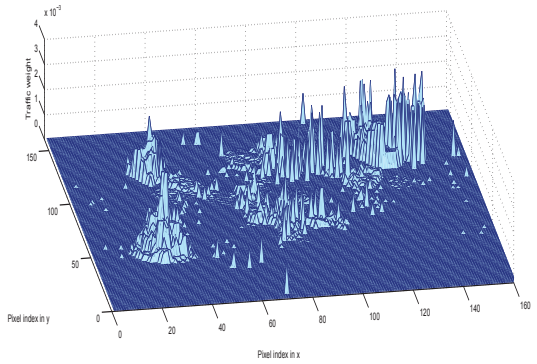

Fig. 3.12 Estimated traffic distribution taking into account real mobile and field imperfections.

Table 3.1 Coordinates of generated and estimated hotspots holding highest traffic weights (x,y) in meters.

Generated hotspot	(1100,960)	(760,940)	(20,980)	(-1020,-640)	(1040,280)	(-200,-120)	(-960,740)	(220,100)	(960,-300)
Estimated hotspot in step 6	(1140,940)	(740,940)	(40,980)	(-1040,-660)	(1200,420)	(-240,-180)	(-940,780)	(320,140)	(940,-280)
Distance to original hotspot position	44.72	20	20	28.28	212.6	72.11	44.72	107.7	28.28
Estimated hotspot in step 7	(1100,960)	(760,900)	(40,980)	(-1020,-660)	(1100,340)	(-180,-120)	(-920,760)	(260,100)	(960,-320)
Distance to original hotspot position	0	40	20	20	84.85	20	44.72	40	20
With imperfections	(1140,920)	(810,900)	(60,880)	(-1020,-660)	(1200,280)	(-160,-60)	(-940,800)	(160,100)	(980,-300)
Distance to original hotspot position	56.57	64	107.7	20	160	72.1	63.24	60	20

from the calculated matrices generating the figures above. From Table 3.1, we find out that the execution of the proposed algorithm until step 6 pinpoints the hotspots generated in the network with a precision of 64.26 meters (see Table 3.1, the mean of the calculated distances between the original and the estimated hotspots in step 6). However, the spatial traffic distribution is quite uniform inside these hotspots. Then, the shape of the estimated traffic distribution is improved after smoothing and the precision becomes about 32.17 meters. In case the estimation is made based on imperfect measurements, the precision of localization becomes less accurate than the previous results and errors of localization are about 69.3 meters.

Fig. 3.13 shows the Cumulative Distribution Function (CDF) of traffic weights attributed to pixels based on the proposed algorithm. To localize the hotspot areas, we are interested only in the region surrounded by the (blue) ellipse in Fig. 3.13 which represents the significant weights.

Fig. 3.13 indicates that using all the 5 KPIs in the network gives better estimation of traffic distribution as compared to the case when using only some of them. In fact, significant weights have a small density when using only one KPI which means that

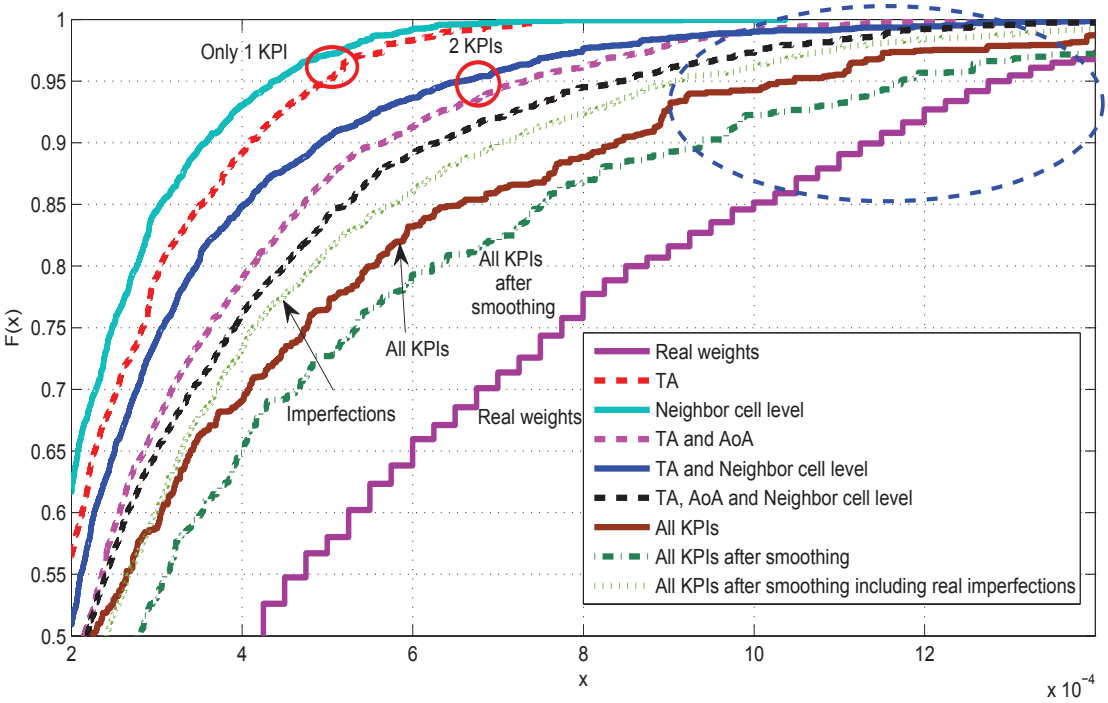

Fig. 3.13 CDF of real and estimated traffic weights.

the traffic distribution is more flat and uniform inside the hotspot area. This density is increased and becomes near the exact distribution when all the KPIs are used and when all the steps of the proposed algorithm are performed.

From the traffic weight distribution, we note that the most useful KPIs are the TA, AoA and the neighbor cell level. The mean throughput and the cell load have also an impact on the estimation and improve further the localization. In addition, smoothing the estimated traffic distribution reduces the difference between the original spatial traffic distribution and the estimated one.

Among the plotted curves in Fig. 3.13, the curve representing the combination between TA and neighboring cell level allows us to compare the solution proposed in [14] to the present proposed algorithm. Results show that our method performs better when compared to the solution disclosed in [14].

From Fig. 3.13, we observe also that including real imperfections clearly impacts the estimation of the spatial traffic distribution. Nevertheless, the observed results are still favorable to further boost the development and the improvement of the proposed traffic tracking solution.

Table 3.2 Percentage of detected hotspots.

Real % of first hotspots	Estimated % with only TA	Estimated % with all KPIs	Estimated % after smoothing	Estimated % with imperfections
0.5	0.12	0.30	0.422	0.22
1	0.26	0.48	0.58	0.42
2	0.46	1.09	1.13	0.95
5	1.12	2.17	2.56	2.03
10	2.29	4.34	4.8	4.11
20	4.87	33.45	9.7	9.1
50	14.22	74.34	27.32	22.47

We compare in Table 3.2 the percentage of detected hotspots that have the highest weights to the original heaviest hotspots in the network. The analysis is based on the fact that weights are sorted in a decreasing order. We determine the coordinates of the pixels which hold 0.5% (1, 2, 5, 10, 20, and 50 respectively) of the traffic in the network (using the real distribution). Then, we calculate the sum of estimated weights in these pixels.

The purpose of the evaluation in Table 3.2 is to see the importance of using all the KPIs and the impact of smoothing on the localization of most significant hotspots. The column showing the performance of using only TA stands to the reason that, in the literature, several traffic tracking techniques are based on only TA. It allows a common comparison of these techniques to the proposed one. Table 3.2 shows that the traffic tracking method is clearly improved when it is based on the 5 KPIs compared to the use of only TA.

From Table 3.2, we also observe that the heaviest hotspots that have the highest weights, are reasonably estimated and this estimation is further enhanced with the step of smoothing. However, when we increase the percentage of the first significant hotspots (from 0.5% to 10%), the estimation shows less efficiency and this is due to the fact that some areas close to the hotspots could take a significant weight without carrying heavy traffic.

Before smoothing, pixels within the same region of a hotspot take the same weight. However, weights of isolated fake hotspot are eliminated after smoothing and weights of pixels in the edge of a hotspot are reduced. Hence, when the percentage of the first significant hotspots is low, only pixels in the center of a hotspot are evaluated and the sum of weights before smoothing is less than the sum after smoothing. In contrast, when the percentage of the first significant hotspots is high, pixels in the edge of the hotspots are also included in the evaluation. As a result, the sum of weights before smoothing is higher than the sum after smoothing since weights of pixels in the edge of hotspots are reduced after smoothing.

The results in Table 3.2 show that including mobile and field imperfections provide also an acceptable estimation of the most important hotspots. This metric shows that the proposed method, in the case when mobile and field imperfections are taken into account, is less accurate when taking more percentage of traffic weights to estimate. This result consolidates the previous results and is due to the same reasons discussed in the case where mobile measurements are assumed to be correct.

3.5 Concluding remarks

In this chapter, we proposed a modular and optimized algorithm that consists in combining several performance metrics projected over a coverage map. The proposed traffic tracking process is tested including data measurement errors due to mobile equipment and field imperfections. Results showed acceptable localization error, in cases of moderate and heavy traffic. Therefore, the use of O&M KPIs projected over a coverage map can be efficient for tracking traffic hotspots as they yield promising results at low operational costs. So, we conclude that this method can be a useful and promising solution to identify areas where a small cell must be deployed or to perform appropriate configurations to lessen congestion in peak traffic areas.

The next step is to evaluate the impact of the imperfect traffic hotspot localization on the deployment of small cells in cellular networks. This subject is investigated in Chapter 4.

Chapter 4

Small cell deployment under perfect and imperfect traffic hotspot localization

Dense urban areas are environments where the spectrum is most scarce, the need for high capacity is urgent and, in addition to the pathloss effect, interferences and shadowing effect have also an important impact on the quality of service. Consequently, a dense network deployment is needed with a topology adapted to the morphology of the environment in order to ensure a best coverage in the entire cell. Understanding the efficiency of small cell deployment in the presence of traffic hotspots can further draw operators' attention to this feature.

In this chapter, we evaluate the impact of imperfect small cell positioning on the network performance. We start by describing the downlink system model with a special focus on radio aspects. After that, we derive the throughput distribution and its mean following a static level analysis, which refers in our context, to a set of decorrelated averaged snapshots of the network where the user location distribution varies only in space. Three different scenarios are studied: i. with macrocells only, ii. with a small cell deployed exactly at the center of the traffic hotspot and iii. with a small cell not perfectly deployed near the traffic hotspot (its position is different from the hotspot one).

We secondly consider the dynamics of the system (widely named flow level analysis), with users arriving to the system at random times and leaving it after a finite duration corresponding to the end of their services, with the service rates derived in the static level analysis. The studied model is based on coupled multi-class Processor Sharing queues (PS). The coupling between the macrocell and the small cell is the consequence

of the interference generated by each one on the other. We derive analytical expressions for several performance metrics depending on the level of accuracy of traffic hotspot localization tools [20].

4.1 System model

4.1.1 System description

We consider a cellular network with an infinite number of macrocells, each one transmitting with power level P. The location of the macrocells is drawn following a hexagonal grid layout (see Fig. 4.1) with inter-site distance denoted by δ. We also add a small cell located in (R_s, θ_s), as illustrated in Fig. 4.1. The transmit power level of the small cell is $P_s = \kappa P$ with $0 \leq \kappa \leq 1$.

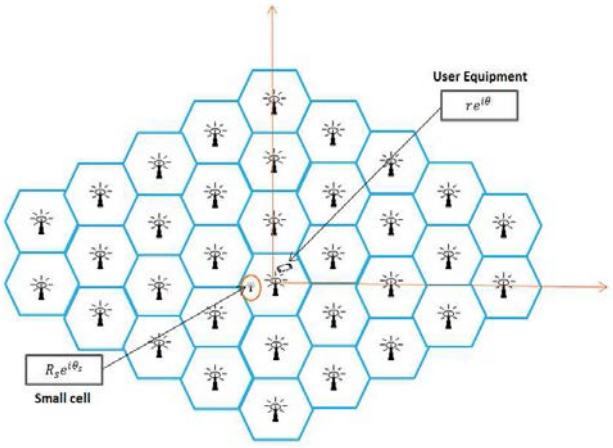

Fig. 4.1 Network layout.

A given User Equipment (UE) m, with polar coordinates (r, θ), is served either by the central macrocell (cell at the origin) or the deployed small cell depending on the relative signal strength coming from both antennas. The rest of the cells play the role of interfering ones.

In order to evaluate the efficiency of the deployed small cells, we consider a traffic hotspot with polar coordinates (R_h, θ_h). Without loss of generality, we assume that this hotspot is located inside the central macrocell of the network. This means that R_h is smaller than the radius of the cell, denoted by R. The choice of R is problematic because the disk circumscribed around the hexagon over-estimates interferences whereas the disk inscribed in the hexagon under-estimates interferences and generates coverage holes. For all the theoretical study, we take an arbitrary R, such that $R < \delta$, but for

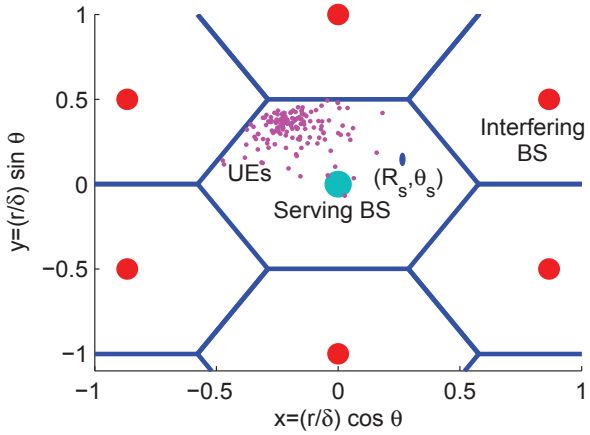

Fig. 4.2 A snapshot of the network with a traffic hotspot in $(R_h = 0.44\delta, \theta_h = \frac{2\pi}{3})$.

the numerical results, we use $R = \delta\sqrt{\frac{\sqrt{3}}{2\pi}}$ which is the radius of the disk having the same area as the hexagon representing the cell. UE locations are spatially distributed in order to form a hotspot centered in (R_h, θ_h); its measure is given by

$$dt(r,\theta) = \frac{1}{2\pi A^2} e^{-\frac{|re^{i\theta} - R_h e^{i\theta_h}|^2}{2A^2}} r dr d\theta \tag{4.1}$$

where A is the standard deviation of the distribution allowing to control the spatial dispersion of the traffic hotspot. An example of the relative spatial distribution is plotted in Fig. 4.2 with $A = 0.2m^2$ (the same value of A is used in simulations).

Remark: Considering more heterogeneity in the spatial traffic distribution is of great importance in the performance evaluation of heterogeneous networks. This aspect and its consequences on performance results are discussed in Subsection 4.3.3. Nevertheless, if we consider more than one traffic hotspot, the impact of imperfect small cell positioning may not make sense since a large error in small cell positioning could help to cover another traffic hotspot. In this way, we may not identify the real impact of imperfect small cell positioning which is the key driver of this work allowing us to obtain the accuracy level that traffic localization tools must attain. Moreover, with many traffic hotspots, it is not possible to know if it is beneficial to deploy small cells near or far from the macrocell position[1] unless all hotspots are generated in the same region (in the edge or in the center).

[1]The macrocell or small cell position means the location of their transmitting antennas. For the studied hexagonal model, the macrocell position is the center of its covered hexagon.

As indicated above, we consider three scenarios: In Scenario 1, there is no small cells in the network. This scenario represents a benchmark allowing the comparison of a network where small cells contribute to offloading traffic to a network without small cells. Scenario 2 considers a small cell inside the central macrocell and it is perfectly deployed in the center of the traffic hotspot, i.e. $(R_h, \theta_h) = (R_s, \theta_s)$. In Scenario 3, we consider a small cell deployed inside the central macrocell as in Scenario 2, but we add imperfections due to the accuracy level of the used traffic hotspot localization method, i.e. $(R_h, \theta_h) \neq (R_s, \theta_s)$.

In order to deduce the performance of Scenario 1 from that of Scenario 3, we consider that in Scenario 3, the small cell is placed far enough from the traffic hotspot and from the macrocell (i.e. $R_s = \infty$) or it is switched in a sleeping mode (i.e. $P_s = 0$).

4.1.2 Channel model and UE association

To model the wireless channel, we consider a distance based pathloss metric with a standard function given by $a|m-C|^{-2b}$, where $|m-C|$ is the distance between the UE m and any cell C in the network, which can be either a macrocell or a small cell, a is a pathloss constant which depends on the type of the environment relative to the type of the cell (indoor, outdoor, rural, urban, etc.) and $2b > 2$ is the pathloss exponent coefficient. Without loss of generality, we consider that the transmit power levels P and P_s include the pathloss constant a, antenna gain, UE antenna gain and body loss.

Based on the proposed pathloss model, the UE located in $m = (r, \theta)$ is served by the small cell if the RSRP of the small cell is higher than the RSRP coming from the macrocell. This can be expressed by the following inequality

$$P_s|re^{i\theta} - R_s e^{i\theta_s}|^{-2b} > Pr^{-2b} \tag{4.2}$$

If the constraint in inequality (4.2) is not satisfied, the UE will be connected to the macrocell.

Based on inequality (4.2), we evaluate the absorption coefficient (denoted by μ) which reflects the percentage of mobile locations (generated according to a given traffic distribution) that can be covered and served by the small cell. This performance metric is given by

$$\mu = \frac{1}{S_0} \int_{S^*} \mathbb{1}\left(P_s|re^{i\theta} - R_s e^{i\theta_s}|^{-2b} > Pr^{-2b}\right) dt(r, \theta) \tag{4.3}$$

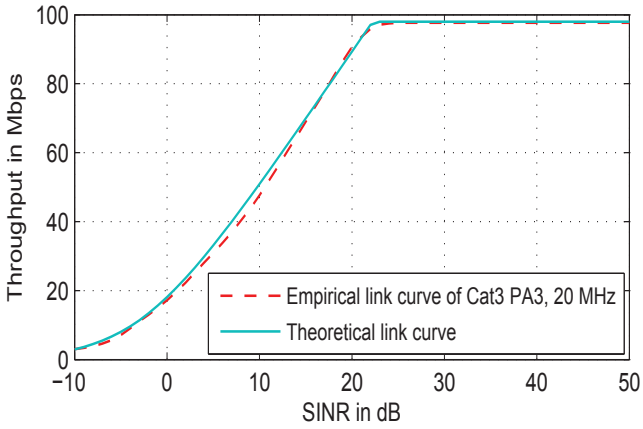

Fig. 4.3 Throughput-SINR link level curve.

where S^* is the covered area by the central macrocell and the deployed small cell.

$$S_0 = \int_{S^*} dt(r,\theta) \tag{4.4}$$

4.1.3 Link level capacity: Throughput vs SINR

The SINR and the throughput of a UE $m = (r,\theta)$ are respectively denoted by $\gamma(r,\theta)$ and $\eta(r,\theta)$ if received from the macrocell and by $\tilde{\gamma}(r,\theta)$ and $\tilde{\eta}(r,\theta)$ if received from the small cell. Independently from the type of the cell, the relationship between γ (in linear scale) and η (in Mbps) depends on the UE capability and receiver characteristics, the available bandwidth, the radio conditions and small scale fading effects, the type of the service and the choice of the Modulation and Coding Schemes (MCS). This relationship gives the peak data rate practically experienced by the UE in any position of the network in the absence of any other active user in the cell. It is often modeled by the modified Shannon formula [71],

$$\eta = \min(K_1 \times W \times \ln(1 + K_2 \times \gamma), \eta_0) \tag{4.5}$$

where K_1 and K_2 are two variables depending on the transmission conditions and can be adapted for each UE speed and category, W is the used bandwidth expressed in MHz and η_0 is the maximum achievable throughput.

For the numerical results, we consider UE category 3 operating at $20MHz$. From a simple fitting of practical data, we find out that, under laboratory measurement conditions, $\eta_0 = 98Mbps$, $K_1 = 0.85$ and $K_2 = 1.9$. Fig. 4.3 provides a comparison

between the theoretical and empirical Throughput-SINR link curve of the specified category of UE.

4.2 Static level analysis

In this section, we evaluate the user throughput obtained in each position of the covered region of the studied macrocell and small cell based on the modified Shannon formula given in equation (4.5). Then, the mean throughput and its Complementary Cumulative Distribution Function (CCDF) are calculated considering a user location variable having a measure $dt(r,\theta)$ as given in equation (4.1), reflecting the presence of a traffic hotspot in the cell.

Definition 1: As mentioned in Subsection 4.1.3, γ and $\tilde{\gamma}$ are the SINRs received at a UE with polar coordinates (r,θ) and served respectively by the macrocell and the small cell. Hence, γ and $\tilde{\gamma}$ are expressed as follows

$$\gamma(r,\theta) = \frac{1}{g(r) + \kappa|re^{i\theta} - R_s e^{i\theta_s}|^{-2b} r^{2b}} \tag{4.6}$$

$$\tilde{\gamma}(r,\theta) = \frac{P_s|re^{i\theta} - R_s e^{i\theta_s}|^{-2b}}{(g(r)+1)\,P r^{-2b}} \tag{4.7}$$

where $g(r)$ represents the interference plus noise factor in a network composed of only macrocells. It is defined by the sum of the power coming from all the interfering macrocells plus the noise power divided by the received power from the serving macrocell.

In order to evaluate the impact of an infinite number of interfering macrocells, we established and validated in [27] an expression of $g(r)$ for the considered hexagonal network model. This formula is expressed as follows:

$$g(r) = 6\alpha \left(\frac{r}{\delta}\right)^{2b} \left(\frac{1 + (1-b)^2 \left(\frac{r}{\delta}\right)^2}{(1 - \left(\frac{r}{\delta}\right)^2)^{2b-1}} + \omega(b) - 1 \right) + \frac{P_N}{P} r^{2b} \tag{4.8}$$

where α is the average cell load over all the interfering macrocells, P_N is the noise power level (exterior to the system and including thermal noise) and

$$\omega(b) = 3^{-b}\zeta(b)\left(\zeta(b,\frac{1}{3}) - \zeta(b,\frac{2}{3})\right)$$

$\zeta(.)$ and $\zeta(.,.)$ are respectively the Riemann Zeta and Hurwitz Riemann Zeta functions [72, pp. 1036].

Definition 2: We define the mean user throughput η_{avg} in the region S^*, covered by the macrocell and the deployed small cell as follows:

$$\eta_{avg} = \eta_{macro} + \tilde{\eta}_{small} \tag{4.9}$$

with

$$\begin{aligned}\eta_{macro} =& \frac{1}{S_0}\int_{S^*} \mathbb{1}\left(P_s|re^{i\theta} - R_s e^{i\theta_s}|^{-2b} < Pr^{-2b}\right) \times \\ & \min(K_1 W \ln(1 + K_2 \times \gamma(r,\theta)), \eta_0) dt(r,\theta)\end{aligned} \tag{4.10}$$

$$\begin{aligned}\tilde{\eta}_{small} =& \frac{1}{S_0}\int_{S^*} \mathbb{1}\left(P_s|re^{i\theta} - R_s e^{i\theta_s}|^{-2b} > Pr^{-2b}\right) \times \\ & \min(K_1 W \ln(1 + K_2 \times \tilde{\gamma}(r,\theta)), \eta_0) dt(r,\theta)\end{aligned} \tag{4.11}$$

where $dt(r,\theta)$ represents the spatial UE location distribution reflecting the presence of a traffic hotspot located in (R_h, θ_h) and $\mathbb{1}(.)$ is the indicator function which returns 1 if the input condition is verified and zero otherwise. S^* is the studied covered area and

$$S_0 = \int_{S^*} dt(r,\theta) \tag{4.12}$$

Definition 3: In the presence of a hotspot (following a spatial distribution such as the one given in equation (4.1)) in the region covered by the central macrocell and the deployed small cell (R_s, θ_s), we define the throughput CCDF for both cells as follows:

$$\begin{aligned}\mathbb{P}(\eta \geq l) =& \frac{1}{S}\int_{S^*} \mathbb{1}\left(P_s|re^{i\theta} - R_s e^{i\theta_s}|^{-2b} \leq Pr^{-2b}\right) \times \\ & \mathbb{1}\left(\min(K_1 W \ln(1 + K_2 \times \gamma(r,\theta)), \eta_0) \geq l\right) dt(r,\theta)\end{aligned} \tag{4.13}$$

$$\begin{aligned}\mathbb{P}(\tilde{\eta} \geq l) =& \frac{1}{\tilde{S}}\int_{S^*} \mathbb{1}\left(P_s|re^{i\theta} - R_s e^{i\theta_s}|^{-2b} > Pr^{-2b}\right) \times \\ & \mathbb{1}\left(\min(K_1 W \ln(1 + K_2 \times \tilde{\gamma}(r,\theta)), \eta_0) \geq l\right) dt(r,\theta)\end{aligned} \tag{4.14}$$

with S^* the studied covered area and

$$S = \int_{S^*} \mathbb{1}\left(P_s|re^{i\theta} - R_s e^{i\theta_s}|^{-2b} \leq Pr^{-2b}\right) dt(r,\theta) \tag{4.15}$$

$$\tilde{S} = \int_{S^*} \mathbb{1}\left(P_s|re^{i\theta} - R_s e^{i\theta_s}|^{-2b} > Pr^{-2b}\right) dt(r,\theta) \tag{4.16}$$

where $dt(r,\theta)$ represents the spatial UE location distribution reflecting the presence of a traffic hotspot located in (R_h, θ_h).

We notice that the performance analysis in Scenario 1 is equivalent to the case of Scenario 3 but with deploying a small cell far enough from the macrocell and hotspot positions. For instance, R_s can be taken as equal to $+\infty$. Hence, the inequality in (4.2) will never be satisfied for UEs located inside the hotspot and it follows that

$$\eta_{avg} = \eta_{macro} \text{ and } \tilde{\eta}_{small} = 0 \tag{4.17}$$

On the other hand, Scenario 2 is illustrated by the equality

$$(R_s, \theta_s) = (R_h, \theta_h) \text{ knowing that } R_h \leq R \tag{4.18}$$

Scenario 3 is eventually depicted by the following conditions

$$(R_s, \theta_s) \neq (R_h, \theta_h) \text{ and } R_s \leq R \tag{4.19}$$

Lemma 4.2.1 *For $l > \eta_0$, the throughput CCDFs in the macrocell and in the small cell are equal to zero since the peak throughput a UE (of a given category) can reach in the best radio conditions, cannot be higher than η_0.*

$$\forall l > \eta_0, \quad \mathbb{P}(\eta \geq l) = 0 \text{ and } \mathbb{P}(\tilde{\eta} \geq l) = 0$$

On the other hand, when $l \leq \eta_0$, the throughput CCDFs are further simplified and are given by

$$\mathbb{P}(\eta \geq l) = \frac{1}{S} \int_{S^*} \mathbb{1}\left(P_s|re^{i\theta} - R_s e^{i\theta_s}|^{-2b} \leq Pr^{-2b}\right) \mathbb{1}\left(\frac{1}{\gamma(r,\theta)} \leq \psi(l)\right) dt(r,\theta) \tag{4.20}$$

$$\mathbb{P}(\tilde{\eta} \geq l) = \frac{1}{\tilde{S}} \int_{S^*} \mathbb{1}\left(P_s|re^{i\theta} - R_s e^{i\theta_s}|^{-2b} > Pr^{-2b}\right) \mathbb{1}\left(\frac{1}{\tilde{\gamma}(r,\theta)} \leq \psi(l)\right) dt(r,\theta) \tag{4.21}$$

with

$$\psi(l) = K_2 \left(e^{\frac{l}{K_1 W}} - 1 \right)^{-1} \tag{4.22}$$

Proof: The proof is based on the fact that the inequality $\min(K_1 W \ln(1 + K_2 \times \tilde{\gamma}(r,\theta)), \eta_0) \geq l$ simplifies to $K_1 W \ln(1 + K_2 \times \tilde{\gamma}(r,\theta)) \geq l$ since $\eta_0 \geq l$. Then, we proceed by performing elementary algebraic transformations. ■

In the rest of the analysis, the throughput CCDF is only calculated for $l \leq \eta_0$ because it is simply equal to zero otherwise.

4.2.1 Case of no small cells deployed in the studied area

As mentioned above, we take $R_s = \infty$ to study the case where the macrocell area does not contain small cells. Then, all the UEs in the hotspot, following $dt(r,\theta)$ defined in equation (4.1), are only served by the macrocell. In this case, the mean user throughput and its CCDF are given by the following propositions.

Proposition 4.2.1 *The mean user throughput in a network of macrocells only in the presence of a traffic hotspot, distributed as given in equation (4.1), is equal to*

$$\begin{aligned} \eta_{avg} = & \frac{2}{S_0} \frac{K_1 W}{2} \frac{1}{A^2} e^{-\frac{R_h^2}{2A^2}} \ln\left(1 + \frac{K_2}{\psi(\eta_0)}\right) \times \int_0^{\Lambda} r e^{-\frac{r^2}{2A^2}} I_0\left(\frac{r R_h}{A^2}\right) dr + \\ & \frac{2}{S_0} \frac{K_1 W}{2} \frac{1}{A^2} e^{-\frac{R_h^2}{2A^2}} \times \int_{\Lambda}^{R} r e^{-\frac{r^2}{2A^2}} \ln\left(1 + \frac{K_2}{g(r)}\right) I_0\left(\frac{r R_h}{A^2}\right) dr \end{aligned} \tag{4.23}$$

where $\psi(\eta_0)$ is given as in equation (4.22), $I_0(.)$ is the first order of the modified Bessel function of the first kind [73], $g(r)$ is given in (4.8) and $\Lambda = \min\left(g^{-1}\left(\psi(\eta_0)\right), R\right)$.

Proof: From the definition of the mean user throughput incorporating the hotspot traffic distribution, one has

$$\begin{aligned} \eta_{avg} = & \frac{2}{S_0} \frac{K_1 W}{2} \frac{1}{A^2} e^{-\frac{R_h^2}{2A^2}} \times \int_0^{R} r e^{-\frac{r^2}{2A^2}} \ln\left(1 + \frac{K_2}{max\left(\psi(l), g(r)\right)}\right) \frac{1}{\pi} \int_0^{\pi} e^{\frac{r R_h cos(\theta)}{A^2}} dr d\theta \\ = & \frac{2}{S_0} \frac{K_1 W}{2} \frac{1}{A^2} e^{-\frac{R_h^2}{2A^2}} \times \int_0^{R} r e^{-\frac{r^2}{2A^2}} \ln\left(1 + \frac{K_2}{max\left(\psi(l), g(r)\right)}\right) I_0\left(\frac{r R_h}{A^2}\right) dr \end{aligned} \tag{4.24}$$

Function g realizes a continuous increasing function from $[0,\ R]$ to $[0,\ g(R)]$. And so, it can be explicitly inversed using series reversion or by switching numerically the x and y axes. A simple and accurate inverse function of g is provided in [29].

Using the monotonicity of g, the expression of η_{avg} is further simplified and we obtain the expressions in equation (4.23) which completes the proof. ■

Proposition 4.2.2 *When the studied area does not contain a small cell, the throughput CCDF in the macrocell, in the presence of UE location distribution defined as in equation (4.1), is expressed by*

$$\mathbb{P}(\eta \geq l) = \frac{1}{S} \frac{e^{-\frac{R_h^2}{2A^2}}}{A^2} \int_0^{\Lambda} r e^{-\frac{r^2}{2A^2}} I_0\left(\frac{r R_h}{A^2}\right) dr \tag{4.25}$$

with $\Lambda = \min\left(g^{-1}\left(\psi(l)\right), R\right)$ *and* $I_0(.)$ *is the first order of the modified Bessel function of the first kind,* ψ *is defined in equation (4.22) and* $g(r)$ *is given in equation (4.8).*

Proof: In the studied scenario, one has $S = \int_{S^*} dt(r,\theta)$ since no small cells are deployed in the evaluated area. Next, from the throughput CCDF definition given in equation (4.20) and based on the monotonicity of g, $\mathbb{P}(\eta > l)$ is expressed as follows

$$\begin{aligned}
\mathbb{P}(\eta \geq l) &= \frac{1}{S} \int_{S^*} \mathbb{1}\left(g(r) \leq \psi(l)\right) dt(r,\theta) \\
&= \frac{1}{S} \int_0^R \int_0^{2\pi} \mathbb{1}\left(r \leq g^{-1}(\psi(l))\right) dt(r,\theta) \\
&= \frac{1}{S} \int_0^{\Lambda} \int_0^{2\pi} dt(r,\theta)
\end{aligned}$$

with $\Lambda = \min\left(g^{-1}\left(\psi(l)\right), R\right)$ and $\psi(l)$ as defined in (4.22).

Finally, replacing $dt(r,\theta)$ by its expression in (4.1) and evaluating the integral on θ, we find (4.25) and complete the proof. ■

4.2.2 Case of small cell deployed in the studied area

When the small cell is deployed in the coverage of the macrocell, the mean user throughput and its CCDF in the system composed of the macrocell and the small cell are given in the following propositions.

Proposition 4.2.3 *When users are located in the hotspot given by $dt(r,\theta)$ and centered in (R_h, θ_h), they are served either by the macrocell or the small cell (with polar coordinates (R_s, θ_s)). Then, the expression of η_{macro} and of $\tilde{\eta}_{small}$ given in definition 2 can be expressed as follows:*

$$\begin{aligned}\eta_{macro} =& \frac{1}{S_0}\frac{K_1 W}{2\pi}\frac{1}{A^2}e^{-\frac{R_h^2}{2A^2}}\int_{[0,\ r_1]\cup[r_2,\ R]} re^{-\frac{r^2}{2A^2}}\int_0^{\pi}\left(e^{\frac{rR_h cos(\theta-\theta_h+\theta_s)}{A^2}}+e^{\frac{rR_h cos(\theta+\theta_h-\theta_s)}{A^2}}\right)\times \\ & \ln\left(1+\frac{K_2}{max\left(\psi(\eta_0), g(r)+\kappa r^{2b}|re^{i\theta}-R_s|^{-2b}\right)}\right)drd\theta \\ & + \frac{1}{S_0}\frac{K_1 W}{2\pi}\frac{1}{A^2}e^{-\frac{R_h^2}{2A^2}}\int_{r_1}^{r_2} re^{-\frac{r^2}{2A^2}}\int_{cos^{-1}(h(r)}^{\pi}\left(e^{\frac{rR_h cos(\theta-\theta_h+\theta_s)}{A^2}}+e^{\frac{rR_h cos(\theta+\theta_h-\theta_s)}{A^2}}\right)\times \\ & \ln\left(1+\frac{K_2}{max\left(\psi(\eta_0), g(r)+\frac{P_s}{P}r^{2b}|re^{i\theta}-R_s|^{-2b}\right)}\right)drd\theta \end{aligned} \tag{4.26}$$

$$\begin{aligned}\tilde{\eta}_{small} =& \frac{1}{S_0}\frac{K_1 W}{2\pi}\frac{1}{A^2}e^{-\frac{R_h^2}{2A^2}}\int_{r_1}^{r_2} re^{-\frac{r^2}{2A^2}}\int_0^{cos^{-1}(h(r))}\left(e^{\frac{rR_h cos(\theta-\theta_h+\theta_s)}{A^2}}+e^{\frac{rR_h cos(\theta+\theta_h-\theta_s)}{A^2}}\right)\times \\ & \ln\left(1+\frac{K_2}{max\left(\psi(\eta_0), (g(r)+1)\frac{1}{\kappa}r^{-2b}|re^{i\theta}-R_s|^{2b}\right)}\right)drd\theta \end{aligned} \tag{4.27}$$

where $r_1 = \frac{R_s}{1+\kappa^{\frac{1}{2b}}}$, $r_2 = \frac{R_s}{1-\kappa^{\frac{1}{2b}}}$, $\psi(\eta_0)$ is defined in (4.22) and

$$h(r) = \frac{R_s^2 + r^2 - \kappa^{\frac{1}{b}}r^2}{2rR_s} \tag{4.28}$$

Proof: First, we start by developing $\mathbb{1}\left(P_s|re^{i\theta}-R_s e^{i\theta_s}|^{-2b} < Pr^{-2b}\right)$ in the expression of η_{macro} given in definition 2:

$$\begin{aligned}\eta_{macro} =& \frac{1}{S_0}\int_{S^*}\mathbb{1}\left(P_s|re^{i\theta}-R_s e^{i\theta_s}|^{-2b} < Pr^{-2b}\right) min(K_1 W\ln(1+K_2\times\gamma(r,\theta)),\eta_0)dt(r,\theta) \\ =& \frac{1}{S_0}\int_{S^*}\mathbb{1}\left(cos(\theta-\theta_s) < h(r)\right) min(K_1 W\ln(1+K_2\times\gamma(r,\theta)),\eta_0)dt(r,\theta)\end{aligned}$$

Then, using the monotonicity of the function $cos(.)$ in $[0,\ \pi]$ and in $[-\pi,\ 0]$ separately, the obtained expression is further transformed to

$$\eta_{macro} = \frac{1}{S_0}\int_0^R\int_0^{\pi} \mathbb{1}\left(\theta-\theta_s > cos^{-1}(h(r)|_{-1}^{1})\right) min(K_1 W \ln(1+K_2\times\gamma(r,\theta)),\eta_0) dt(r,\theta) + \frac{1}{S_0}\int_0^R\int_{-\pi}^{0} \mathbb{1}\left(\theta-\theta_s < cos^{-1}(h(r)|_{-1}^{1})\right) min(K_1 W \ln(1+K_2\times\gamma(r,\theta)),\eta_0) dt(r,\theta)$$

with

$$h(r)|_{-1}^{1} = \begin{cases} h(r)\ if\ -1 < h(r) < 1 \\ -1\ if\ h(r) < -1 \\ 1\ if\ h(r) > 1 \end{cases} \tag{4.29}$$

Knowing that $cos^{-1}(h(r)|_{-1}^{1})$ can be expressed as in equation (4.30) and after performing algebraic transformations notably in the expression of the traffic distribution $dt(r,\theta)$, we obtain equation (4.26) and complete the first part of the proof.

$$cos^{-1}(h(r)|_{-1}^{1}) = \begin{cases} cos^{-1}(h(r)) & \text{if } r_1 < r < r_2 \\ 0 & \text{otherwise} \end{cases} \tag{4.30}$$

We follow the same steps to prove the resulting expression of $\tilde{\eta}_{small}$ in equation (4.27). ■

Remark: When the small cell position matches with the hotspot's one (Scenario 2), the mean throughput of UEs served by the macrocell is further simplified and its expression becomes as follows

$$\begin{aligned} \eta_{macro} = & \frac{2}{S_0}\frac{K_1 W}{2\pi}\frac{1}{A^2} e^{-\frac{R_h^2}{2A^2}} \int_{[0,\ r_1]\cup[r_2,\ R]} r e^{-\frac{r^2}{2A^2}} \int_0^{\pi} e^{\frac{rR_h cos(\theta)}{A^2}} \\ & \ln\left(1+\frac{K_2}{max\left(\psi(\eta_0), g(r)+\kappa r^{2b}|re^{i\theta}-R_h|^{-2b}\right)}\right) dr d\theta + \\ & \frac{2}{S_0}\frac{K_1 W}{2\pi}\frac{1}{A^2} e^{-\frac{R_h^2}{2A^2}} \int_{r_1}^{r_2} r e^{-\frac{r^2}{2A^2}} \int_{cos^{-1}(h(r))}^{\pi} e^{\frac{rR_h cos(\theta)}{A^2}} \\ & \ln\left(1+\frac{K_2}{max\left(\psi(\eta_0), g(r)+\kappa r^{2b}|re^{i\theta}-R_h|^{-2b}\right)}\right) dr d\theta \end{aligned} \tag{4.31}$$

Likewise, the mean throughput of UEs served by the small cell is given by

$$\tilde{\eta}_{small} = \frac{2}{S_0}\frac{K_1 W}{2\pi}\frac{1}{A^2} e^{-\frac{R_h^2}{2A^2}} \int_{r_1}^{r_2} r e^{-\frac{r^2}{2A^2}} \int_0^{cos^{-1}(h(r))} e^{\frac{rR_h cos(\theta)}{A^2}} \times \ln\left(1 + \frac{K_2}{max\left(\psi(\eta_0), (g(r)+1)\frac{1}{\kappa} r^{-2b} |re^{i\theta} - R_h|^{2b}\right)}\right) dr d\theta \tag{4.32}$$

Proposition 4.2.4 *In the presence of a traffic hotspot with a probability measure $dt(r,\theta)$, the throughput CCDFs in the macrocell and in the small cell (with polar coordinates (R_s, θ_s)) are given by the following expressions*

$$\mathbb{P}(\eta \geq l) = \frac{1}{S}\int_{\Lambda_0}^{\Lambda}\int_0^{2\pi} \mathbb{1}\left(cos(\theta - \theta_s) \leq g_2(r)\right) dt(r,\theta) + \frac{1}{S}\int_0^{\Lambda_0}\int_0^{2\pi} \mathbb{1}\left(cos(\theta - \theta_s) \leq g_1(r)\right) dt(r,\theta) \tag{4.33}$$

$$\mathbb{P}(\tilde{\eta} \geq l) = \frac{1}{\tilde{S}}\int_{\Lambda_0}^{R}\int_0^{2\pi} \mathbb{1}\left(cos(\theta - \theta_s) \geq g_3(r)\right) dt(r,\theta) + \frac{1}{\tilde{S}}\int_0^{\Lambda_0}\int_0^{2\pi} \mathbb{1}\left(cos(\theta - \theta_s) > g_1(r)\right) dt(r,\theta) \tag{4.34}$$

with $\Lambda_0 = \min(g^{-1}(\psi(l) - 1), R)$, $\Lambda = \min\left(g^{-1}\left(\psi(l)\right), R\right)$, ψ and g are given in equations (4.22) and (4.8) respectively.

$$g_1(r) = \frac{R_s^2 + r^2 - \kappa^{1/b} r^2}{2rR_s}$$

$$g_2(r) = \frac{R_s^2 + r^2 - \kappa^{\frac{1}{b}} r^2 \left(\psi(l) - g(r)\right)^{-1/b}}{2rR_s}$$

$$g_3(r) = \frac{R_s^2 + r^2 - \left(\psi(l)\kappa\right)^{\frac{1}{b}} r^2 \left(g(r)+1\right)^{-1/b}}{2rR_s}$$

Proof: First, we replace $\gamma(r,\theta)$ in equation (4.20) by its expression given in definition 1. Next, we consider Ω defined by

$$\Omega = \mathbb{1}\left(g(r) + \kappa r^{2b} |re^{i\theta} - R_s e^{i\theta_s}|^{-2b} \leq \psi(l)\right)$$

If $g(r) \geq \psi(l)$, then $\Omega = 0$. Consequently, since g is an increasing function in $[0,\ R]$, $\mathbb{P}(\eta \geq l)$ becomes as follows

$$\begin{aligned}\mathbb{P}(\eta \geq l) =& \frac{1}{S}\int_0^{\Lambda}\int_0^{2\pi} \mathbb{1}\left(\kappa|re^{i\theta} - R_s e^{i\theta_s}|^{-2b} \leq r^{-2b}\right) \times \\ & \mathbb{1}\left(g(r) + \kappa r^{2b}|re^{i\theta} - R_s e^{i\theta_s}|^{-2b} \leq \psi(l)\right) dt(r,\theta)\end{aligned}$$

with $\Lambda = \min\left(g^{-1}\left(\psi(l)\right), R\right)$ and $\psi(l)$ as defined in equation (4.22).

Subsequently, applying elementary transformations yields to

$$\mathbb{P}(\eta \geq l) = \frac{1}{S}\int_0^{\Lambda}\int_0^{2\pi} \mathbb{1}\left(cos(\theta - \theta_s) \leq \min\{g_1(r), g_2(r)\}\right) dt(r,\theta)$$

Then, one has $g_1(r) < g_2(r)$ if and only if $g(r) < \psi(l) - 1$. Knowing that g^{-1} is the inverse function of an increasing one, it follows that $g^{-1}\left(\psi(l)\right) \geq g^{-1}\left(\psi(l) - 1\right)$. Finally, we obtain equation (4.33) which completes the first part of the proof.

The throughput CCDF in the small cell is defined in equation (4.21). We replace $\tilde{\gamma}(r,\theta)$ by its expression given in definition 1 and we apply elementary transformations in order to obtain

$$\mathbb{P}(\tilde{\eta} \geq l) = \frac{1}{\tilde{S}}\int_0^{R}\int_0^{2\pi} \mathbb{1}\left(cos(\theta - \theta_s) > g_1(r)\right) \times \mathbb{1}\left(cos(\theta - \theta_s) \geq g_3(r)\right) dt(r,\theta)$$

Furthermore, one has $g_1(r) < g_3(r)$ if and only if $g(r) > \psi(l) - 1$. Hence, we obtain the expression in equation (4.34). ■

Remark: The advantage of the obtained expressions is the simplification of the integral with the reduction of the double use of the indicator function in the entire disk to become a simple one in each subarea. In fact, numerical computations of the original expressions in equations (4.10), (4.11), (4.13) and (4.14) are time consuming and their simplifications in equations (4.23), (4.26), (4.27), (4.25), (4.33) and (4.34) reduce significantly the computational costs. This kind of expressions are often implemented in planning and performance prediction tools as a complementary layer to the Monte Carlo simulations' module.

4.3 Dynamic level analysis

In this section, we derive performance metrics based on a dynamic level analysis. First, we define the term flow, regularly used in the rest of the analysis, to refer to a session

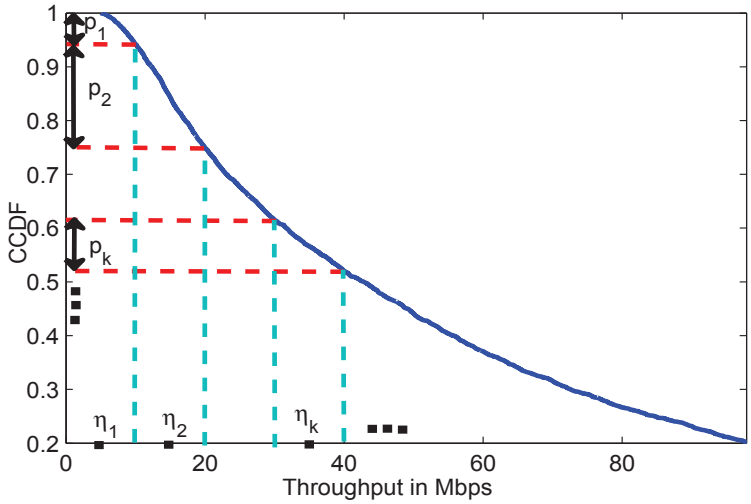

Fig. 4.4 Extraction of $(p_k, \tilde{p}_l)$ and $(\eta_k, \tilde{\eta}_l)$.

where a user initiates and finishes his transmission successfully. It is characterized by a starting time, corresponding to the time the user arrives to the system, and the size of the file to be transferred. We focus, in this work, on the case of best effort traffic. Flows may belong to different classes where the notion of class reflects the different clusters of users experiencing approximately the same radio conditions. For each class, the arrival rate and the peak data rate are extracted from the static level analysis as described in the next subsection.

4.3.1 Inputs extracted from the static level analysis

The distribution of users in each flow class can be extracted from the CQI distribution for a cell already installed and operational. However, during the planning task, this information is not available. The throughput distribution, obtained from the static level analysis in the presence of non-uniform spatial traffic distribution (adapted to real scenarios), can be therefore a relevant alternative to predict the distribution of radio conditions in the studied area. Following this approach, we extract from the throughput CCDF the distribution of radio conditions involving the spatial traffic distribution as follows: First, we denote by p_k and $\tilde{p}_l$ $(k = 1..K$ and $l = 1..L)$ the proportion of users in each class of radio conditions where K and L represent the number of classes in the macrocell and the small cell respectively. Second, in Fig. 4.4, the x-axis of the throughput is discretized in order to divide users into classes of flows according to their peak data rates. Each class is characterized by η_k for the macrocell and $\tilde{\eta}_l$ for the small cell which corresponds to the mean (or the max [30, 32]) of peak data rates in this

class. Third, the proportion of users p_k in class k (or p_l in class l for the small cell) is directly extracted from the y-axis by simply taking the value of $\mathbb{P}(\eta_{min,k} \leq \eta \leq \eta_{max,k})$, where $\eta_{min,k}$ and $\eta_{max,k}$ represent the boundaries of the interval of class k peak data rate.

4.3.2 Traffic characteristics and dynamic system model

For both cells, random arrivals of data flows are modeled by multi-class flows; the flow classes are sorted according to the associated peak data rate η_k (or $\tilde{\eta}_l$ for small cell) in an increasing order. All users of the same class have approximately the same data rate when scheduled in the same cell, however the data rate differs from a flow class to another one. We assume that each flow of class k for macrocell and l for small cell arrives to the network following a Poisson process of intensity $\lambda_k = \lambda p_k = \lambda_{Tot} \frac{S}{S+\tilde{S}} p_k$ in the macrocell and $\tilde{\lambda}_l = \tilde{\lambda} \tilde{p}_l = \lambda_{Tot} \frac{\tilde{S}}{S+\tilde{S}} \tilde{p}_l$ in the small cell, where λ_{Tot} is the total arrival intensity in the studied system.

Flow sizes, denoted by σ, are assumed to be mutually independent and exponentially distributed with mean σ_0 in Mbits. Traffic is assumed to be FTP-like data. Such elastic flows result from the transfer of electronic documents like peer-to-peer file sharing, typically characterized by a file size and a variable duration which depends on the network capacity and load, and also on the radio conditions of the user.

Cell capacity is assumed to be shared between all transmissions according to a multi-class $M/G/1$ Processor Sharing discipline wherein resources are equally shared between all the users and all the classes. Moreover, the service in the macrocell and the small cell are coupled because the peak data rate of the macrocell users and small cell ones depends on the existence of an active user in the small cell and in the macrocell, respectively. Indeed, macrocell interference on small cell users is accounted for when there is at least one active user in the macrocell. Similarly, small cell interference on macrocell users is accounted for when there is at least one active user in the small cell. Therefore, the service data rates η_k and $\tilde{\eta}_l$ of each class take each one two values depending on the presence of an active user in the interfering cell. Their expressions

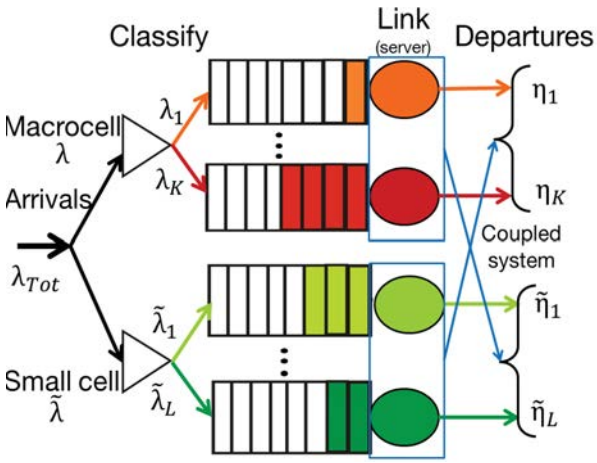

Fig. 4.5 Dynamic system model.

are given as follows

$$\forall k = 1..K,\ \eta_k = \begin{cases} \eta_{k,0} \text{if no user is served by the small cell} \\ \eta_{k,1} \text{otherwise} \end{cases} \tag{4.35}$$

$$\forall l = 1..L,\ \tilde{\eta}_l = \begin{cases} \tilde{\eta}_{l,0} \text{if no user is served by the macrocell} \\ \tilde{\eta}_{l,1} \text{otherwise} \end{cases} \tag{4.36}$$

where $\eta_{k,0}$ is given by the throughput distribution curve of Subsection 4.2.1 (equation (4.25)) and $\eta_{k,1}$ is given in Subsection 4.2.2 (equation (4.33)). For the small cell, $\tilde{\eta}_{l,0}$ is simply given by deleting the contribution of the macrocell in the interference experienced by the small cell's UEs. $\tilde{\eta}_{l,1}$ is also derived from the throughput distribution curve of Subsection 4.2.2 (equation (4.34)). An explanatory scheme of the dynamic system model and its specifications is depicted in Fig. 4.5.

4.3.3 Performance analysis

Preliminary analysis of the model

We denote by ρ and $\tilde{\rho}$ the load of the macrocell and the small cell respectively. In the quasi-stationary regime, i.e. the rate processes evolve on an infinitely slow time scale, ρ and $\tilde{\rho}$ are given by

$$\rho = \sum_{k=1}^{K} \lambda_k \mathbb{E}\left(\frac{\sigma}{\eta_k}\right)\ ,\ \tilde{\rho} = \sum_{l=1}^{L} \tilde{\lambda}_l \mathbb{E}\left(\frac{\sigma}{\tilde{\eta}_l}\right) \tag{4.37}$$

At instant t, we denote by $n_k(t)$ and $\tilde{n}_l(t)$ the number of flows in each class of the macrocell and the small cell respectively. Then, $(n(t),\tilde{n}(t)) = (n_k,\tilde{n}_l)_{\ k=1..K,l=1..L}$ represents an irreducible Markov process (Fig. 4.6) with non-null transition rates from state $(n,\tilde{n})$ to state $(m,\tilde{m})$ given by

$$
\begin{aligned}
&q((n,\tilde{n}),(n+e_k,\tilde{n})) = \lambda_k \\
&q((n,\tilde{n}),(n-e_k,\tilde{n})) = \mathbb{1}(n_k>0)\frac{\eta_k}{|n|} \\
&q((n,\tilde{n}),(n,\tilde{n}+e_l)) = \tilde{\lambda}_l \\
&q((n,\tilde{n}),(n,\tilde{n}-e_l)) = \mathbb{1}(\tilde{n}_l>0)\frac{\tilde{\eta}_l}{|\tilde{n}|}
\end{aligned}
$$

where the states $n=(n_1,..,n_K)$ and $\tilde{n}=(\tilde{n}_1,..,\tilde{n}_L)$ respectively in the macrocell and the small cell represent the number of simultaneously active flows in each flow class. We denote by $|n| = \sum_{k=1}^{K} n_k$ and $|\tilde{n}| = \sum_{l=1}^{L} \tilde{n}_l$ the cardinality of all the active flows in the macrocell and the small cell respectively and e_k or e_l the row vectors with all components equal to 0 except the k^{th} and l^{th} one equal to 1.

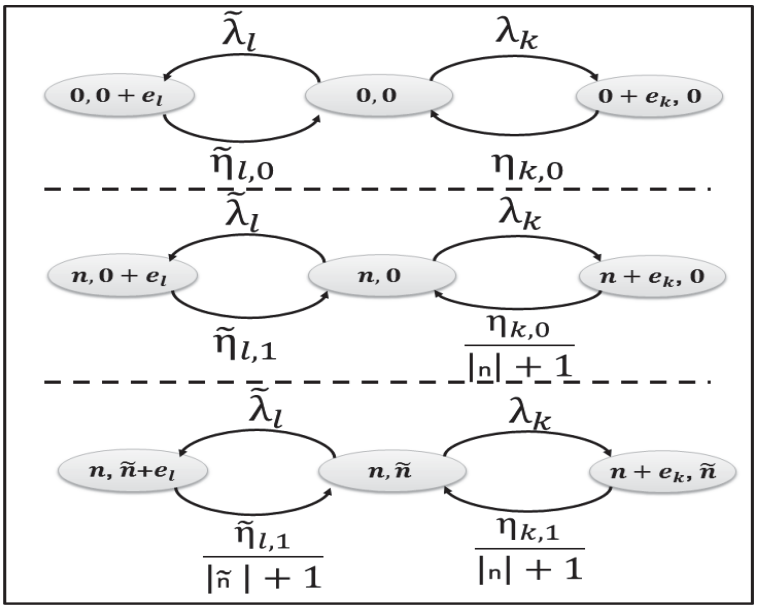

Fig. 4.6 Markov process of the Macro-Small cells system.

The transition from state $(n,\tilde{n})$ to $(n+e_k,\tilde{n})$ means that a new macrocell user arrived with radio conditions of class k. Likewise, the transition from state $(n,\tilde{n})$ to $(n,\tilde{n}+e_l)$ means that a new small cell user arrived with radio conditions of class l. However, transition from state $(n,\tilde{n})$ to $(n-e_k,\tilde{n})$ signifies that a user of class k

attached to the macrocell has successfully finished his service. The same applies for the transition from $(n,\tilde{n})$ to $(n,\tilde{n}+e_l)$ where a user of class l in the small cell completed its transmission and quit the system.

Furthermore, we take

$$q((n,\tilde{n}),(n,\tilde{n})) = -\sum_{(m,\tilde{m})\neq(n,\tilde{n})} q((n,\tilde{n}),(m,\tilde{m})) \tag{4.38}$$

Knowing that $\rho,\tilde{\rho}<1$, there exists a unique invariant probability distribution $\pi_{n,\tilde{n}}$, $(n,\tilde{n})\in\mathbb{Z}_+^K\times\mathbb{Z}_+^L$ satisfying

$$\pi Q = 0 \quad and \sum_{(n,\tilde{n})\in\mathbb{Z}_+^K\times\mathbb{Z}_+^L} \pi_{n,\tilde{n}} = 1 \tag{4.39}$$

where $\pi=[\pi_{n,\tilde{n}}]_{\ (n,\tilde{n})\in\mathbb{Z}_+^K\times\mathbb{Z}_+^L}$ is the row vector composed of the stationary probabilities in each state and $Q=[q((n,\tilde{n}),(m,\tilde{m}))]_{\ n,m\in\mathbb{Z}_+^K\ and\ \tilde{n},\tilde{m}\in\mathbb{Z}_+^L}$ is the matrix of transition rates.

The relative balance equations of the defined Markov process are given by

$$\begin{aligned}&\sum_{k=1}^{K}\left(\mathbb{1}(n_k>0)\lambda_k\pi_{n-e_k,\tilde{n}}+\frac{\eta_k}{|n|+1}\pi_{n+e_k,\tilde{n}}\right)+\sum_{l=1}^{L}\left(\mathbb{1}(\tilde{n}_l>0)\tilde{\lambda}_l\pi_{n,\tilde{n}-e_l}+\frac{\tilde{\eta}_l}{|\tilde{n}|+1}\pi_{n,\tilde{n}+e_l}\right)\\&=\pi_{n,\tilde{n}}\left(\sum_{k=1}^{K}\mathbb{1}(n_k>0)\frac{\eta_k}{|n|}+\lambda_k+\sum_{l=1}^{L}\mathbb{1}(\tilde{n}_l>0)\frac{\tilde{\eta}_l}{|\tilde{n}|}+\tilde{\lambda}_l\right)\end{aligned} \tag{4.40}$$

Resolution of the model

The interaction between the macrocell and the small cell with a multi-class PS system makes an exact analysis very complex and impractical since the derivation of the exact solution to the system of equations defined in (4.39) or in (4.40) is very difficult. Therefore, we propose, for tractability issues, to transform the system model as described next.

Lemma 4.3.1 *Under the stability condition, i.e. $\rho,\tilde{\rho}<1$, the average loads in equation (4.37) is given by*

$$\rho = 1-P_0 \quad , \quad \tilde{\rho} = 1-\tilde{P}_0 \tag{4.41}$$

where P_0 and $\tilde{P}_0$ are the probabilities of the steady states where no user is in the macrocell and the small cell respectively.

Proof: As largely considered in literature, the load is equal to the percentage of time where the cell's resources are occupied by UEs. In the studied model, if at least one

UE is active, all the available resources in the cell will be occupied by it or shared with other UEs since the traffic generated is elastic. Based on this elastic sharing process, the load is equal to the percentage of time when there is at least one active flow in the cell. Hence, $\rho = 1 - P_0,\ \tilde{\rho} = 1 - \tilde{P}_0$. ■

In the studied system, macrocell flows experience permanent interference-limited service rate $\eta_{k,1}$ during a proportion $1-\tilde{P}_0$ of the total observation time and interference-free service rate $\eta_{k,0}$ during the rest of the observation time (a proportion of $\tilde{P}_0$). The same applies for the small cell. It follows that, based on the expression of the load given in equation (4.37) and under the stability condition, ρ becomes as follows

$$\rho = \sum_{k=1}^{K} \left[\tilde{P}_0 \frac{\lambda_k \sigma_0}{\eta_{k,0}} + \left(1 - \tilde{P}_0\right) \frac{\lambda_k \sigma_0}{\eta_{k,1}} \right] \tag{4.42}$$

Similarly, the load $\tilde{\rho}$ in the small cell is given by

$$\tilde{\rho} = \sum_{l=1}^{L} \left[P_0 \frac{\tilde{\lambda}_l \sigma_0}{\tilde{\eta}_{l,0}} + (1 - P_0) \frac{\tilde{\lambda}_l \sigma_0}{\tilde{\eta}_{l,1}} \right] \tag{4.43}$$

Theorem 4.3.1 *In the coupled multi-class processor sharing system defined above, the stationary probability of having at least one active flow in the macrocell (in the small cell respectively) is equal to the cell load. The latter is given by*

$$\rho = \frac{\sum\limits_{k=1}^{K} \left[\frac{\lambda_k \sigma_0}{\eta_{k,0}} + \left(\frac{\lambda_k \sigma_0}{\eta_{k,1}} - \frac{\lambda_k \sigma_0}{\eta_{k,0}} \right) \times \sum\limits_{l=1}^{L} \left[\frac{\tilde{\lambda}_l \sigma_0}{\tilde{\eta}_{l,0}} \right] \right]}{1 - \sum\limits_{k=1}^{K} \left(\frac{\lambda_k \sigma_0}{\eta_{k,1}} - \frac{\lambda_k \sigma_0}{\eta_{k,0}} \right) \times \sum\limits_{l=1}^{L} \left(\frac{\tilde{\lambda}_l \sigma_0}{\tilde{\eta}_{l,1}} - \frac{\tilde{\lambda}_l \sigma_0}{\tilde{\eta}_{l,0}} \right)} \tag{4.44}$$

$$\tilde{\rho} = \frac{\sum\limits_{l=1}^{L} \left[\frac{\tilde{\lambda}_l \sigma_0}{\tilde{\eta}_{l,0}} + \left(\frac{\tilde{\lambda}_l \sigma_0}{\tilde{\eta}_{l,1}} - \frac{\tilde{\lambda}_l \sigma_0}{\tilde{\eta}_{l,0}} \right) \times \sum\limits_{k=1}^{K} \left[\frac{\lambda_k \sigma_0}{\eta_{k,0}} \right] \right]}{1 - \sum\limits_{l=1}^{L} \left(\frac{\tilde{\lambda}_l \sigma_0}{\tilde{\eta}_{l,1}} - \frac{\tilde{\lambda}_l \sigma_0}{\tilde{\eta}_{l,0}} \right) \times \sum\limits_{k=1}^{K} \left(\frac{\lambda_k \sigma_0}{\eta_{k,1}} - \frac{\lambda_k \sigma_0}{\eta_{k,0}} \right)} \tag{4.45}$$

with σ_0, λ_k, $\tilde{\lambda}_l$, $\eta_{k,0}$, $\tilde{\eta}_{l,0}$, $\eta_{k,1}$ and $\tilde{\eta}_{l,1}$ are as defined in Subsection 4.3.2.

Proof: In order to find equation (4.44), we take, at first, the expression of the load ρ given in equation (4.42). Based on the equality given in Lemma 4.3.1, we replace $\tilde{P}_0$ by $1-\tilde{\rho}$ in equation (4.42). Then, $\tilde{\rho}$ is also replaced by its expression given in equation

(4.43) and we obtain the following identity, equivalent to equation (4.44),

$$\rho = \sum_{k=1}^{K} \left[\frac{\lambda_k \sigma_0}{\eta_{k,0}} + \left(\frac{\lambda_k \sigma_0}{\eta_{k,1}} - \frac{\lambda_k \sigma_0}{\eta_{k,0}} \right) \times \sum_{l=1}^{L} \left[\frac{\tilde{\lambda}_l \sigma_0}{\tilde{\eta}_{l,0}} + \left(\frac{\tilde{\lambda}_l \sigma_0}{\tilde{\eta}_{l,1}} - \frac{\tilde{\lambda}_l \sigma_0}{\tilde{\eta}_{l,0}} \right) \rho \right] \right] \tag{4.46}$$

Transforming equation (4.46) to extract ρ yields equation (4.44).
The same steps are followed to obtain equation (4.45). ■

Based on the expressions given in equations (4.44) and (4.45), the stationary distribution is derived in the following proposition.

Proposition 4.3.1 *Under the stability condition ($\rho, \tilde{\rho} < 1$), the stationary distribution of the state $(n, \tilde{n})$ becomes equal to*

$$\pi_{n,\tilde{n}} = \frac{|n|!(1-\rho)}{\prod_{k=1}^{K} (\tilde{\rho} n_k)! \left((1-\tilde{\rho}) n_k\right)!} \frac{|\tilde{n}|!(1-\tilde{\rho})}{\prod_{l=1}^{L} (\rho \tilde{n}_l)! \left((1-\rho)\tilde{n}_l\right)!} \prod_{k=1}^{K} \frac{(\lambda_k \sigma_0)^{n_k}}{\eta_{k,0}^{(1-\tilde{\rho})n_k} \eta_{k,1}^{\tilde{\rho} n_k}} \prod_{l=1}^{L} \frac{\left(\tilde{\lambda}_l \sigma_0\right)^{\tilde{n}_l}}{\tilde{\eta}_{l,0}^{(1-\rho)\tilde{n}_l} \tilde{\eta}_{l,1}^{\rho \tilde{n}_l}} \tag{4.47}$$

Proof: For each class k of flows in the macrocell, the queuing system can be modeled with a proportion $\tilde{P}_0$ of flows experiencing a peak data rate equal to $\eta_{k,0}$ and a proportion $1 - \tilde{P}_0$ of flows experiencing a peak data rate equal to $\eta_{k,1}$. The same applies for the small cell. The system is partially modified and behaves like a network with two types of classes in both the macrocell and the small cell: macro and small cell flow classes suffering all the time from interference coming from the small cell and the macrocell respectively and flow classes not affected by this interference. Consequently, the service rate in each cell does not depend anymore on the queue state of the other interfering cell. Under the stability condition and following [74, Chap. 7, p. 119], the stationary distributions are directly derived as in equation (4.47), which completes the proof. ■

Remark: Considering more heterogeneity in the traffic distribution can be depicted by two main possible scenarios: The first one consists in adding a uniform traffic distribution in addition to the hotspot distribution. In this case, analysis is not significantly altered since a uniform traffic will approximately add the same proportion of users in each class of flows which leads to obtain the same results but for higher value of $\lambda_{Tot} = \lambda_{Hotspot} + \lambda_{Uniform}$. The second scenario consists in considering more than one traffic hotspot (but not too many because otherwise the traffic becomes as if

it is uniformly distributed in the macrocell). Despite its inability to respond to the main objective of this study for the reasons cited in Subsection 4.1.1, the scenario of more than one traffic hotspot can be a particular case of our study and would simplify the system mainly for the dynamic level analysis. For instance, if the deployed small cell is serving a traffic hotspot and the macrocell is serving other traffic hotspots, then the load in the macrocell will tend to 1. Consequently, the coupling defined in equation (4.36) will disappear since there will be always at least one active user in the macrocell.

From equation (4.47) and following [32], the mean number of flows in each class is equal to

$$N_k = \tilde{\rho}\frac{\lambda_k \sigma_0}{(1-\rho)\eta_{k,1}} + (1-\tilde{\rho})\frac{\lambda_k \sigma_0}{(1-\rho)\eta_{k,0}} \tag{4.48}$$

$$\tilde{N}_l = \rho\frac{\tilde{\lambda}_l \sigma_0}{(1-\tilde{\rho})\tilde{\eta}_{l,1}} + (1-\rho)\frac{\tilde{\lambda}_l \sigma_0}{(1-\tilde{\rho})\tilde{\eta}_{l,0}} \tag{4.49}$$

Applying Little's law to the presented ergodic process implies that the mean service time of class k flows in the macrocell is $\tau_k = \frac{N_k}{\lambda_k}$. For class l in the small cell, it is equal to $\tilde{\tau}_l = \frac{\tilde{N}_l}{\tilde{\lambda}_l}$.

Let υ_k and $\tilde{\upsilon}_l$ be the stationary throughputs of class k flows in the macrocell and class l flows in the small cell, respectively. Then, from equations (4.42), (4.43) and the expression of service time for each class, we have the following identities:

$$\upsilon_k = \tilde{\rho}\eta_{k,1}(1-\rho) + (1-\tilde{\rho})\eta_{k,0}(1-\rho) \tag{4.50}$$

$$\tilde{\upsilon}_l = \rho\tilde{\eta}_{l,1}(1-\tilde{\rho}) + (1-\rho)\tilde{\eta}_{l,0}(1-\tilde{\rho}) \tag{4.51}$$

According to the previous expressions, when the load is very small in the macrocell, the flow throughput υ_k is at its maximum. It then decreases linearly with its own cell load. When the load is very small in the small cell, the flow throughput in the macrocell is at its maximum and decreases linearly with the load in the small cell.

4.4 Numerical results

We now evaluate the different performance metrics of the studied scenarios at static and dynamic levels. We show in Table 4.1 the most relevant parameters used in the numerical evaluation (taken from the 3GPP LTE-Advanced specifications [75] and also from operational network settings). In the legends of the obtained figures, MC and SC stand for macrocell and small cell respectively, HS stands for the traffic hotspot and

Table 4.1 Parameters' configuration.

Macro deployment	infinite hexagonal with $\delta = 1$ km
Association	UE associated to highest RSRP
Pathloss model MtoUE	$151 + 37.6log_{10}(d_{km})$
Pathloss model StoUE	$148 + 36.7log_{10}(d_{km})$
BS power	Macro:46dBm, Small:30dBm
Antenna gain with cable loss	Macro:18dBi, Small:6dBi
Antenna mask	Macro:Omni, Small:Omni
Frequency/Bandwidth	2.6 Ghz / 20 Mhz
Thermal noise per Hertz	-174dBm/Hz
Noise figure	8dB
UE category/Throughput	3 / $\eta_0 = 98Mbps,\ K_1 = 0.85,\ K_2 = 1.9$
UE antenna gain/Body loss	0dB / 2dB
File size/Scheduling/Traffic type	2Mb / PS (Round Robin Scheduling) / FTP

perfect SC means that the small cell is deployed in the center of the hotspot (perfect in terms of positioning). MUeTh refers to the mean user throughput.

4.4.1 Static level results

In this section, we firstly vary the position of the hotspot by varying R_h and then θ_h and determine the minimum distance to the macro BS from which the small cell deployment can be considered as an efficient solution. We assume the error of small cell positioning to be constant relative to the position of the hotspot, taking the following values: error of 0 meters (perfect hotspot localization), 60 meters (accuracy provided in [20]) and 120 meters (current accuracy when using probes) between the variables R_h and R_s and we suppose that θ_s is equal to θ_h (equal to $\frac{\pi}{3}$). Then, the mean user throughput is calculated as a function of R_h. Next, we take $R_s = R_h = 0.4km$, and we consider the error between θ_h and θ_s to be equal to 0, $\pi/6$ and $\pi/3$ respectively and we evaluate the same performance metrics as in the first part of the simulations.

After that, we secondly fix the position of the traffic hotspot in $0.35e^{i\frac{\pi}{6}}$ and $0.52e^{i\frac{\pi}{2}}$ respectively. Then, the mean user throughput and the absorption coefficient are plotted as a function of the small cell position by varying R_s (with $\theta_s = \theta_h$) at first and then by varying θ_s (with $R_s = R_h$).

From Fig. 4.7a, we observe that deploying a small cell near the macrocell does not generate additional capacity gains since the interference in this case is very high compared to the SNR received either from the serving small cell or macrocell. In fact, for a traffic hotspot in position of less than 300 meters far from the macrocell, the evaluation of the impact of bad localization of the traffic hotspot is worthless and not

justified because the offloading gain[2] is negative even with a perfect positioning. Hence, the deployment of a small cell near the macrocell does not help to offload the traffic and it deteriorates the throughput in the macrocell. However, the deployment of a small cell improves significantly the overall performance of the macrocell in the presence of the traffic hotspot at cell edge. In the latter case, the small cell still generates positive offloading gains even when its position does not match exactly with the hotspot's one.

Moreover, from Fig. 4.7b, it is clear that when the hotspot is in the center of the cell,

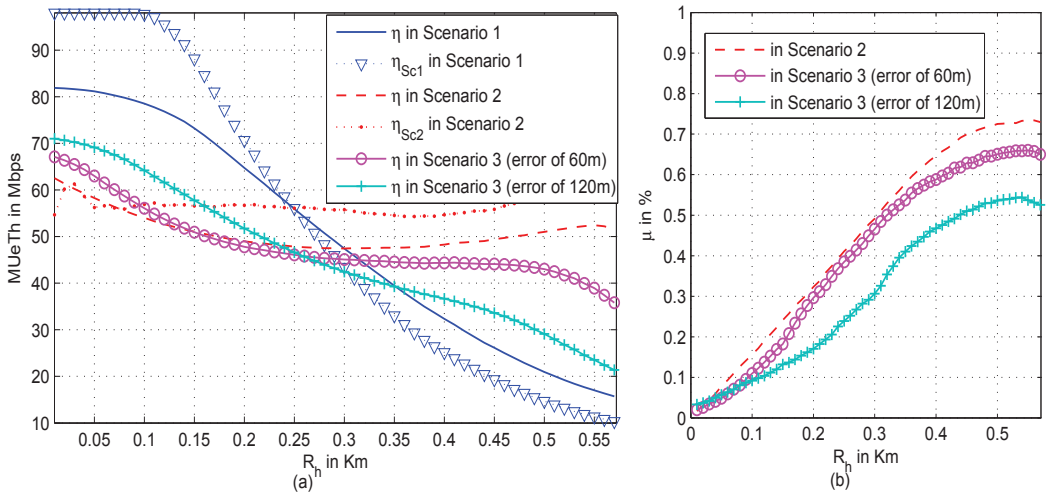

Fig. 4.7 The mean user throughput (a) and the absorption coefficient (b) for different locations of the traffic hotspot with varying R_h.

the RSRP received from the macrocell is often higher than the RSRP received from the small cell. As a result, the absorption coefficient relative to the presence of the small cell is very small even with a perfect positioning of this latter. This coefficient is more important when the hotspot is at cell edge. Moreover, deploying a small cell with errors in its positioning remains a useful solution to offload an important percentage of traffic located at cell edge.

We also notice that for a hotspot in the cell center, a small percentage of UEs can be offloaded by the small cell but the mean throughput in the small cell (denoted by η_{Sc2}) in Scenario 2 is not improved compared to the mean throughput in Scenario 1 (denoted by η_{Sc1} which means that the mean user throughput is calculated only in the same region as the served area by the small cell in Scenario 2). This is due to the high interference in the center between the small cell and the macrocell. This observation is

[2]The offloading gain is the extra capacity effectively exploited in the deployed small cell. It is defined by $\iota = \frac{\eta_{Scenario\ 2,3} - \eta_{Scenario\ 1}}{\eta_{Scenario\ 1}}$

deduced from the extra curves represented with triangles for η_{Sc1} and dotted line for η_{Sc2} in Fig. 4.7a.

We observe in Fig. 4.8a that the mean throughput in Scenario 2 is higher than that in Scenario 1. However, when we introduce an error of $\pi/6$, the mean throughput becomes lower because most of the traffic is served by the macrocell and the small cell will play the role of an interfering cell. When the error is taken higher than $\pi/6$, the mean user throughput is improved since the interference is attenuated.

Fig. 4.8b shows that when θ_h is different from θ_s and especially if this difference

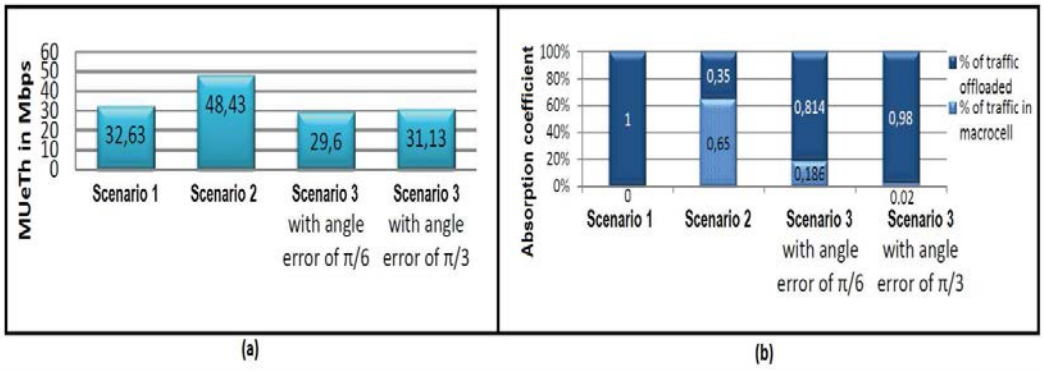

Fig. 4.8 The mean user throughput (a) and the absorption coefficient (b) for different locations of the hotspot with varying θ_h.

is high, the absorption coefficient is reduced as compared to the case of a perfectly deployed small cell.

In Fig. 4.9a, we compare the mean user throughput in the presence of a traffic hotspot and with varying the position of the small cell. When the small cell is deployed near the macrocell, the traffic located in the cell center (hotspot located at $0.35Km$ far from the macrocell) and served by the macrocell will be significantly interfered by the small cell. If this small cell is deployed near the traffic hotspot, most of the traffic will be offloaded by the small cell and the mean user throughput is improved. However, we observe also that when the distance between R_s and R_h increases, the mean user throughput is approximately constant (function of R_h) and its value is equal to the mean user throughput of a network without small cells (offloading gain near 0%). This means that when the small cell is deployed far from the traffic hotspot and from the macrocell, the performance of Scenario 1 is approximately the same as that of Scenario 3.

On the other hand, we observe that when the traffic hotspot is in the cell edge, the small cell is an appropriate solution to offload the congesting traffic and errors of small cell positioning are more tolerated compared to the case of a hotspot located near the

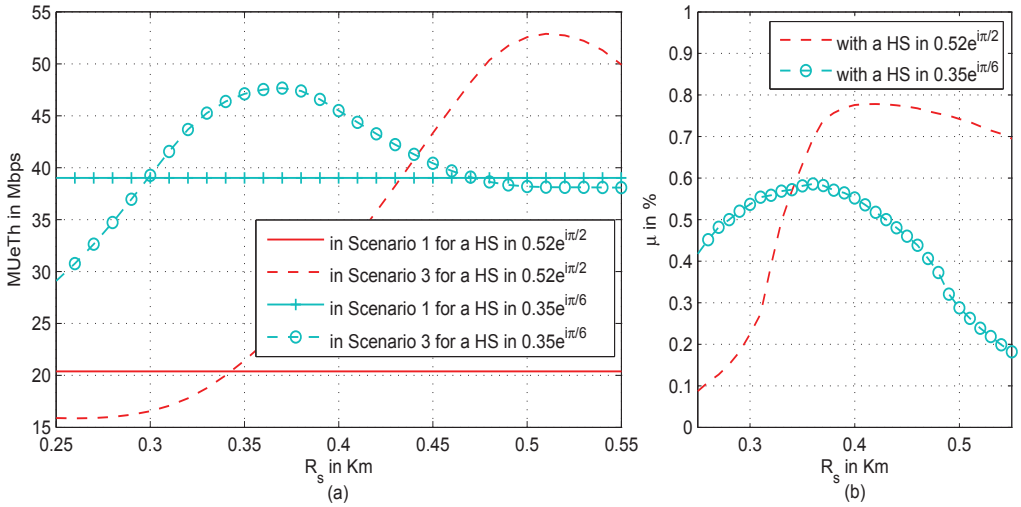

Fig. 4.9 The mean user throughput (a) and the absorption coefficient (b) for different locations of the small cell relative to the hotspot position with varying R_s.

macrocell position. In fact, for a traffic hotspot $520m$ far from the macrocell, the small cell still improves the mean user throughput in the macrocell even with an error of hotspot localization of $160m$ which is not the case for a hotspot $350m$ far from the macrocell. In such scenarios, some traffic hotspot localization techniques [20, 21] can be implemented and used in operational small cell planning tools.

Results in Fig. 4.9b show that more traffic is served by the small cell when its coordinates approaches those of the hotspot. The absorption coefficient is higher for a hotspot at cell edge and is reduced when the hotspot gets nearer to the macrocell.

Fig. 4.10a shows that when the hotspot is in the cell edge, the performance of the macrocell is improved with deploying a small cell with $\theta_s - \theta_h$ less than a certain threshold. This can be explained by the fact that UEs in bad radio conditions and previously taken in charge by the macrocell are now offloaded to the small cell which is near the traffic hotspot. Moreover, we observe that the impact of error related to θ_s is very important and may cause significant degradation of the system performance when the distance between the hotspot and the macrocell increases. This can be explained by the fact that the distance between the small cell and the hotspot is proportionally increased with the difference between θ_s and θ_h.

Fig. 4.10b consolidates the different observations of Fig. 4.10a and it further shows that the absorption coefficient is more important when the hotspot is at cell edge and the error of small cell positioning is more tolerated.

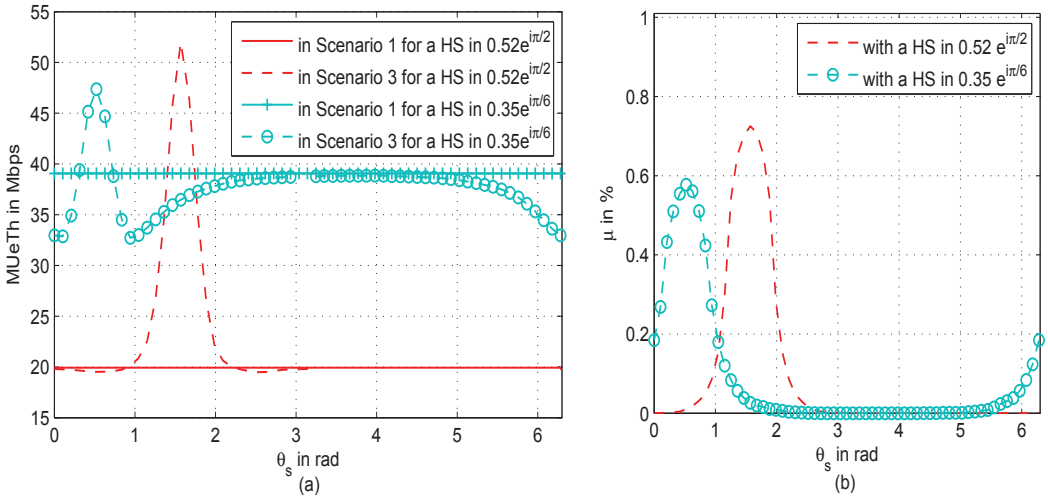

Fig. 4.10 The mean user throughput (a) and the absorption coefficient (b) for different locations of the small cell relative to the hotspot position with varying θ_s.

In the rest of the numerical results, we consider a specific scenario ($R_h = 0.5, \theta_h = \frac{\pi}{3}$) where the traffic hotspot is in an area where the deployment of a small cell is more eligible to generate positive gains. Like in the previous results, we fix an error of 0 meters, 60 meters and 120 meters respectively between the variables R_h and R_s. θ_s and θ_h are taken equal to $\frac{\pi}{3}$ since the small cell deployment is practically insensitive to the angle coordinate as we verified in [27].

The throughput CCDF is plotted for the different proposed scenarios in Fig. 4.11. From Fig. 4.11, we observe that the perfect positioning of the deployed small cell improves significantly the capacity of the system (composed of the macrocell and the small cell deployed within its covered area) since user locations with degraded throughputs will be covered by the small cell and hence will experience a better SINR level. Moreover, we note that, even with taking into consideration the imperfect traffic hotspot localization (60 meters), the system capacity is improved compared to the scenario where only macrocells are operating in the studied area. However, when the distance between the small cell and the hotspot increases due to inaccurate traffic hotspot localization technique, the solution of deploying small cells becomes useless because the cell throughput distribution is not improved anymore compared to a network without small cells. Based on these results, we conclude that the efficiency of small cell deployment depends mainly on the precision of the traffic hotspot localization process in addition to the position of the hotspot with respect to the macrocell's position.

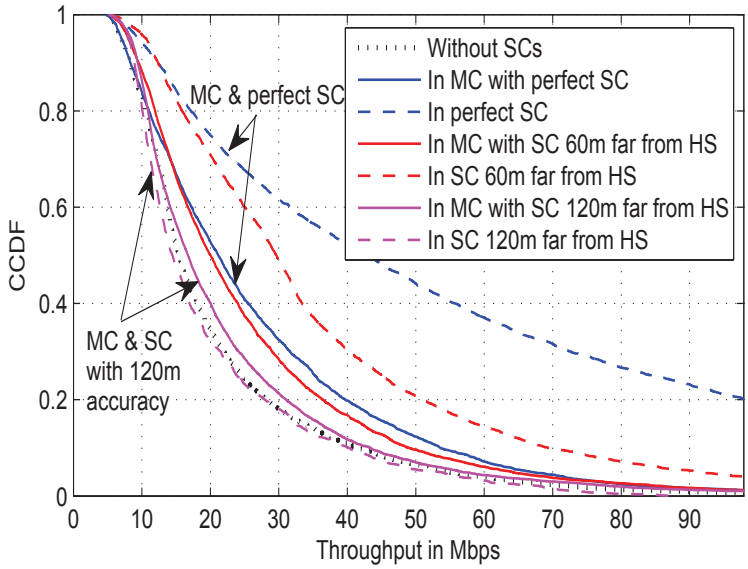

Fig. 4.11 Throughput CCDF in the 3 scenarios defined in the static level study.

4.4.2 Dynamic level results

We now turn to the system performance at the dynamic level. In Fig. 4.12, we plot, for the different studied scenarios, the evolution of the load in the macrocell and the small cell when the arrival intensity λ_{Tot} increases. In addition to the analytical expressions of the load, simulations are also performed so as to validate the obtained expressions.

From Fig. 4.12, we observe that the load is significantly reduced with the deployment of a small cell even when it is not perfectly located near the hotspot. Moreover, we notice that the load in the small cell is less than the load in the macrocell. This can be explained by the fact that the traffic hotspot is in the cell edge and interference experienced by users in cell edge is more significant when they are attached to the macrocell compared to users attached to the small cell.

Furthermore, we observe that, when the small cell is slightly deviated from its perfect position, the load in the macrocell reduces and the load in the small cell increases. In fact, when the small cell is deployed in the center of the traffic hotspot, it absorbs most of the traffic which leads to more interference on the macrocell users due to the coupling between the macrocell and the small cell.

On the other hand, the load in the perfectly deployed small cell is marginally reduced compared to the load of the small cell slightly deviated from its perfect position (60 meters far from the hotspot). This is due to the increase of the proportion of users having good radio conditions in the perfectly deployed small cell. However, when this

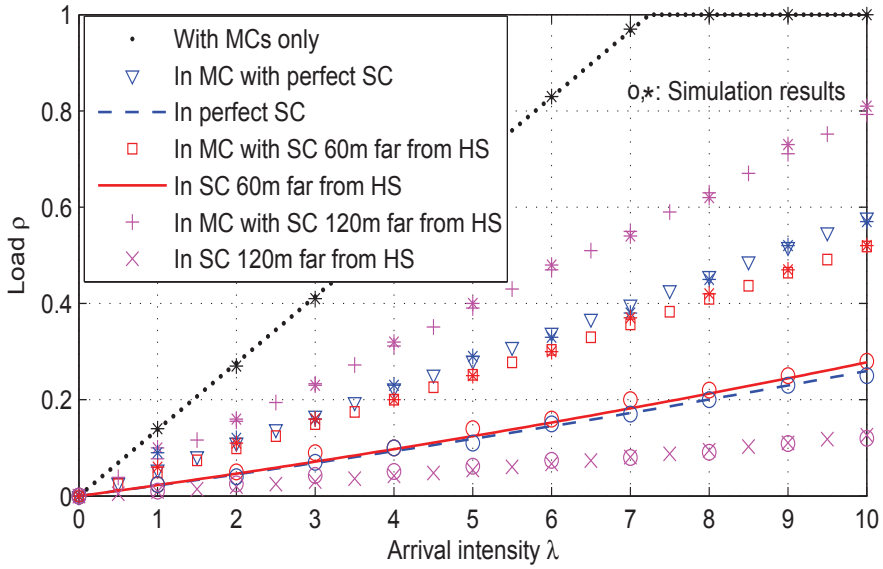

Fig. 4.12 The load in the small cell and the macrocell.

latter is slightly far from its perfect position, a significant proportion of traffic becomes with degraded radio conditions while its absorption coefficient still remain more or less the same as for perfectly deployed small cell (see Fig. 4.7b). In addition, when the proportion of traffic absorbed by a small cell 120 meters far from the hotspot is significantly reduced (see Fig. 4.7b), its load becomes smaller than the load in perfectly deployed small cell even with users exclusively located at small cell edge. Nevertheless and still in the scenario with small cell 120 meters far from the hotspot, the load of the macrocell is significantly increased compared to the perfect deployment scenario.

In Figs. 4.13 and 4.14, we plot the average number of active flows and the mean flow throughput in the macrocell and the small cell. The analytical expressions derived from equations (4.49) and (4.51) are compared with simulation results and we show that the approximations made are accurate for evaluating the system performance. The same conclusions as before regarding the load are recovered for the average number of active flows. First, when the small cell is significantly far from the hotspot, the mean number of active flows in the small cell is reduced compared to a perfectly deployed small cell. On the other hand, this metric is increased for the macrocell when the small cell is not perfectly positioned near the hotspot since it will take more traffic. Besides, more active flows are observed in macrocell with perfect small cell positioning than in the case of a slightly deviated small cell. In addition to the explanation given in the evaluation of the load, this is related to the large proportion of users that are at the small cell edge and attached to the macrocell (see the absorption coefficient in Fig.

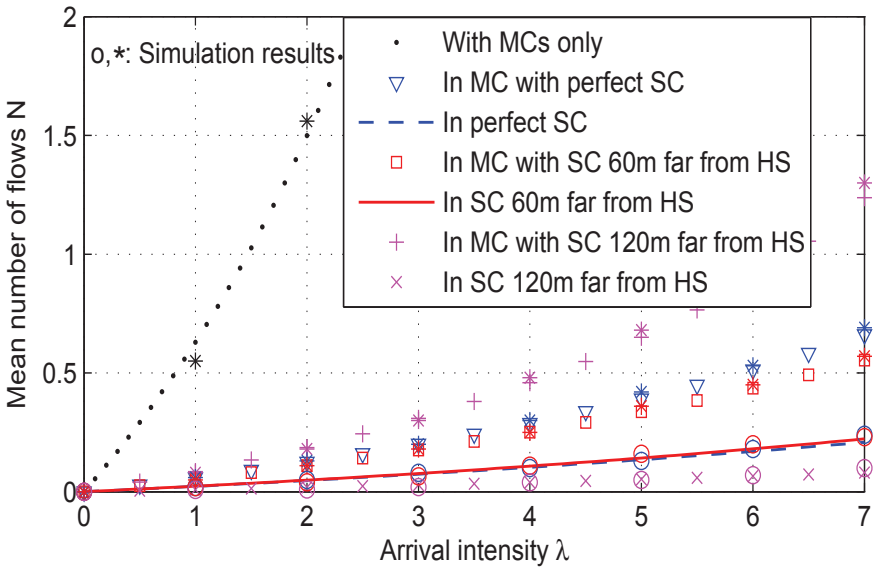

Fig. 4.13 Average number of active flows.

4.7b). And so, these users are highly interfered by the small cell and will stay longer in the system to complete their transfers. Results from Fig. 4.14 confirm once again the different observations concluded from the load and mean number of flows' analysis. Contrary to the static level results, the mean flow throughput in the small cell and the macrocell is improved when the traffic hotspot is partially absorbed by the small cell (the small cell is not deployed exactly in the center of the hotspot). This can be further explained by the fact that more users will share the small cell resources when it is perfectly deployed and so their transmission rates will be slightly reduced. We also notice that the flow throughput in the small cell deployed far enough from the hotspot is improved conversely to the flow throughput in the macrocell. The increase of the throughput in the small cell is reasonable since the number of active flows is reduced and the cell resources are divided between a smaller number of flows (see the absorption coefficient in Fig. 4.7b).

Finally, we conclude that deploying small cells represents always a good way to offload traffic but improving the efficiency of this solution depends on many constraints in addition to those identified in the static level results. First, the small cell must cover all the hotspot in order to reduce the proportion of macrocell users located near the small cell and experiencing high interference from this latter. Second, the capacity of the small cell and the size of its carried traffic are also important to take as an input in the HetNet planning process. Third, in the case where the small cell does not completely cover the hotspot, the interference coming from the small cell on macrocell

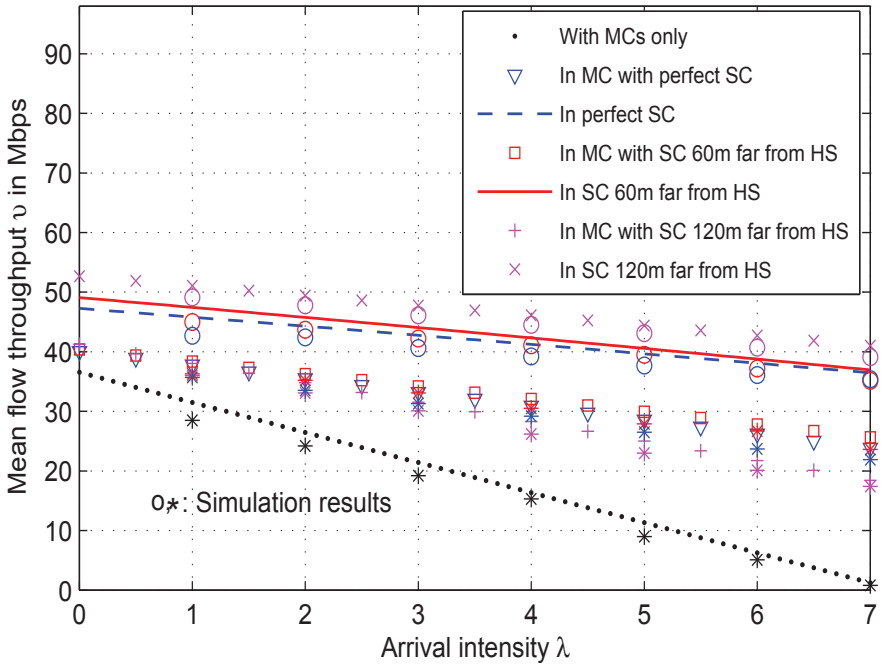

Fig. 4.14 Mean flow throughput.

users represents a crucial limitation leading thus to the need of improving interference mitigation techniques.

4.5 Concluding remarks

We have studied, in this chapter, the impact of deploying a small cell in the presence of traffic hotspot inside a macrocell. We have firstly performed our modeling following a static level analysis to assess the mean throughput and its distribution and also the absorption coefficient of the small cell. We have secondly investigated the dynamic level analysis where users come to the system at random times and leave it after being served with data rates derived from the static level part.

If one considers analysis at static level only, results show that the efficiency of deploying small cells to offload traffic in the congested macrocell depends mainly on the precision of the traffic hotspot localization process and also on the hotspot's position within the cell as well as the small cell's position with respect to the macrocell location.

Moreover, we conclude that when the hotspot is at the cell edge, the imperfections of the hotspot localization are more tolerated and the system performance can still be improved by deploying small cells as compared to a network composed of only macrocells. However, when the hotspot is at cell center, even a perfect positioning of

the small cell is not beneficial for the overall system performance and does not bring offloading gains.

Dynamic level analysis allows us to observe that, for small cell deployments with positive gains (obtained from the static level analysis), the perfect positioning of the small cell with respect to the hotspot position is sufficient to obtain better performance but it is not sufficient to obtain the best one. This latter depends on several input parameters such as the radio range of the small cell (if it covers all the hotspot or a part of it when this latter is more flat), the small cell capacity and the amount of traffic it carries as well as the level of interference generated by the small cell.

Chapter 5

Moving small cells in 5G networks under the presence of mass events

In this chapter, the concept of moving small cells in mobile networks is presented and evaluated taking into account the dynamics of the system. We consider a small cell moving according to a Manhattan mobility model which is the case when the small cell is deployed on the top of a bus following a predefined trajectory in areas which are generally crowded. Taking into account the distribution of user locations, we study the dynamic system level considering a queuing model composed of multi-class Processor Sharing queues combined with a coupling due to the mutual interference generated by each cell to the other (since they are operating in the same bandwidth).

5.1 Manhattan mobility model

Manhattan model is used to emulate the movement pattern of the small cell. The city is modeled by Manhattan style grid composed of horizontal and vertical streets. All streets are two-way, with one lane in each direction and small cells movements are constrained by these lanes which represent the main characteristic and the geographic restriction of this model. At an intersection of a horizontal and a vertical street, the small cell can turn left, right or go straight. In Fig. 5.1, the trajectory of the moving small cell is defined.

Moreover, the velocity of the small cell at a time slot is dependent on its velocity at the previous time slot. It is also restricted by the velocity of the road traffic on the same lane of the street and by the stops where the bus must take passengers.

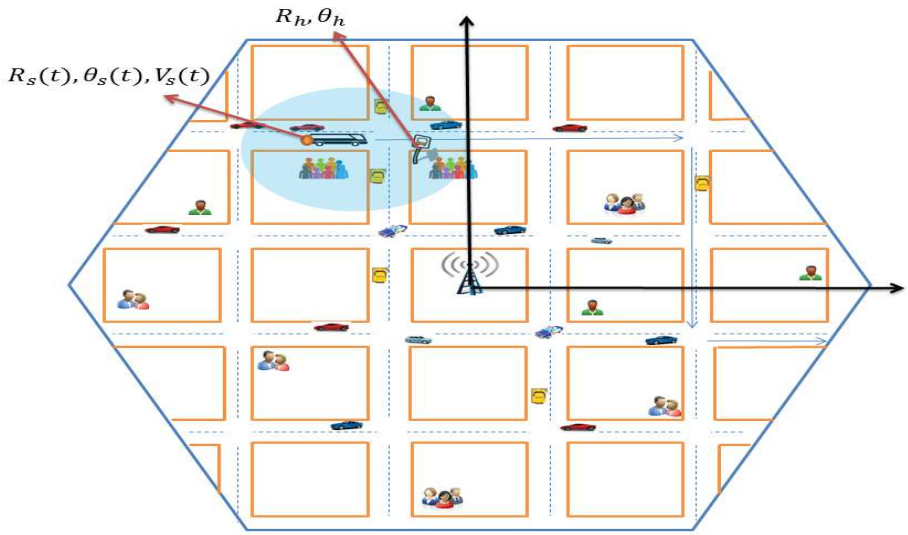

Fig. 5.1 A moving small cell according to Manhattan mobility model.

We model the mobility of the small cell in position $L_s(t) = (R_s(t), \theta_s(t))$ moving, at time t, with a speed of $V_s(t)$ by the following expression

$$V_s(t+dt) = \min(V_{max}, V_s(t) + \beta dV_s(t)) \tag{5.1}$$

where V_{max} is the maximum allowed velocity, $V_s(t)$ and $dV_s(t)$ are respectively the current speed and the acceleration of the small cell and $\beta \in [-1, 1]$. If β is negative, then the moving small cell is decelerating. The small cell position at time $t+dt$ is likewise given by

$$L_s(t+dt) = L_s(t) + V_s(t)dt \tag{5.2}$$

Note that $V_s(t)$ and $L_s(t)$ are complex numbers (in $\mathbb{C}$) since the small cell is moving in a bi-dimensional space.

5.2 Downlink system model

As in Chapter 4, we consider a hexagonal cellular network where the inter-site distance is denoted by δ and the transmitting power level is equal to P. At time t, a moving small cell is located at position $L_s(t)$ and offloading data traffic in its coverage area, as illustrated in Fig. 5.1. The transmit power level of the small cell is $P_s = \kappa P$ with $0 \leq \kappa \leq 1$.

In order to evaluate the efficiency of moving small cells, we consider a stationary traffic hotspot with polar coordinates (R_h, θ_h). The traffic hotspot is assumed to be located inside the central macrocell, i.e. $R_h < R$ with R the approximated radius of the cell. UE locations are spatially distributed in order to form a traffic hotspot centered in (R_h, θ_h) with a standard deviation denoted by A; its measure is given by equation (4.1).

We consider two scenarios: In the first scenario, only macrocells are operational. This scenario represents a benchmark allowing the comparison of a network where moving small cells contribute in offloading traffic to a network without smalls cells. Scenario 2 considers a small cell moving near the traffic hotspot.

The wireless channel is modeled as in Subsection 4.1.2. At time t, the SINR received by the UE and its throughput are respectively denoted by $\gamma_t(r,\theta)$ and $\eta_t(r,\theta)$ if it is received from the macrocell and by $\tilde{\gamma}_t(r,\theta)$ and $\tilde{\eta}_t(r,\theta)$ if it is received from the small cell.

Independently of the time t and of the cell size (macro, small), the relationship between γ (in linear scale) and η is modeled by the modified Shannon formula given in equation (4.5).

5.3 Preliminary analysis

We first evaluate the instantaneous user throughput obtained in each position of the covered region of the studied macrocell and its moving small cell. Then, the instantaneous throughput CCDF is calculated considering the distribution of user locations given in equation (4.1).

The instantaneous SINRs received from the macrocell and the small cell are expressed as follows

$$\gamma_t(r,\theta) = \frac{1}{g(r) + \kappa |re^{i\theta} - R_s(t)e^{i\theta_s(t)}|^{-2b} r^{2b}} \tag{5.3}$$

$$\tilde{\gamma}_t(r,\theta) = \frac{P_s |re^{i\theta} - R_s(t)e^{i\theta_s(t)}|^{-2b}}{(g(r)+1)\, P r^{-2b}} \tag{5.4}$$

where $g(r)$ is as defined in equation (4.8).

We define the instantaneous throughput CCDF for both the macrocell and the moving small cell $(R_s(t), \theta_s(t))$ as in equations (4.13) and (4.14), by only replacing the static position of the small cell by its instantaneous coordinates.

As in Chapter 4, the following results still apply:

$$\forall l > \eta_0, \;\; \mathbb{P}(\eta_t \geq l) = 0 \;\; \text{and} \;\; \mathbb{P}(\tilde{\eta}_t \geq l) = 0$$

$$\forall l \leq \eta_0, \;\; \mathbb{P}(\eta_t \geq l) = \frac{1}{S_t} \int_{S^*} \mathbb{1}\left(P_s |re^{i\theta} - R_s(t)e^{i\theta_s(t)}|^{-2b} \leq Pr^{-2b}\right) \times \mathbb{1}\left(\frac{1}{\gamma_t(r,\theta)} \leq \psi(l)\right) dm(r,\theta) \tag{5.5}$$

$$\mathbb{P}(\tilde{\eta}_t \geq l) = \frac{1}{\tilde{S}_t} \int_{S^*} \mathbb{1}\left(P_s |re^{i\theta} - R_s(t)e^{i\theta_s(t)}|^{-2b} > Pr^{-2b}\right) \times \mathbb{1}\left(\frac{1}{\tilde{\gamma}_t(r,\theta)} \leq \psi(l)\right) dm(r,\theta) \tag{5.6}$$

Besides, when the moving small cell leaves the coverage of the studied macrocell and goes far enough from it, all UEs in the traffic hotspot (R_h, θ_h) will be served by the macrocell. Hence, the throughput CCDF can be simply given by the expression in equation (4.25).

5.4 Dynamic level analysis of moving small cells

5.4.1 Dynamic system model description

As in Chapter 4, we focus, in this work, on the case of best effort traffic where flow sizes, denoted by σ, are assumed to be mutually independent and exponentially distributed with mean σ_0 in Mbits. Flows may belong to different classes depending on the radio conditions of mobile users. Then, flow classes are sorted, for tractability issues, in an increasing order according to the associated data rate, denoted by $\eta_{k,t}, \tilde{\eta}_{l,t}, \; k = 1..K, l = 1..L$, index k for macrocell user classes and index l for moving small cell ones. The probabilities $p_{k,t}, \tilde{p}_{l,t}, \; k = 1..K, l = 1..L$ denote the density of each flow class in the macrocell and the moving small cell respectively. Each class follows a Poisson Process of intensity $\lambda_{k,t} = \lambda_t p_{k,t} = \lambda_{Tot} \frac{S_t}{S_t + \tilde{S}_t} p_{k,t}, \; k = 1..K$ in the macrocell and $\tilde{\lambda}_{l,t} = \tilde{\lambda}_t \tilde{p}_{l,t} = \lambda_{Tot} \frac{\tilde{S}_t}{S_t + \tilde{S}_t} \tilde{p}_{l,t}, \; l = 1..L$ in the moving small cell. Data rates and flows' arrival intensities are extracted from the preliminary analysis as depicted in Fig. 4.4.

Due to the mutual interference between the macrocell and the moving small cell, the coupling between the two cells is expressed by

$$\forall k = 1..K,\ \eta_{k,t} = \begin{cases} \eta_{k,t,0} \text{ if no user is served by the small cell} \\ \eta_{k,t,1} \text{ otherwise} \end{cases} \tag{5.7}$$

$$\forall l = 1..L,\ \tilde{\eta}_{l,t} = \begin{cases} \tilde{\eta}_{l,t,0} \text{ if no user is served by the macrocell} \\ \tilde{\eta}_{l,t,1} \text{ otherwise} \end{cases} \tag{5.8}$$

where $\eta_{k,t,0}$ is obtained from the throughput distribution of a macrocell network in Section 5.3 and $\eta_{k,t,1}$ is obtained from the scenario involving a deployed moving small cell. However, for the moving small cell, $\tilde{\eta}_{l,t,0}$ is simply given by deleting the contribution of the central macrocell in the interference experienced by the small cell's UEs. $\tilde{\eta}_{l,t,1}$ is also derived from the throughput distribution curve obtained in Section 5.3.

Moreover, we assume that users near the small cell (i.e. in its coverage area or in the coverage area of the macrocell but experiencing a significant interfering signal coming from the small cell) change from a flow class to another adjacent class after exponential durations due to the mobility of the small cell and also of the users. Handovers are also taken into account. Therefore, we assume that users handed over from a cell to another will affect the system only in the first flow class of each cell since users with bad radio conditions are the most eligible to trigger a handover and they will be highly interfered by their previous serving cell. The transition rates from a flow class to another vary according to the mobility of the small cell and their values are extracted from the evolution of the throughput CCDF in time. This represents the main difference to the dynamic system model studied in Chapter 4. Hence, at time t, these transitions rates are denoted by $\nu_{k,k+1,t}$, $\nu_{k,k-1,t}$, $\tilde{\nu}_{l,l+1,t}$ and $\tilde{\nu}_{l,l-1,t}$ (see Fig. 5.2). Similarly, ν_t and $\tilde{\nu}_t$ denote the instantaneous handover rates from the macrocell to the small cell and inversely. The dynamic system model is depicted in Fig. 5.2.

5.4.2 System coupling

We denote by ρ and $\tilde{\rho}$ the load of the macrocell and the small cell respectively and by P_0, $\tilde{P}_0$ the steady state probabilities when no user is in the macrocell and the small cell respectively. Without considering the mobility of the small cell, we apply the same decoupling approach as in Chapter 4. So, for each class k of flows in the macrocell, the queuing system can be modeled with a proportion $\tilde{P}_0 = 1 - \tilde{\rho}$ of flows experiencing a

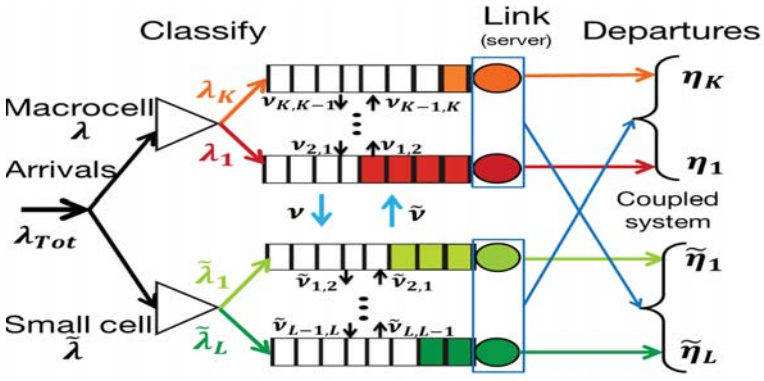

Fig. 5.2 Dynamic system model

data rate equal to $\eta_{k,0}$ and a proportion $1-\tilde{P}_0$ of flows experiencing a data rate equal to $\eta_{k,1}$ and the same for the small cell. Hence, the stationary distribution of the state $(n=(n_1,..,n_K),\tilde{n}=(\tilde{n}_1,..,\tilde{n}_L))$ is expressed as in equation (4.47).

5.4.3 Performance analysis

Analysis taking into account the mobility of the small cell is not affected by the system coupling detailed in the previous subsection since transition rates (between classes and between cells) does not depend on the queue state of the interfering cell.

The probability of having an active flow of class k for the macrocell (of class l for the small cell) is given by

$$\forall k=1..K,\ P_k=\frac{E_t[n_{k,t}]}{\sum\limits_{i=1}^{K}E_t[n_{i,t}]+\sum\limits_{j=1}^{L}E_t[\tilde{n}_{j,t}]} \tag{5.9}$$

$$\forall l=1..L,\ \tilde{P}_l=\frac{E_t[\tilde{n}_{l,t}]}{\sum\limits_{i=1}^{K}E_t[n_{i,t}]+\sum\limits_{j=1}^{L}E_t[\tilde{n}_{j,t}]} \tag{5.10}$$

where $n_t=(n_{1,t},..,n_{K,t})$ and $\tilde{n}_t=(\tilde{n}_{1,t},..,\tilde{n}_{L,t})$ represent the queue state in each cell and of each class at time t and $E_t[h(t)]=\frac{1}{t}\sum_{s=0}^{t}h(s)$.

With the deployment of moving small cells and in the presence of traffic hotspots, the system presents two important characteristics allowing to derive several performance metrics: a high mobility and a heavy system load. Hence, following [76], the probability

that a user is of class k (or of class l) satisfies

$$\forall k = 1..K,\ q_k = \frac{E_t\left[\frac{\tilde{\nu}_t}{\nu_t}\prod_{i=1}^{k-1}\frac{\nu_{i,i+1,t}}{\nu_{i+1,i,t}}\prod_{j=1}^{L-1}\frac{\tilde{\nu}_{j,j+1,t}}{\tilde{\nu}_{j+1,j,t}}\right]}{\sum_{i=1}^{K} q_i + \sum_{j=1}^{L}\tilde{q}_j} \tag{5.11}$$

$$\forall l = 1..L,\ \tilde{q}_l = \frac{E_t\left[\frac{\nu_t}{\tilde{\nu}_t}\prod_{j=1}^{l-1}\frac{\tilde{\nu}_{j,j+1,t}}{\tilde{\nu}_{j+1,j,t}}\prod_{i=1}^{K-1}\frac{\nu_{i,i+1,t}}{\nu_{i+1,i,t}}\right]}{\sum_{i=1}^{K} q_i + \sum_{j=1}^{L}\tilde{q}_j} \tag{5.12}$$

Under the round robin policy and with considering the proposed coupling approach, it follows that the K and L queues are equivalent to one PS queue with service data rate given by

$$\begin{aligned}\bar{\eta} = &\sum_{k=1}^{K} q_k E_t\left[\tilde{\rho}_t\eta_{k,t,1} + (1-\tilde{\rho}_t)\eta_{k,t,0}\right] + \\ &\sum_{l=1}^{L}\tilde{q}_l E_t\left[\rho_t\tilde{\eta}_{l,t,1} + (1-\rho_t)\tilde{\eta}_{l,t,0}\right]\end{aligned} \tag{5.13}$$

where ρ_t and $\tilde{\rho}_t$, representing the load in both cells at time t, are supposed to be in $[0,\ 1]$, otherwise they are taken equal to 1 in the analysis. It is important to notice that this assumption affects only the coupling statement where the proportion of users with data rate $\eta_{k,t,0}$ plus those with data rate $\eta_{k,t,1}$ are equal to 100% when we have, respectively, $\tilde{\rho}_t \geq 1$ and $\rho_t \geq 1$.

The load of the cells may be higher than one since the mobility of the small cell allows to offload the extra load from a cell to another and the system remains stable. In this context, it is proved in [76], that mobility increases the stability region in wireless networks. Then, under the stability condition, i.e. $\bar{\rho} = \frac{\lambda_{Tot}\sigma}{\bar{\eta}} < 1$, the stationary probability of state $(n = (n_1, .., n_K), \tilde{n} = (\tilde{n}_1, .., \tilde{n}_L))$ is given by

$$\pi_{n,\tilde{n}} = \frac{(1-\bar{\rho})|n+\tilde{n}|!\prod_{k=1}^{K} q_k^{n_k}\prod_{l=1}^{L}\tilde{q}_l^{\tilde{n}_l}}{\prod_{k=1}^{K}(\tilde{\rho}n_k)!\,((1-\tilde{\rho})n_k)!\prod_{l=1}^{L}(\rho\tilde{n}_l)!\,((1-\rho)\tilde{n}_l)!} \tag{5.14}$$

with $\rho = \lim_{t\to\infty} E_t[\rho_t]$ and $\tilde{\rho} = \lim_{t\to\infty} E_t[\tilde{\rho}_t]$.

The traffic conservation equation, which still applies, is expressed by

$$\lambda_{Tot}\sigma = \sum_{k=1}^{K} E_t\left[\eta_{k,t}\Phi_k(n_t)\right] + \sum_{l=1}^{L} E_t\left[\tilde{\eta}_{l,t}\tilde{\Phi}_l(\tilde{n}_t)\right] \tag{5.15}$$

where $\Phi_k(n_t) = \frac{n_{k,t}}{|n_t|}$ and $\tilde{\Phi}_l(\tilde{n}_t) = \frac{\tilde{n}_{l,t}}{|\tilde{n}_t|}$, with the round robin scheduling, represent the proportion of allocated resources to users of class k and l in their serving cells.

Subsequently, the mean flow throughput is given by

$$R = \sum_{k=1}^{K} P_k E_t\left[\frac{\eta_{k,t}\Phi_k(n_t)}{n_{k,t}}\right] + \sum_{l=1}^{L} \tilde{P}_l E_t\left[\frac{\tilde{\eta}_{l,t}\tilde{\Phi}_l(\tilde{n}_t)}{\tilde{n}_{l,t}}\right] \tag{5.16}$$

5.5 Numerical results

The most important parameters used in the numerical evaluation are already given in the results' section of Chapter 4 (Table 4.1). In the figures' legend, MC and SC stand for macrocell and small cell respectively, HS stands for traffic hotspot.

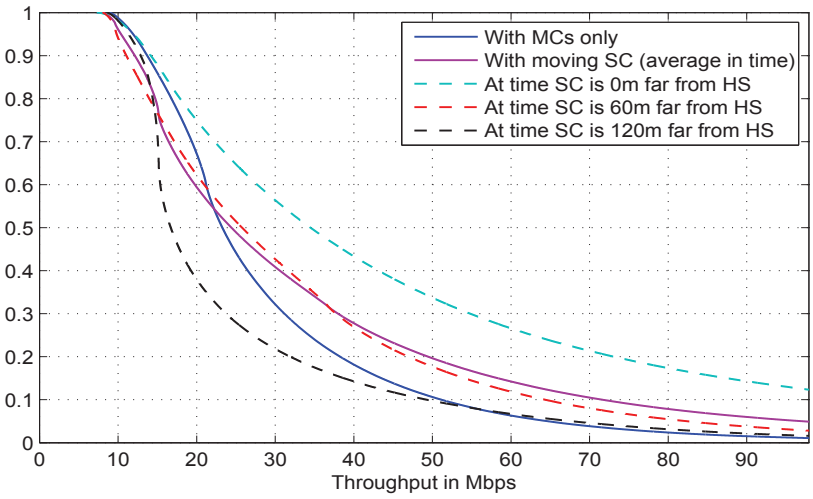

Fig. 5.3 Throughput CCDF defined in the preliminary study.

We consider a specific scenario where the position of the traffic hotspot is equal to $(R_h = 0.5, \theta_h = \frac{\pi}{3})$. We plot in Fig. 5.3, the throughput CCDF in a network without small cells, and also in a network with a moving small cell in different times (when the

small cell is $0m$, $60m$ and $120m$ far from the hotspot) and also on average (during the observation time).

From Fig. 5.3, we observe that the deployment of a moving small cell improves significantly the capacity of the system when it moves near the traffic hotspot since user locations with degraded radio conditions will be covered by the moving small cell and hence will experience a better SINR level. Moreover, we note that, even when the small cell moves far from the hotspot (60 meters), the system capacity is improved compared to scenario where only macrocells are operating in the studied area. In average and during all the simulation period, the deployment of a moving small cell generates positive gains and improves the distribution of radio conditions compared to a network without small cells.

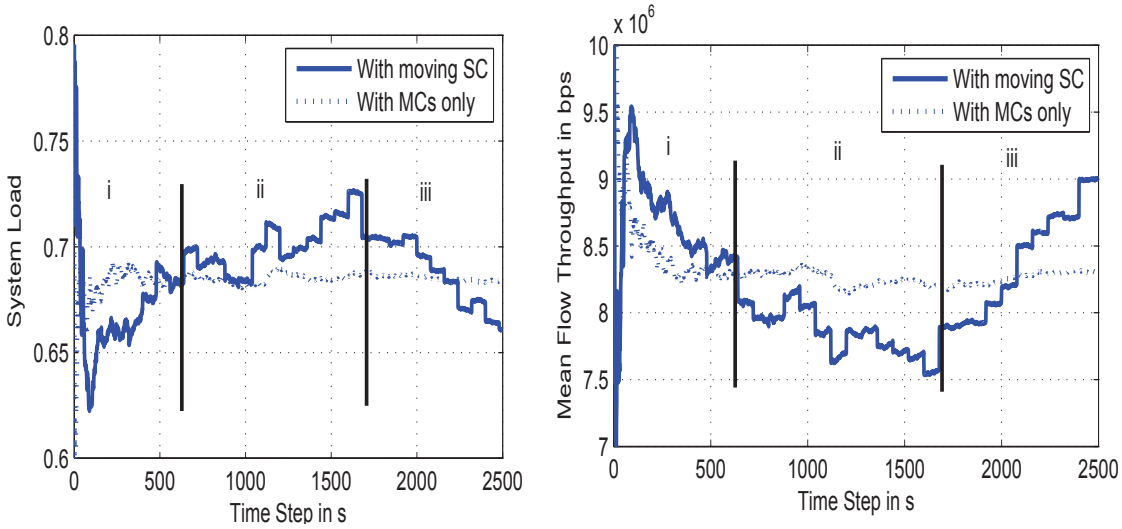

Fig. 5.4 The load $\bar{\rho}$ (left) and the mean flow throughput R (right) in the system before and after the deployment of a moving cell.

In Fig. 5.4, we plot the evolution of the load and the mean flow throughput in time for the studied scenarios: with and without a moving small cell. This latter is moving according to Manhattan mobility model and is supposed to pass by the traffic hotspot periodically (after each 30 minutes) since it is located on top of buses. Curves are divided into three intervals.

In interval i, the load in the system is reduced with the deployment of a moving small cell and the mean flow throughput is higher than in a network with macrocells only. This is explained by the fact that the small cell is moving near the traffic hotspot located in $(0.5km, \frac{\pi}{3})$. In interval ii, the small cell is moving far away from the traffic hotspot and higher interference (between the macrocell and the small cell) is

experienced by users compared to the first interval of time. Consequently, we observe that the load is increased with the deployment of a small cell and the mean flow throughput is reduced. This means that when the small cell is near the traffic hotspot but covering a small proportion of it, the system performance is degraded due to the significant interference on macrocell users and the increase of the proportion of cell edge users in the small cell. In interval iii, we notice that the load is reduced again and the mean flow throughput is improved. This is explained by the fact that the small cell is moving again near the traffic hotspot (since small cells are supposed to be deployed on the top of buses, the existence of small cells near the traffic hotspot is periodic which leads to the periodicity of the network performance).

5.6 Concluding remarks

We studied in this chapter the impact of deploying a moving small cell in the presence of stationary traffic hotspot inside a macrocell. We studied the system taking into account its dynamics where users' radio conditions may vary during service and allow then to move from a class to another.

Results show that the efficiency of deploying moving small cells to offload traffic in the congested macrocell can be a beneficial solution when the small cell is moving near the traffic hotspot and covers a significant proportion of it. However, when the small cell is moving far away from the traffic hotspot, the system performance is degraded compared to a network composed of only macrocells due to the high mutual interference between macro and small cell users.

Aiming to better exploit the mobility of cells, we develop in the next chapter a mechanism allowing to control the mobility of small cells in order to cover traffic hotspots and reduce congestion in cellular networks so as to make this promising technology a cost-effective investment.

Chapter 6

Drone small cells in 5G Networks

In this chapter, we develop a new traffic offloading mechanism using drone cells. First, we describe the different steps of the whole mechanism including several possible scenarios. Second, the access mode is discussed. Third, a study of the performance of the proposed mechanism is realized. Finally, the advantages and the limitations of the drone-based mechanism are investigated.

6.1 Description of the proposed offloading mechanism

In this section, we start by presenting the different parameters, variables and states involved in the proposed drone-based mechanism to reduce congestion. After that, we describe the different steps related to specific scenarios such as the appearance, disappearance and movement of traffic hotspots.

6.1.1 Definitions and notations

Drone & Macrocell states

It is clear that the drone is not active all the time. It is activated only when some specific conditions (mainly related to the macrocell load and the location of traffic) are verified. So, we define the following drone activity modes: Idle/Stand-by/Active/Ready. In Idle mode, the drone is connected to a powering terminal to recharge its battery and all its Radio Frequency (RF) and flying components are deactivated. The Stand-by mode is conceived in order to enhance the reactivity of the drone and anticipate the appearance of a traffic hotspot. In this mode, the drone activates several flying

components in an energy-saving mode. If there is congestion due to heavy load in the macrocell, the drone switches to Active mode and moves to the hotspot position but its RF components are not yet activated to serve users (only the communication with the macro Base Station (BS) remains running). Finally, when the drone settles up near the traffic hotspot, it switches to Ready mode and starts serving users while behaving like a small cell.

Since activity modes of the drone are dependent on the congestion state of the macrocell, we define the following congestion states: Green/Yellow/Red. Green state means that the macrocell is not congested and the its load is not high. Yellow state means that a possible congestion may occur in the macrocell. Red state means that the macrocell is facing a serious congestion problem and it needs immediately a solution to offload traffic.

If the traffic hotspot is located close to the macro BS, it was shown in recent studies [36, 37] that deploying small cells, using the same spectrum as the macrocell, degrades the overall system performance. This is explained by the fact that the interference coming from the macrocell on the small cell users will be very high. Consequently, users spend more time to finish their transmissions and the useful data rate is reduced since more bits are required to protect the transmitted signal. Similarly, if the drone is working with the same frequencies as the macro BS, deploying drones near macro BSs does not represent a good solution. Moreover, the only way to offload a traffic hotspot at cell center is to review the capacity dimensioning of the macrocell. That is why, incorporating the hotspot's position in the activation of the drone is very important to make its deployment a beneficial solution.

In order to efficiently use the drone-based mechanism, we combine these two criteria as depicted in Fig. 6.1: the hotspot's position and the cell load. In the green region, the drone is in Idle mode. The blue region is conceived to trigger the switch to Idle mode given that the drone is already in Active or Ready mode. The yellow region is related to the Stand-by mode where the drone is waiting the order from the macro BS to move. Finally, the red region represents the situation where the drone must switch from Stand-by mode to Active or must stay in Ready mode. The parameters set in Fig. 6.1 are defined in the next subsection.

Measurement variables and parameters

In Fig. 6.1, the x-axis, denoted by *Cell_Load* represents the measured load in the cell (e.g. load of the cell evaluated by Physical Resource Block (PRB) usage in 3GPPP

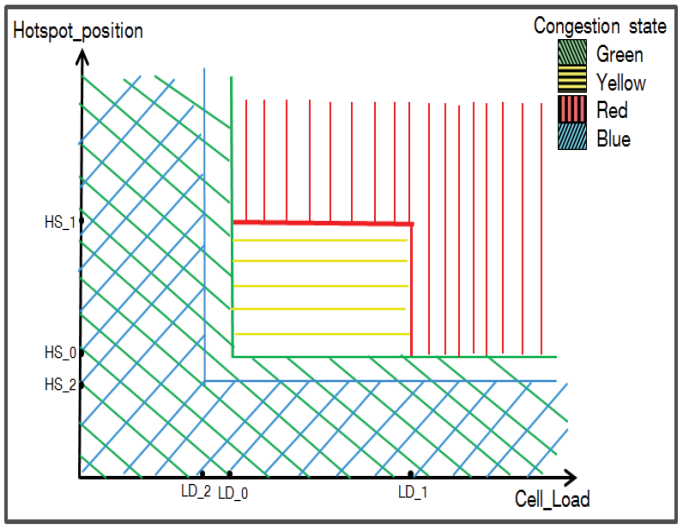

Fig. 6.1 State Diagram controlling the drone.

LTE-A networks). $Hotspot\_position$ is defined as the position of the hotspot calculated through a hotspot localization method executed in the macro BS [20].

To define the different events that may occur in the macrocell, we firstly define the following thresholds related to the cell load and to the traffic hotspot's position. LD_0 is the threshold of macrocell load to switch from green state to yellow one when the traffic hotspot position is between HS_0 and HS_1 and from green state to red one when the traffic hotspot position is higher than HS_1. Note that when the traffic hotspot position is smaller than HS_0, nothing will happen because, as explained before, deploying a small cell near the macro BS, in case they are operating in the same frequency band, does not bring any positive gains and it even degrades the overall system performance. LD_1 represents the threshold of cell-load to switch from yellow state to red one when the traffic hotspot position is between HS_0 and HS_1. To ensure the resumption of a normal situation, the hotspot position must be less than HS_2 and the cell-load less than LD_2.

We define $\{TP_i, i = 1..n\}$ as a set of locations planned during the network design process for positioning drones to allow the best possible coverage. Furthermore, SEL_offset, HO_hys and HO_offset are three additional parameters used for the process of UEs' selection and handover. N_{UE} is the number of users served by the drone.

6.1.2 Designed mechanism and followed steps

In Fig. 6.2, a general overview of the designed mechanism with its performed operations is presented.

Initial state of the drone

Each drone is initially attached to one of the already-planned set of possible locations $\{TP_i, i = 1..n\}$. These locations are defined in the planning step to be in strategic positions (covering most of the areas where the signal from macrocell is not good mainly because of shadowing). These positions can be the top of a lamppost or a high building which has the advantage that the drone is always able to choose a place where it can be in line-of-sight with its attached macrocell and also with the users, source of the congestion in the macrocell. Moreover, it is possible to install power terminals in some of these points capable of efficiently charging the drones' batteries. When the macrocell is not congested ($Cell\_Load \leq LD_0$), the drone stays in Idle mode.

Detection of congestion symptoms in the macrocell

Once the congestion level in the macrocell exceeds a certain threshold but is still less than a second predefined threshold ($LD_0 < Cell\_Load \leq LD_1$), an $event\_D$ is triggered in the macrocell. Subsequently, a traffic hotspot localization process (see for example [20]) starts to be periodically executed each T_0 to estimate the possible position of the hotspot generating the congesting traffic. Performing periodically the traffic localization allows also to predict the mobility profile of the hotspot. If the resulting hotspot position is near the macro BS ($Hotspot\_position \leq HS_0$), the drone will not be notified of this event. However, if the hotspot is not near the macro BS, we have to deal with one of two different situations. The first one is when $HS_0 < Hotspot\_position \leq HS_1$ and $LD_0 < Cell\_Load \leq LD_1$. In this case, a notification message is sent to the drone in order to be in Stand-by mode. The second situation is when $Hotspot\_position > HS_1$ and $Cell\_Load > LD_0$ resulting in the activation of the drone in the next step.

Preparation for possible congestion

In this step, we have two different situations:

When $Hotspot\_position > HS_1$ and $Cell\_Load > LD_0$, the drone switches to Stand-by mode and the macrocell waits the expiration of a timer T_1 and verifies if the two previous conditions are still satisfied or not. If the congestion persists with the

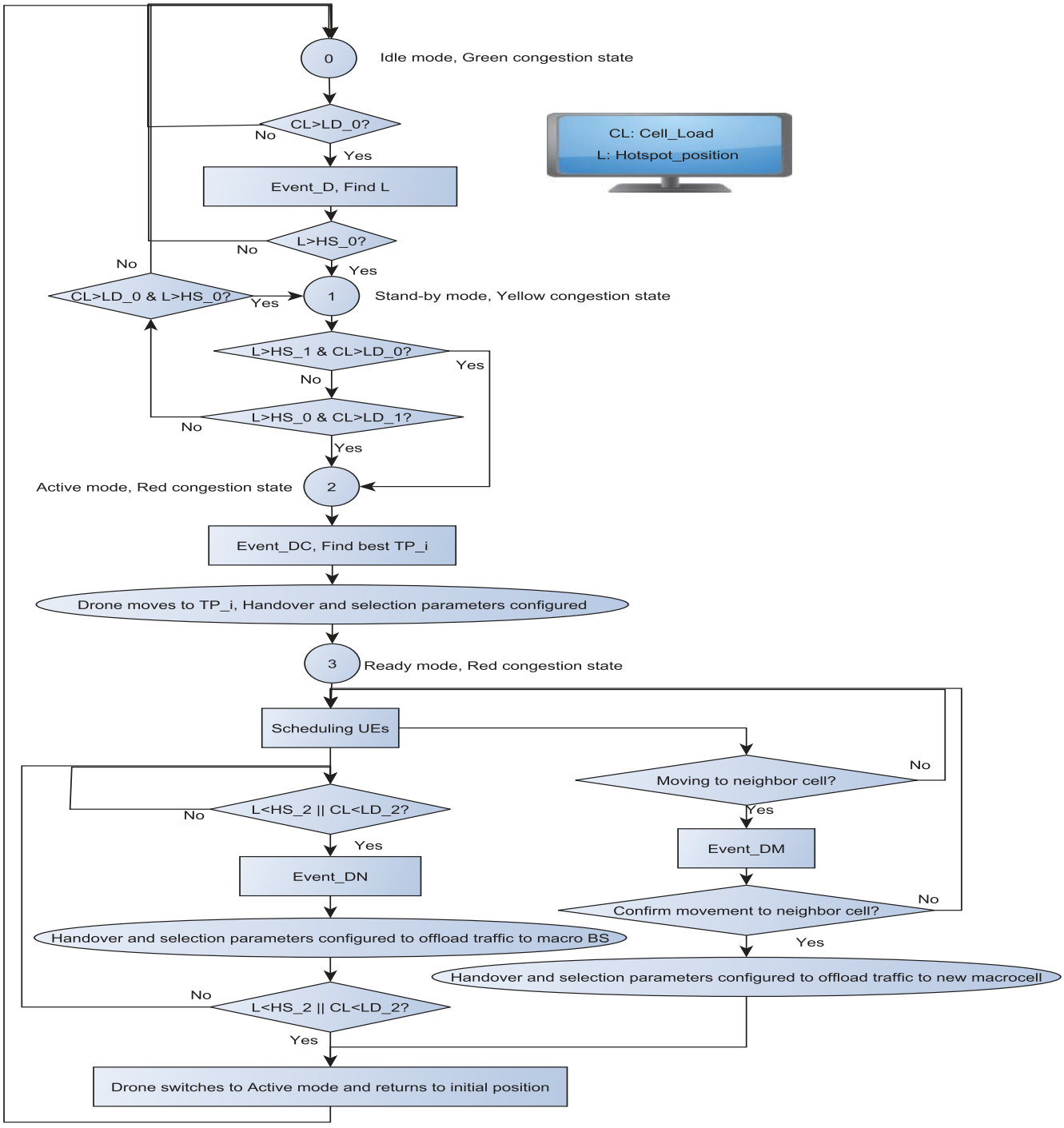

Fig. 6.2 Offloading mechanism.

same previous conditions, the macrocell triggers the *event_DC* meaning that it needs the intervention of the drone to reduce the congestion level in the cell. However, if $Hotspot\_position \leq HS_1$ or $Cell\_Load \leq LD_0$, two possible cases can be identified. In the first one, $Hotspot\_position$ is less than HS_0 or $Cell\_Load \leq LD_0$. Then, after expiration of T_2, if $Hotspot\_position$ is still less than HS_0 or $Cell\_Load \leq LD_0$, the macrocell sends a message to the drone in order to return to Idle mode. In the second case, $Hotspot\_position > HS_0$ and $Cell\_Load > LD_0$, the drone stays in Stand-by mode.

When $HS_0 < Hotspot\_position < HS_1$ and $LD_0 < Cell\_Load < LD_1$, the macrocell waits the expiration of a timer T_3 and verifies if the two previous conditions are still satisfied or not. After T_3, if $HS_0 < Hotspot\_position < HS_1$ and $LD_0 < Cell\_Load < LD_1$, the drone is still in Stand-by mode. Otherwise, if the distance to the hotspot becomes smaller than HS_0 or the load becomes less than LD_0, the macrocell waits until the expiration of T_2. Then, if the same conditions are still valid, the macrocell sends a message to the drone in order to return to Idle mode. However, if after T_3, $Hotspot\_position > HS_1$ and $Cell\_Load > LD_0$, the macrocell triggers the *event_DC*.

Persistent congestion and activation of the drone

The action following *event_DC* is that the macrocell sends an activation message with the information of the position where the drone must move. Based on this information, the drone switches to Active mode and moves to the communicated position, chosen between the set of points $\{TP_i, i = 1...n\}$, and settles up on the top of it. This position is properly determined allowing to minimize the distance and to ensure line-of-sight condition to the traffic hotspot.

Mobility control of the hotspot

Drones are controlled by an intelligent entity connected to the macrocell which communicates the positions to which the drone needs to move. A database, filled with predefined trajectories to each position in $\{TP_i, i = 1...n\}$, is checked by the drone in order to find the best path to arrive to the communicated position. The drone is also equipped with a GPS module allowing to adjust and update its trajectory.

The macrocell tries also to anticipate and predict the mobility profile of UEs so that the drone can move and settle up in the next position in order to cover most of it for long periods of time. That is why, the hotspot localization process is periodically performed (each T_0) while the drone is in Active mode.

Parameters' configuration

After being landed in the right position, the drone switches to Ready mode. In the scope of Self Organizing Networks (SON) technology [67, 77], parameters' configuration of the drone and of the macro BS are done as follows: Selection and handover parameters (SEL_offset, HO_hys and HO_offset) of the drone-cell are auto-configured in order to absorb more traffic and quickly anticipate the handover to the drone. The HO_hys between the macrocell and its drone is increased in such a way that the drone will take most of the UEs in its covered area. However, the individual HO_offset of the drone is decreased in order to make all the drone-served UEs stay larger periods connected to it. The SEL_offset is also increased to allow the drone to handle new arrivals.

State evolution of the macrocell

Once the experienced load in the macrocell (including the traffic served by the drone) becomes less than a threshold LD_2 or the hotspot position becomes less than HS_2, $event\_DN$ is triggered and a timer T_4 is activated in order to test if the situation in the macrocell is still the same or not. If T_4 times out and the previous condition persists, this means that the macrocell can serve all the traffic generated inside its covered region without using the drone. Consequently, the macrocell switches its congestion state to blue which is the green mode after regaining a normal situation with minimized risk of congestion in the macrocell. Then, parameters SEL_offset, HO_hys and HO_offset are auto tuned allowing the drone to offload all its served UEs to the macrocell and it waits in Ready mode until the expiration of T_5. If the congestion state in the macrocell is still blue, the drone switches from Ready to Active mode and moves to the nearest position where a power charger is available (if it does not dispose of sufficient energy for an upcoming mission). Once the drone arrives at this position, it switches to Idle mode. However, if $Cell\_Load$ becomes higher than LD_0 and $Hotspot\_position > HS_0$ after T_4, the drone will continue to serve the UEs in Ready mode.

The traffic hotspot is moving to another macrocell

If users move from a macrocell to another, $event\_DM$ is triggered and a warning message will be sent to the new serving macrocell informing it about the arriving hotspot. Based on its congestion state, the new macrocell executes the same steps as described above based on measurements sent by the first macrocell (mainly the

position and the size of the hotspot in terms of number of UEs N_{UE}). While the new macrocell is only searching for the best solution (nothing is activated yet), if the next hotspot localization report of the first macrocell (after T_1) says that the traffic hotspot is still in the same cell, nothing will happen in the second macrocell and the drone will remain in Ready mode. However, if this hotspot localization report still gives a position belonging to the covered region of the new macrocell, the first drone can still offload traffic temporarily until the expiration of timer T_6. The new macrocell proceeds with the activation of its own drone if it is congested. Once a message is sent to the initial serving macrocell informing it that the new macrocell is ready to serve its arriving hotspot of UEs, HO_offset of the drone will be increased and all UEs of the first drone will be connected to the new macrocell directly or via its drone. SEL_offset of the original drone is decreased in order to be inaccessible for new arrivals. Next, a message from the first macrocell is sent to the drone informing it about the next position where to move to either serve a new hotspot or to be in Stand-by mode or to switch into Idle mode. The HO_hys between the macrocell and the drone is also set to the initial value.

The drone recharges its battery

With the development of the drone technology, drones can remain for longer times in the air without the need to be connected to a power terminal. Moreover, as described in the proposed mechanism, the drone flies only when it moves to cover a traffic hotspot or when it returns to its initial position. When the drone arrives at the desired position, it lands on the top of it and then all its flying components are deactivated. Consequently, less energy is consumed by the drone during its service since only RF components are active.

To recharge its battery, the drone needs to find the nearest point where a recharging equipment is installed and then moves to reach this position and settle up on it. The best solution is to exploit the well-distributed network of lampposts and install in some of them electric feeders allowing to recharge the drone. It follows that operators could negotiate with the government on how to allow them to use the public electric resources with reasonable costs.

6.2 Specification of access mode between macrocell, drone and UEs

The communication between the backhaul and the drone can be transported through wire-lined links installed in each strategic point (defined in subsection 6.1.1) or realized through directive antennas with dedicated frequency band. However, in order to save the spectrum resources, the connection to the backhaul will be performed, in this work, through the dedicated band attributed to the macrocell. Indeed, a proportion of the macrocell FDD (Frequency Division Duplexing) frequency, used formerly to serve mobile users, is exclusively allocated to the drone when it is activated.

Communications between the drone cell and UEs is based either on licensed spectrum if the required resources are available or on unlicensed spectrum otherwise. WiFi, as a well known unlicensed spectrum based technology and currently available in most of commercialized smartphones and other connected devices, allows operators to generate extra income from the access of WiFi-only-devices. However, billing and security still require hardware and software upgrades for the WiFi module. Moreover, interference in WiFi band cannot be controlled due to the wide use of this unlicensed band in other applications such as in medical, scientific and industrial fields or even for domestic personal use. For the licensed spectrum, each operator actually has licensed TDD (Time Division Duplexing) frequency bands constituting an important investment. However, they are not favorably exploited in operational networks which represents a waste of resources. This can be explained by the fact that, with large scale distances, the uplink/downlink guard time in TDD mode is not enough to overcome the interferences between the two transmission links. Nevertheless, TDD mode is known to perform efficiently for small scale distant communications. So, using TDD mode between the drone and its users is recommended and henceforth applied in the present work.

6.3 Performance analysis of the proposed drone-based offloading mechanism

6.3.1 System model

Network layout and traffic distribution

As in Section 4.1.1, we consider a hexagonal macrocell network where each cell is transmitting with power level P. The inter-site distance and the antenna elevation

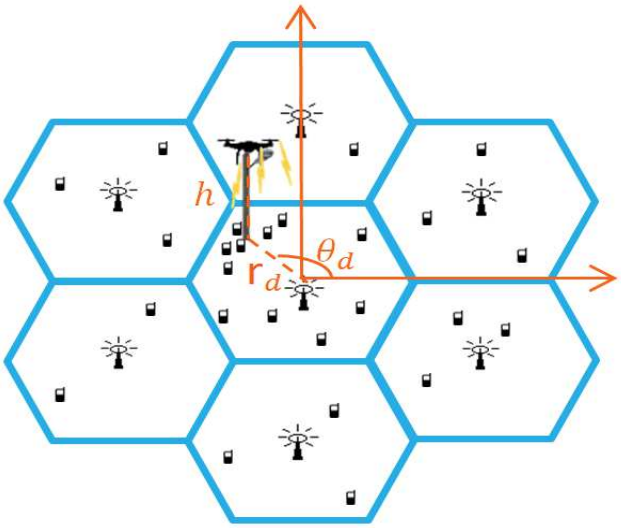

Fig. 6.3 Network layout

are denoted by δ and ϵ, respectively. We also add a drone located in $(r_d(t),\theta_d(t))$ depending on the instantaneous position of the traffic hotspot. $(r_d(t),\theta_d(t))$ does not depend on time during the time interval where it is installed in a serving position since it stays in the same position to serve users until the hotspot moves out of the drone coverage (so, for notational simplicity, we replace $(r_d(t),\theta_d(t))$ by (r_d,θ_d) in each serving position). The altitude of the drone is denoted by h typically representing the height of the serving points (Fig. 6.3). The transmit power of the drone is $P_d = \kappa P$ with $0 \leq \kappa \leq 1$.

In order to connect the drone to the backhaul, a proportion, denoted by α of the radio resources of the macrocell used to serve mobile users is exclusively allocated to the drone when it is activated. A given UE m, with polar coordinates (r,θ), is served either by the central macrocell (cell at the origin) or the deployed drone depending on the relative signal strength coming from both antennas. For notational simplicity, the altitude of the UE is incorporated in the values of ϵ and h cited above.

In order to evaluate the efficiency of the deployed mechanism, we consider a traffic hotspot with polar coordinates, at time t, $(r_h(t),\theta_h(t))$. Without loss of generality, we assume that this hotspot moves inside the central macrocell of the network according to the Manhattan mobility model [47] (with $r_h(t)$ smaller than the radius of the macrocell $R < \delta$).

UE locations are spatially distributed in order to form a hotspot centered in $(r_h(t),\theta_h(t))$; its measure at time t is given as in equation (4.1).

The wireless channel is modeled as in Subsection 4.1.2 with pathloss coefficients denoted by (a,b) for the macrocell and by $(\tilde{a},\tilde{b})$ for the drone cell. In fact, for the channel between the drone and the users, the signal at the receiver is principally composed of strong LOS component. In fact, according to the planning of the serving points where the drone can be settled up, the probability of occurrence of LOS signals is near to one and it is quite credible to neglect NLOS components. Consequently, incorporating this specification in the system model can be realized by using the same propagation model as the one of the macrocell but with different pathloss coefficients $\tilde{a}$ and $\tilde{b}$ [78].

All the users in the radio range of the drone will be exclusively served by the drone even if the received macrocell signal level is better than the RSRP received from the drone. This decision is in accordance with the initial objective of deploying drones which is the fact that the congested macrocell needs to offload a high proportion of traffic using the drone. Consequently, the drone handles all the users in its coverage area. We denote by $\tilde{R}$ the radius of the disk that the drone can cover with a certain quality of service represented by an Signal to Noise Ratio (SNR) threshold $\tilde{\gamma}_0$.

$$\tilde{R} = \sqrt{\left(\frac{\tilde{a}P_d}{\tilde{\gamma}_0 P_N}\right)^{\frac{1}{\tilde{b}}} - h^2} \tag{6.1}$$

where P_N is the thermal noise power.

At time t, the SINR received by the UE and its throughput are respectively denoted by $\gamma_t(r,\theta)$ and $\eta_t(r,\theta)$ if it is received from the macrocell and by $\tilde{\gamma}_t(r,\theta)$ and $\tilde{\eta}_t(r,\theta)$ if it is received from the drone cell. The relationship between γ (in linear scale) and η is modeled by the modified Shannon formula given in equation (4.5).

Let us consider that W (in equation (4.5)) is the total bandwidth used in the network. Then, when the drone is activated, the drone will occupy $\alpha \times W$ and the macrocell will operate only in $(1-\alpha)W$ to serve its users. This coefficient α is set before the activation of the drone according to the macrocell congestion state evolution.

Since the backhaul of the drone involves the connection to the macrocell like a mobile equipment, the interference coming from the neighboring macrocells must be included in the derivation of the drone capacity, denoted by $\tilde{\eta}_d$. Consequently, the drone capacity becomes as follows:

$$\tilde{\eta}_0 = min(K_1 \alpha W \ln(1 + K_2 \tilde{\gamma}_d), \alpha\eta) \tag{6.2}$$

with

$$\tilde{\gamma}_d = \frac{1}{g(r_d)} \tag{6.3}$$

where $g(r)$ is given by equation (4.8) but with including further the different antennas' elevations.

$$g(r) = \frac{P_N}{P}(r^2+\epsilon^2)^b + 6\chi_0 \left(\frac{r^2+\epsilon^2}{\delta^2}\right)^b \left(\frac{1+(1-b)^2\left(\frac{r}{\delta}\right)^2}{\left(1-\left(\frac{r}{\delta}\right)^2\right)^{2b-1}} + \omega(b) - 1\right) \tag{6.4}$$

where χ_0 is the average cell load over all the interfering macrocells and $\omega(b)$ is expressed in equation (4.2).

Remark: The studied system model is different from the systems studied in Chapter 4 and 5. In fact, the interference of the drone cell on macrocell users and of the macrocell on drone cell users is equal to zero since the drone is serving its users using a different spectrum bandwidth. Moreover, the access to the network, in this case, is not based anymore on the highest received signal power (RSRP) but it is directly linked to the radio range of the drone cell defined in equation (6.1).

6.3.2 Throughput distribution definition and derivation

To communicate with its users, the deployed drone operates in TDD frequency band, a fixed proportion of the FDD frequency band (used by the macrocell to serve its users) is exclusively allocated to the drone to be connected to the backhaul. Consequently, the co-channel interference on macrocell users comes only from the neighboring macrocells. However, drone users will not experience interference from macrocells. Based on these specifications, we provide the following definitions of SINRs and throughputs.

Definition 1: Let γ_t and $\tilde{\gamma}_t$ be the instantaneous SINRs received at a UE (r,θ) from the macrocell and the drone respectively, at time t. Then, γ_t and $\tilde{\gamma}_t$ are expressed as follows

$$\gamma_t(r,\theta) = \frac{1}{g(r)} \tag{6.5}$$

$$\tilde{\gamma}_t(r,\theta) = \frac{P_d}{P_N}\left(|re^{i\theta} - r_d e^{i\theta_d}|^2 + h^2\right)^{-\tilde{b}} \tag{6.6}$$

Remark:

- The elevation distance (denoted by ϵ) between the UE and the neighboring macrocells is not considered in the evaluation of the interference coming from them since the ground distances between the UE and these cells are very high and can be suitable to approximate the distance including this elevation.
- If a neighbor macrocell is also using its drone (r_n, θ_n), it is better to simply have a synchronization between the two drones in order to avoid the overlapping between the uplink of one transmission and the downlink of another one. Nevertheless, the mutual interference between downlink transmissions of both drones is not avoided in this case. So, the experienced SINR by UE in position m is given by

$$\tilde{\gamma}(r,\theta) = \frac{\left(|re^{i\theta} - r_d e^{i\theta_d}|^2 + h^2\right)^{-\tilde{b}}}{\left(|re^{i\theta} - r_n e^{i\theta_n}|^2 + h^2\right)^{-\tilde{b}} + \frac{P_N}{P_d}} \tag{6.7}$$

Definition 2: In the presence of a hotspot (following a spatial distribution such as the one given in equation (4.1)) in the region covered by the central macrocell and the deployed drone, we define the instantaneous throughput CCDF, at time t, as follows:

$$\begin{aligned}\mathbb{P}(\eta_t \geq y) = \frac{1}{S_t}\int_{S^*} \mathbb{1}\left(|re^{i\theta} - r_d e^{i\theta_d}| > \tilde{R}\right) \times \\ \mathbb{1}\left(\min(K_1(1-\alpha)W\ln(1+K_2\gamma_t(r,\theta)), \eta_0) \geq y\right) dm(r,\theta,t)\end{aligned} \tag{6.8}$$

$$\begin{aligned}\mathbb{P}(\tilde{\eta}_t \geq y) = \frac{1}{\tilde{S}_t}\int_{S^*} \mathbb{1}\left(|re^{i\theta} - r_d e^{i\theta_d}| \leq \tilde{R}\right) \times \\ \mathbb{1}\left(\min(K_1 W\ln(1+K_2\tilde{\gamma}_t(r,\theta)), \tilde{\eta}_0) \geq y\right) dm(r,\theta,t)\end{aligned} \tag{6.9}$$

where

$$\begin{aligned}S_t &= \int_{S^*} \mathbb{1}\left(|re^{i\theta} - r_d e^{i\theta_d}| > \tilde{R}\right) dm(r,\theta,t) \\ \tilde{S}_t &= \int_{S^*} \mathbb{1}\left(|re^{i\theta} - r_d e^{i\theta_d}| \leq \tilde{R}\right) dm(r,\theta,t)\end{aligned}$$

with $dm(r,\theta,t)$ the measure representing the spatial UE location distribution reflecting the presence of a traffic hotspot located in $(r_h(t), \theta_h(t))$.

In the analysis, we only derive the throughput CCDF for $l \leq \eta_0$ for the macrocell and for $l \leq \tilde{\eta}_0$ for the drone because, as explained in [37], this quantity is simply equal to zero otherwise.

Proposition 6.3.1 *When the position of the traffic hotspot matches exactly with the position of the drone, i.e.* $(r_h(t), \theta_h(t)) = (r_d, \theta_d)$*, the throughput CCDFs in the macrocell and in the drone cell are given by the following expressions*

$$\mathbb{P}(\eta_t \geq l) = \frac{2e^{-\frac{r_h(t)^2}{2A^2}}}{2\pi A^2 S_t} \int_0^{g^{-1}(\psi(l))} re^{-\frac{r^2}{2A^2}} \int_{\cos^{-1}\left(h(r)|_{-1}^{1}\right)}^{\pi} e^{-\frac{r_h(t) r \cos\theta}{A^2}} dr d\theta \tag{6.10}$$

$$\mathbb{P}(\tilde{\eta}_t \geq l) = \frac{1}{\tilde{S}_t} \int_0^R \int_0^{\cos^{-1}\left(s(r)|_{-1}^{1}\right)} dm(r, \theta, t) \tag{6.11}$$

with $\psi(l) = K_2 \left(e^{\frac{l}{K_1(1-\alpha)W}} - 1 \right)^{-1}$, $\tilde{\psi}(l) = K_2 \left(e^{\frac{l}{K_1 W}} - 1 \right)^{-1}$ *and*

$$h(r) = \frac{r^2 + r_h(t)^2 - r_h(t)^2}{2 r_h(t) r}$$

$$s(r) = \frac{r^2 + r_h(t)^2 - \min\left(r_h(t)^2, \left(\frac{P_N}{P_d} \tilde{\psi}(l) \right)^{-\frac{1}{b}} - h^2 \right)}{2 r_h(t) r}$$

The function u *stands for* h *in equation (6.10) and* s *in equation (6.11) and is defined by*

$$u(r)|_{-1}^{1} = \begin{cases} u(r) \ if \ -1 < u(r) < 1 \\ -1 \ if \ u(r) < -1 \\ 1 \ if \ u(r) > 1 \end{cases}$$

6.3.3 Flow level analysis of system performance

As in Subsection 5.4.1, we derive performance metrics based on a dynamic level analysis. We focus on the case of best effort traffic. Cell capacity is assumed to be shared between all transmissions according to a multi-class $M/G/1$ Processor Sharing discipline. Users of the same class have the same data rate denoted by $\eta_{k,t}$ for the macrocell and $\tilde{\eta}_{l,t}$ for the drone, $k \leq K$ and $l \leq L$. We assume that we have K classes in the macrocell and L classes in the drone cell when it is activated. We define the arrival rate $\lambda_{k,t}$ for the

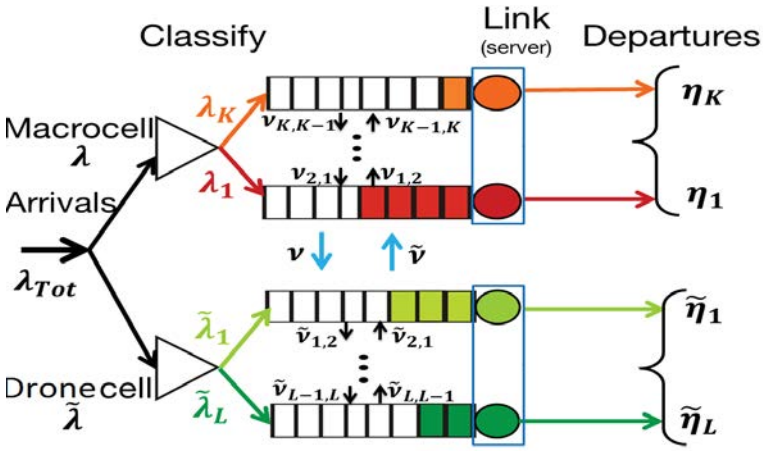

Fig. 6.4 Dynamic system model

macrocell and $\tilde{\lambda}_{l,t}$ for the drone cell when it is activated. Flow sizes are assumed to be mutually independent and exponentially distributed with mean σ_0 in Mbits.

As mentioned in the dynamic level analysis of Chapter 4, flow classes are sorted, for tractability issues, in an increasing order according to the associated data rate, denoted by $\eta_{k,t}, \tilde{\eta}_{l,t},\ k = 1..K, l = 1..L$. The probabilities $p_{k,t}, \tilde{p}_{l,t},\ k = 1..K, l = 1..L$ denote the density of each flow class in the macrocell and the drone cell respectively observed at time t. Each class follows a Poisson process of intensity $\lambda_{k,t} = \lambda_t p_{k,t} = \lambda_{Tot} \frac{S_t}{S_t + \tilde{S}_t} p_{k,t},\ k = 1..K$ in the macrocell and $\tilde{\lambda}_{l,t} = \tilde{\lambda}_t \tilde{p}_{l,t} = \lambda_{Tot} \frac{\tilde{S}_t}{S_t + \tilde{S}_t} \tilde{p}_{l,t},\ l = 1..L$ in the drone cell when it is activated (with $\lambda_{Tot} = \lambda_t + \tilde{\lambda}_t$ the total arrival intensity of the system composed of the macrocell and the drone cell). Data rates and flows' arrival intensities are extracted from analysis in Chapter 4 as explained in Fig. 4.4.

Due to the mobility of the traffic and also of the drone, we keep the same notations for transition rates as in Chapter 5. The dynamic system model is depicted in Fig. 6.4. The main difference to the dynamic system model studied in Chapters 4 and 5 is that there is no coupling between the macrocell and the drone cell since they are operating in different spectrum bandwidths.

The derived performance metrics remain the same as in Chapter 5 but without the coupling between the transmissions. So, under the round robin policy and with heavy mobile traffic, only the expression of the service data rate $\bar{\eta}$ and of the stationary probability will be modified to become as follows

$$\bar{\eta} = \sum_{k=1}^{K} q_k E_t \left[\eta_{k,t}\right] + \sum_{l=1}^{L} \tilde{q}_l E_t \left[\tilde{\eta}_{l,t}\right] \tag{6.12}$$

$$\pi_{n,\tilde{n}} = \frac{(1-\bar{\rho})|n+\tilde{n}|! \prod_{k=1}^{K} q_k^{n_k} \prod_{l=1}^{L} \tilde{q}_l^{\tilde{n}_l}}{\prod_{k=1}^{K} n_k! \prod_{l=1}^{L} \tilde{n}_l!} \tag{6.13}$$

6.3.4 Numerical results

We now evaluate the different performance metrics and investigate the efficiency of deploying drones in offloading traffic. The same parameters' configuration as in Chapters 4 and 5 is set. The parameters configuration is also the same for TDD and FDD mode (the only difference is that in TDD mode, we use another frequency band in $2.6GHz$ with the same band size of $20MHz$ and we need to specify the type of UL/DL configuration).The transmission power of the drone is $20dBm$ and its pathloss equation is given by $115 + 26log_{10}(d_{km})$. The arrival rate in the network is equal to 6 and α is taken equal to 50%. For the TDD mode, the UL/DL configuration is taken as the configuration 1 (see 3GPP TS 36.211 [79]) which stands for a resource partition as follows: 40% DL, 40% UL and 20% for special subframes. The hotspot is moving with a speed of 3km/h (the reference speed for pedestrian users [80]).

We consider a specific scenario where the traffic hotspot is moving inside the macrocell constraining the drone to move from a strategic point to another to get closer to the hostpot. We plot in Fig. 4.11 the mean (over time) of the throughput CCDF in a network without drones where the hotspot is moving from $(0.5km, \frac{\pi}{3})$ to $(0.5km, \frac{4\pi}{3})$ while passing through $(0.5km, \frac{2\pi}{3})$ in straight lines according to Manhattan model. The mean throughput CCDF (during the movement of the hotspot and the drone) is also plotted after the deployment of the proposed drone mechanism. The drone starts working in position $(0.5km, \frac{\pi}{3})$. After 5 minutes of service in that position, it moves to $(0.5km, \frac{2\pi}{3})$. Then, after 4 minutes and 30 seconds, the drone moves to the next position $(0.5km, \frac{4\pi}{3})$. The obtained results are further compared to the throughput CCDF of a network using a classic small cell operating in FDD mode (with the same spectrum as the macrocell) and to small cells operating in TDD mode (with paramters configured as for the drone cell). In these two evaluated scenarios, the position of the deployed small cell will be equal to the initial position of the moving hotspot.

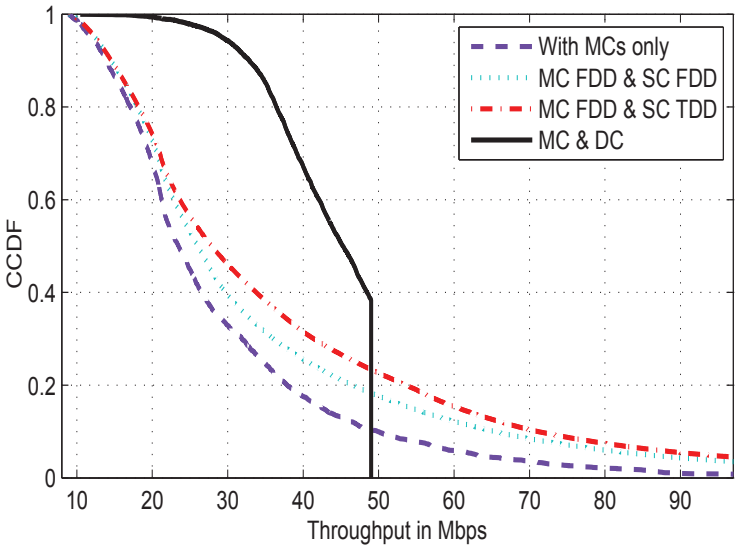

Fig. 6.5 Throughput CCDF in the different compared scenarios.

In the figures' legend, MC, SC and DC stand for macrocell, small cell and drone cell respectively, HS stands for the traffic hotspot.

From Fig. 4.11, we observe that the deployment of the drone improves the capacity of the system composed of only macrocells since user locations with degraded throughputs will be covered by the drone. So, these users will experience a better SINR level since radio conditions are less impacted by fading and shadowing effects and also thanks to the exploitation of TDD bands. When the hotspot is moving, the mean of the throughput CCDF over time shows that deploying drones gives better performance than small cells especially for small data rates which are significantly improved. With drone cells, more than 40% of the traffic can be offloaded with approximately $50Mbps$. However, the best performance that we can obtain from the other solutions is more than 75% of the traffic offloaded with less than $50Mbps$. Compared to the deployment of a small cell operating whether in TDD or FDD mode, the system capacity is still competitive admitting that the drone has less capacity allocated to its users with $\alpha = 50\%$.

Besides, we observe that deploying drones performs better than small cells for small throughput values meaning that the small cell edge users experience better QoS when they are connected to the drone. So, deploying drone cells allows to have more homogeneous user experience all over its covered area which is illustrated by the decreasing proportion of users with high data rates in favor of medium data rates.

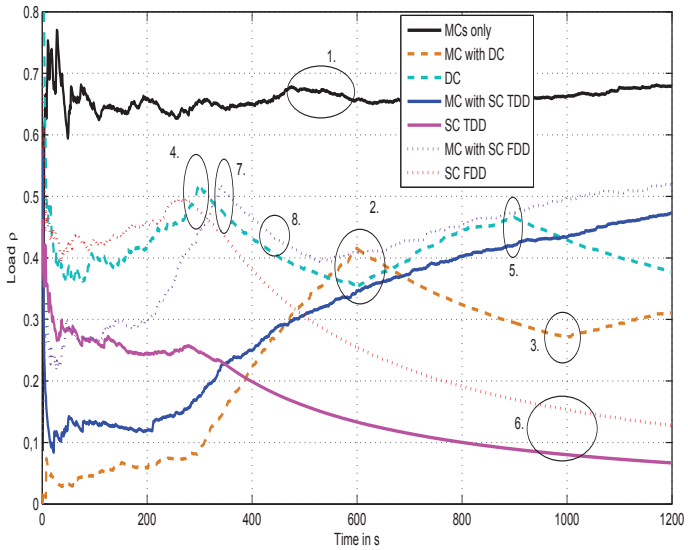

Fig. 6.6 Load in each cell.

In Fig. 6.6, we plot, for the four deployment scenarios defined as in Fig. 6.5, the evolution (over time) of the load in the network. From situations 1. and 2. in Fig. 6.6, we observe that the load is significantly reduced in the macrocell with the deployment of a drone located near the traffic hotspot. This can be explained by the fact that the users served by the drone have better radio conditions and experience less interference than the scenario with only macrocells. The peak of the load in the macrocell obtained in 2. is due to the fact that the traffic hotspot is getting far from the drone cell. Consequently, more users are handed over to the macrocell.

Next, in situation 3. of Fig. 6.6, the load in the macrocell (in the scenario of deployed drone) is reduced again thanks to the drone which changed its position to get nearer to the hotspot. The reached load in situation 4. for the drone cell is explained by the fact that the hotspot is approaching again to the drone. In situation 5., we observe that the load in the macrocell (with a deployed small cell either operating in TDD or FDD mode) is increasing since the small cells are not anymore covering the hotspot. Furthermore, the same conclusion is consolidated by the results in situation 6. showing that the load in the small cell is considerably decreased when the hotspot is moving far from this latter. The peak in situation 7. for the macrocell with a small cell operating in FDD mode is explained by the increase of the number of users near the small cell edge and thus receiving more interference from the small cell.

After that, as illustrated in situation 8., the impact of the interference is reduced when the hotspot gets far from the small cell edge. Finally, we observe that users

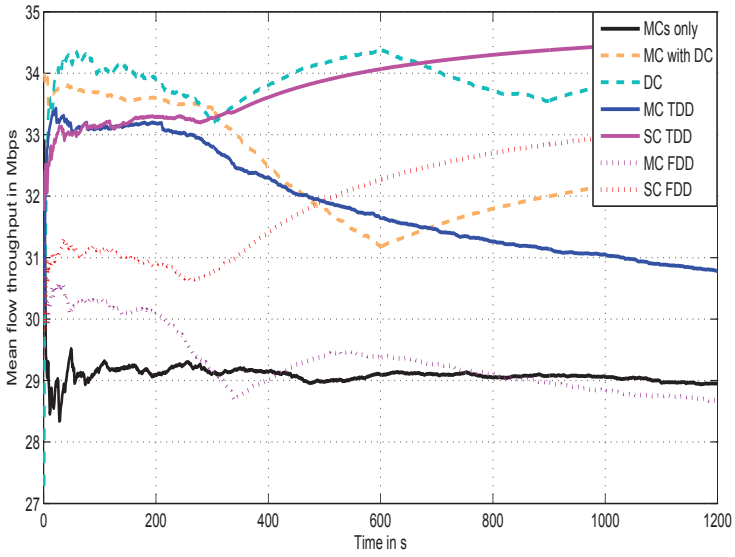

Fig. 6.7 Mean flow throughput in each scenario.

generating the traffic hotspot can efficiently exploit the available resources resulting in the reduction of the load in the drone cell and also in the macrocell (even better than the scenario of small cell because good radio conditions are always guaranteed).

Regarding the deployment of classic small cells, we notice that the load in the macrocell is most of the time higher than the one in the scenario of deploying a drone which is also in accordance with the results of Fig. 4.11.

In summary, we conclude that the drone deployment could be a relevant solution to offload moving traffic hotspots, whereas the classic small cells does not always deliver good performance especially when the mobility of the traffic is considered.

The different observations deduced from Fig. 4.12 are also consolidated by the results obtained in Fig. 6.7 illustrating the evolution of the mean flow throughput in each scenario. Moreover, we observe that the mean flow throughput in the small cell (either operating in TDD or FDD mode) is improved when the traffic hotspot moves far from it. This is explained by the fact that the load is reduced. So, even with users exclusively located at small cell edge, they will be served with more radio resources. The mean flow throughput in a network composed of only macrocells is in specific cases better than the one in a macrocell with a small cell operating in FDD mode with the same spectrum as the macrocell. In fact, when the traffic hotspot moves far from the small cell, this latter will not actively offload the traffic and it will play the role of an only interfering cell leading thus to the degradation of the macrocell performance.

6.4 Discussion on the blocking points and the key advantages of the proposed mechanism

Nowadays, drones are at the peak of their development and many constructors are investing in research in order to produce viable professional and commercial models which are safe, autonomous, stable and power-efficient. Nevertheless, until recently, exploiting drones for professional use is still missing in the government regulations. It needs exhaustive investigations about their control to create new rules mainly related to the national security and also the interference with other applications.

Concerning the security aspects, many companies, mainly working in military projects, are developing new solutions to control drones, identify their owners and the reason for which it is flying in a specific region and this by intercepting and analyzing all its transmissions.

The cost efficiency of deploying drones, such as described in the proposed mechanism, is guaranteed since one drone can efficiently replace many classic small cells in an energy-saving way. In fact, even the case of low battery power cannot be addressed because with the advanced achievements in the design of drones and also with the described drone mobility mechanism, energy consumption will not be a limitation for this type of communications. Consequently, the cost of drones does not represent anymore a limitation factor for their deployment.

Another limiting factor is the coexistence with other flying devices and interference with other applications. This point can be treated by identifying and avoiding the probable collisions with other operating applications and flying devices.

Several advantages can be obtained by deploying the proposed drone-based mechanism in offloading traffic. First, drones guarantee the line-of-sight condition to UEs and also to the macrocell which reduces interferences and energy consumption of macrocells. In fact, with such channel model based on a strong line-of-sight condition, the relationship between the transmitted and received signals is not highly dependent on fast fading and shadowing effects. Consequently, the network performance can be upgraded without complex signal processing computations.

Second, using drones rapidly improves radio conditions of UEs in unpredictable events such as accidents and infrequently occurring events such as street shows. Furthermore, it is possible to cover unknown dead spots difficult to be predicted by operators' planning tools.

Third, the need to relay communications with complex systems with more than two hops and to have cooperative relays doesn't exist anymore since the drone will be in line-of-sight with the macrocell and UEs also.

Fourth, the mobility of drones helps the macrocell to cover a mobile hotspot located in cell edge or in coverage holes for long periods of time. Consequently, handover interruptions are notably reduced since handovers are only triggered when UEs quit the coverage of the drone cell.

Fifth, a better control of drones leads to enhanced homogeneous user experience all over the covered area and to a better control of the coverage and capacity expected in the planning process.

Sixth, with deploying drones (especially as explained in the proposed mechanism), no strict installation guidelines are imposed with respect to planning and site-acquisition.

Most of the raised advantages are further confirmed through the obtained numerical results specifically the homogeneous user experience, the good radio conditions and the reduction of the system load.

In addition to the advantages enumerated in the previous paragraph, the mobility of the drone is an important characteristic allowing to significantly improve network performance (for instance, a drone serving a hotspot of UEs in a mass event). When this hotspot is moving, the drone anticipates this movement and chooses the next best location where to settle up to continue serving this hotspot. Following this concept, the next generation network design process will be related to the initial planning of the set of best drone locations where it can move to cover traffic hotspots. Furthermore, it is important to note that the planned drone locations will not contain specific equipment; they are only used to specify location points where the drone can be placed. Nevertheless, it is possible to install power terminals in some of these positions in order to recharge drones' batteries. The second important element in the proposed mechanism is that the drone moves near the traffic hotspot to land on the communicated position and deactivates all its flying components before starting to serve users. This allows to make from deploying drones in cellular networks a more feasible solution since it reduces significantly the energy consumption. An additional point, raised from the performance analysis section, is that deploying drones always provides additional capacity gains since radio conditions are improved inside the macrocell and its UEs are not impacted by interference coming from the drone when this latter is operating in TDD band.

6.5 Concluding remarks

In this chapter, a new offloading mechanism is developed to reduce congestion in cellular networks. We propose to use drone cells in an efficient and energy-saving way. Drones instantly react in response to the appearance of traffic hotspots and allow to efficiently offload traffic with providing better radio conditions. The disappearance and the movement of the traffic hotspot are also addressed in order to make a complete, reliable and feasible offloading mechanism. The performance of the deployed mechanism is also investigated in terms of system load evolution in time and throughput distribution. The obtained results are compared to the ones of a classic small cell deployment showing that deploying drones improves further the capacity and the quality of service in the network (especially for users with bad radio conditions) in an efficient and cost-effective way.

To further highlight the benefits of the deployment of drone cells, a study on the efficiency in terms of reactivity and the energy consumed when applying the proposed mechanism is indispensable.

Chapter 7

Conclusion and future works

7.1 Summary

Traffic hotspots' localization and HetNets' deployment are among the main topics facing the existing and the future generations of cellular networks. Dealing with these issues is challenging, especially in the context of meeting the ever-growing capacity and coverage requirements of cellular networks. Indeed, depending only on macrocell deployments cannot meet the demand users are currently imposing on cellular operators. Therefore, recent wireless systems are constantly upgraded with new parameterizations and features that aim to improve both the users' experience and the system capacity. A core goal of this thesis is to develop a new traffic localization method and to assess the impact of the limited accuracy of traffic hotspot localization tools on small cell deployments. Aiming to boost capacity and coverage in cellular networks, the second objective of this thesis was to propose and evaluate the performance of new offloading mechanisms, that capitalize on future HetNet deployments.

Chapter 1 started by presenting the background and the general context of our work. It covered also the targeted problems in this thesis and our original contributions.

Chapter 2 provided an overview of the topics related to traffic localization and HetNet deployment. The accuracy and the limitations of developed methods in the literature were investigated. Then, the motivations behind our developed localization method were presented. HetNet deployments and the performance of each studied scenario in the literature were also investigated. This spanned classic, moving and drone small cells. Likewise, the motivations behind the realized studies were presented in order to understand the difference between the developed study and previous ones.

Chapter 3 investigated the problem of traffic hotspot localization in high-traffic urban environments to provide an important information in the HetNet planning

process. We proposed a new traffic hotspot localization method based on O&M KPIs and projected over the coverage map. The accuracy of the proposed method is evaluated and our results demonstrated that this solution was able to provide improved traffic tracking precision at low operational and computational costs.

Chapter 4 presented a study on the impact of imperfect traffic hotspot localization on small cells deployment, namely to quantify potential performance gains of classic small cells when they are not perfectly covering traffic hotspots. Specifically, we chose to study three different scenarios: i. with macrocells only, ii. a network of macrocells with a small cell deployed exactly at the center of the traffic hotspot and iii. with a small cell not perfectly deployed near the traffic hotspot (its position is different from the hotspot one). The study is realized in two stages: static level and flow level.

In the static level, the throughput CCDF and the mean user throughput are investigated in the presence of non-uniform traffic distribution in the network. In the dynamic level, user arrivals and departures are generated according to the defined spatial traffic distribution reflecting the presence of a traffic hotspot. We also examined the achievable performance gains in terms of load, mean number of active users and mean flow throughput.

Our analytical and simulation results indicated that deployment of a small cell is less impacted by the imperfect positioning with respect to traffic hotspot location when this latter is in cell edge. In addition, our results demonstrated that there are no potential gains when small cells are deployed to cover traffic hotspots at cell center. In areas close to the cell edge, dynamic level results showed that it is sufficient to obtain better performance with the deployment of small cells but it is not sufficient to obtain the best ones. This latter depends, in addition to the spatial traffic distribution in the network, on several input parameters such as the radio range of the small cell (if it covers all the hotspot or a part of it when this latter is more flat), the small cell capacity and the amount of traffic it has to offload as well as the level of the mutual interference generated by both the small cell and the macrocell.

In Chapter 5, we introduced the mobility of small cells in the network of macrocells. Moving small cells are deployed in this case on top of vehicles (for example public transportation means since they are generally moving in crowded areas which maintains appropriate levels of small cells utilizations). Deploying moving cells allows to cover more traffic hotspots with less investments since one mobile small cell can replace many classic small cells. Static and dynamic level results showed that moving small cell can be a beneficial solution with positive capacity gains as compared to a network with only macrocells. Nevertheless, the mobility control of mobile cells is still an

important challenge for cellular operators. In fact, when the traffic hotspot is far from the deployed small cell, the system performance is not improved due to the additional interference generated by this latter on macrocell users. That's why, following the trajectory of the traffic hotspot represents a major concern.

Finally, in Chapter 6, we proposed a novel traffic offloading mechanism based on drone small cells. Overloaded macrocells activate their drones and move them near the heaviest traffic hotspots. Then, each drone starts to serve the users generating the traffic hotspot in an energy-efficient way since it will settle up on strategic points defined in the planning process. The key advantages and the limiting factors of the solution were investigated in order to show the potential gains and also the blocking issues or non treated ones related to drone deployments. The performance of the proposed mechanism was compared to classic small cell solutions and to networks with macrocells only so as to assess the additional capacity that is obtained from drones. Our results showed that using drones according to the proposed mechanism makes this new deployment solution a beneficial one. In fact, deploying drones was shown to be useful to further improve the capacity and the quality of service in the network (especially for users with bad radio conditions) in an efficient and cost-effective way.

7.2 Conclusions

Throughout this thesis, and from the evaluated scenarios and developed mechanisms, we can conclude the following:

- The accuracy of the actual traffic hotspot localization tools still need to be improved if radio engineers are tempted by exploiting the output of these tools in the HetNet design process. Otherwise, deploying small cell based on these tools will be always risky and could lead to possible losses in terms of expenditures and also of capacity.
- The O&M KPIs and the coverage map represent relevant inputs for traffic localization methods and their combination with more sophisticated tools could lead to high accuracy.
- Deploying classic small cells in areas receiving good radio signals from the macrocell degrades the overall network performance. Indeed, the interference from the macrocell on small cell users will be very high leading thus to degraded service data rate for these users.

- Deploying small cells in cell edge areas is often a beneficial solution even with errors in traffic localization. This is explained by the fact that the radio conditions will be always improved in these areas.
- Deploying moving cells can be further efficient solution in terms of capacity improvement and also of costs. Nevertheless, the incapability to control the mobility of these cells is still a major concern and constitutes an open research question for this solution to reach maturity.
- Drone small cells is a new promising alternative to offload congesting traffic in cellular networks. It will be surely an open research topic for future generation technologies.

7.3 Future works

The main focus of the work in this thesis is to efficiently localize and offload traffic hotspots in cellular networks through the deployment of heterogeneous networks. In view of this, several directions of future works can be established in order to address the challenges and the deployment issues helping operators to leverage potential gains of HetNets.

First, new traffic localization methods can be developed and studied while exploiting the new features activated in cellular networks such as Device-to-Device (D2D) communications and Minimizing Drive Tests (MDT) techniques. A hybrid localization process based on O&M KPIs and also on D2D technology is of interest since it can be a good solution for indoor and outdoor localization with a good accuracy.

Secondly, this work analyzes the impact of imperfect traffic hotspot localization on the performance of small cell deployment. However, we consider that all the deployed sites are omni-directional and we do not consider shadowing. For real networks, these assumptions are not always verified especially in urban areas due to underlying design issues or inherent environment characteristics. The challenge to incorporate the shadowing and to study a network composed of tri-sectorial sites can be a future work. Furthermore, considering the network structure as a perturbed hexagonal one (site location is perturbed by a random variable) can be also an interesting scientific opening for future studies. In fact, perturbed hexagonal network model approximates more than any other model the geometry of the real network [26]. Consequently, performance of perturbed hexagonal model would be closer to the performance of a real network.

Although the performance evaluation in this thesis was carried out for different traffic offloading solutions (classic, moving and drone small cells) and was limited to metrics linked to the quality of service and radio conditions, a study on the cost and on the energy consumption of each deployed solution is also envisaged.

Another interesting problem would be to add a data caching feature to these small cells to increase offloading throughput and relieve cellular networks by storing frequently requested information. What, where and when to cache to achieve certain objectives, is still an open question.

Moreover, the developed work is mainly related to the impact of imperfect traffic hotspot localization. So, only one small cell is considered since more traffic hotspots or more small cells will not allow to achieve the goal of this study. Nevertheless, the case where multiple small cells are deployed in the network of macrocells, can be studied in order to gain a more comprehensive and coherent understanding of real-time behavior.

Besides, the mobility of cells represents an interesting option that can be further developed in terms of mobility control in order to improve the overall system performance. In this context, handover metrics also present a relevant performance study to investigate.

Finally, another open research problem lies in the efficient use of the WiFi capabilities in addition to the licensed spectrum in order to offload the heavy data traffic in cellular networks.

References

[1] Dongwoon Bai, Cheolhee Park, Jungwon Lee, Hoang Nguyen, Jaspreet Singh, Ankit Gupta, Zhouyue Pi, Taeyoon Kim, Chaiman Lim, Min-Goo Kim, et al. LTE-advanced modem design: challenges and perspectives. *IEEE Communications Magazine*, 50(2):178–186, 2012.

[2] Ekram Hossain and Monowar Hasan. 5G cellular: key enabling technologies and research challenges. *IEEE Instrumentation & Measurement Magazine*, 18(3):11–21, 2015.

[3] Jeffrey G Andrews, Stefano Buzzi, Wan Choi, Stephen V Hanly, Aurelie Lozano, Anthony CK Soong, and Jianzhong Charlie Zhang. What will 5G be? *Selected Areas in Communications, IEEE Journal on*, 32(6):1065–1082, 2014.

[4] Aleksandar Damnjanovic, Juan Montojo, Yongbin Wei, Tingfang Ji, Tao Luo, Madhavan Vajapeyam, Taesang Yoo, Osok Song, and Durga Malladi. A survey on 3GPP heterogeneous networks. *Wireless Communications, IEEE*, 18(3):10–21, 2011.

[5] Woon Hau Chin, Zhong Fan, and Robert Haines. Emerging technologies and research challenges for 5G wireless networks. *IEEE Wireless Communications*, 21 (2):106–112, 2014.

[6] Tao Chen, Yang Yang, Honggang Zhang, Haesik Kim, and Kari Horneman. Network energy saving technologies for green wireless access networks. *Wireless Communications, IEEE*, 18(5):30–38, 2011.

[7] E Nan, Xiaoli Chu, Weisi Guo, and Jie Zhang. User data traffic analysis for 3G cellular networks. In *Communications and Networking in China (CHINACOM), 2013 8th International ICST Conference on*, pages 468–472. IEEE, 2013.

[8] Thomas Louail, Maxime Lenormand, Oliva G Cantu Ros, Miguel Picornell, Ricardo Herranz, Enrique Frias-Martinez, José J Ramasco, and Marc Barthelemy. From mobile phone data to the spatial structure of cities. *Scientific reports*, 4, 2014.

[9] Meisam Mirahsan, Rainer Schoenen, and Halim Yanikomeroglu. HetHetNets: Heterogeneous traffic distribution in heterogeneous wireless cellular networks. *Selected Areas in Communications, IEEE Journal on*, 33(10):2252–2265, 2015.

[10] Dongheon Lee, Sheng Zhou, Xiaofeng Zhong, Zhisheng Niu, Xuan Zhou, and Honggang Zhang. Spatial modeling of the traffic density in cellular networks. *IEEE Wireless Communications*, 21(1):80–88, 2014.

[11] Henrik Klessig, Vinay Suryaprakash, Oliver Blume, Albrecht Fehske, and Gerhard Fettweis. A framework enabling spatial analysis of mobile traffic hot spots. *IEEE Wireless Communications Letters*, 3(5):537–540, 2014.

[12] Silvia Martin-leon, Mustafa Ahmed, and Timothy David Hurley. Traffic location in mobile cellular telecommunications systems, August 23 2001. US Patent 20,010,016,490.

[13] Olivier Ho-A-Chuck. Process for analyzing traffic localization within a cellular radio communication network, October 27 1998. US Patent 5,828,962.

[14] Tomi Vaara and Risto Aalto. Traffic hot spot locating method, November 20 2001. US Patent 6,321,083.

[15] Qiang Xu, Alexandre Gerber, Zhuoqing Morley Mao, and Jeffrey Pang. AccuLoc: practical localization of performance measurements in 3G networks. In *Proceedings of the 9th international conference on Mobile systems, applications, and services*, pages 183–196. ACM, 2011.

[16] Martin Azizyan, Ionut Constandache, and Romit Roy Choudhury. SurroundSense: mobile phone localization via ambience fingerprinting. In *Proceedings of the 15th annual international conference on Mobile computing and networking*, pages 261–272. ACM, 2009.

[17] C.S. Randriamasy. Geographic representation of traffic load in a mobile radio communication network, January 2 2002. EP Patent App. EP20,010,401,494.

[18] Akshay Athalye, Vladimir Savic, Miodrag Bolic, and Petar M Djuric. Novel semi-passive RFID system for indoor localization. *Sensors Journal, IEEE*, 13(2): 528–537, 2013.

[19] A. Roxin, J. Gaber, M. Wack, and A. Nait-Sidi-Moh. Survey of wireless geolocation techniques. In *Globecom Workshops, 2007 IEEE*, pages 1–9, Nov 2007.

[20] Aymen Jaziri, Ridha Nasri, and Tijani Chahed. Traffic hotspot localization in 3G and 4G wireless networks using OMC metrics. In *Personal, Indoor, and Mobile Radio Communication (PIMRC), 2014 IEEE 25th Annual International Symposium on*, pages 270–274. IEEE, Sept 2014.

[21] Aymen Jaziri, Ridha Nasri, and Tijani Chahed. Tracking traffic peaks in mobile networks using statistics of performance metrics. *accepted with major revisions in International Journal of Wireless Information Networks*, 2016.

[22] Xiaoli Chu, David Lopez-Perez, Yang Yang, and Fredrik Gunnarsson. *Heterogeneous Cellular Networks: Theory, Simulation and Deployment*. Cambridge University Press, 2013.

[23] Harpreet S Dhillon, Radha Krishna Ganti, Francois Baccelli, and Jeffrey G Andrews. Modeling and analysis of k-tier downlink heterogeneous cellular networks. *Selected Areas in Communications, IEEE Journal on*, 30(3):550–560, 2012.

[24] Harpreet S Dhillon, Marios Kountouris, and Jeffrey G Andrews. Downlink mimo hetnets: Modeling, ordering results and performance analysis. *Wireless Communications, IEEE Transactions on*, 12(10):5208–5222, 2013.

[25] Robert W Heath, Marios Kountouris, and Tianyang Bai. Modeling heterogeneous network interference using Poisson point processes. *Signal Processing, IEEE Transactions on*, 61(16):4114–4126, 2013.

[26] Anjin Guo and Martin Haenggi. Spatial stochastic models and metrics for the structure of base stations in cellular networks. *Wireless Communications, IEEE Transactions on*, 12(11):5800–5812, 2013.

[27] Ridha Nasri and Aymen Jaziri. On the analytical tractability of hexagonal network model with random user location. *in IEEE Transactions on Wireless Communications*, 15(5):3768–3780, 2016.

[28] Jean-Marc Kelif, Stephane Senecal, and Marceau Coupechoux. Impact of small cells location on performance and QoS of heterogeneous cellular networks. In *Personal Indoor and Mobile Radio Communications (PIMRC), 2013 IEEE 24th International Symposium on*, pages 2033–2038. IEEE, 2013.

[29] Ridha Nasri and Aymen Jaziri. Tractable approach for hexagonal cellular network model and its comparison to Poisson point process. *in Wireless Communications Symposium, IEEE Globecom 2015, San Diego*, 2015.

[30] Thomas Bonald and Alexandre Proutière. Wireless downlink data channels: user performance and cell dimensioning. In *Proceedings of the 9th annual international conference on Mobile computing and networking*, pages 339–352. ACM, 2003.

[31] Richard Combes, Zwi Altman, and Eitan Altman. Self-organization in wireless networks: a flow-level perspective. In *INFOCOM, 2012 Proceedings IEEE*, pages 2946–2950. IEEE, 2012.

[32] Ahlem Khlass, Thomas Bonald, and Salah Eddine Elayoubi. Flow-level performance of intra-site coordination in cellular networks. In *Modeling & Optimization in Mobile, Ad Hoc & Wireless Networks (WiOpt), 2013 11th International Symposium on*, pages 216–223. IEEE, 2013.

[33] Xiaohu Ge, Tao Han, Yan Zhang, Guoqiang Mao, Cheng-Xiang Wang, Jing Zhang, Bin Yang, and Sheng Pan. Spectrum and energy efficiency evaluation of two-tier femtocell networks with partially open channels. *Vehicular Technology, IEEE Transactions on*, 63(3):1306–1319, 2014.

[34] Louai Saker, Salah Eddine Elayoubi, Tijani Chahed, and Azeddine Gati. Energy efficiency and capacity of heterogeneous network deployment in LTE-advanced. In *European Wireless, 2012. EW. 18th European Wireless Conference*, pages 1–7. VDE, 2012.

[35] Louai Saker, Salah-Eddine Elayoubi, and Tijani Chahed. How femtocells impact the capacity and the energy efficiency of LTE-advanced networks. In *Personal Indoor and Mobile Radio Communications (PIMRC), 2011 IEEE 22nd International Symposium on*, pages 177–181. IEEE, 2011.

[36] Aymen Jaziri, Ridha Nasri, and Tijani Chahed. Performance analysis of small cells' deployment under imperfect traffic hotspot localization. *In IEEE Globecom, Wireless Networks Symposium*, 2015.

[37] Aymen Jaziri, Ridha Nasri, and Tijani Chahed. System level analysis of heterogeneous networks under imperfect traffic hotspot localization. *in IEEE Transactions on Vehicular Technology, DOI: 10.1109/TVT.2016.2530844*, 2016.

[38] Yutao Sui, Jaakko Vihriala, Agisilaos Papadogiannis, Mikael Sternad, Wei Yang, and Tommy Svensson. Moving cells: a promising solution to boost performance for vehicular users. *Communications Magazine, IEEE*, 51(6):62–68, 2013.

[39] Cheng Xiang Wang, Fourat Haider, Xiqi Gao, Xiao-Hu You, Yang Yang, Dongfeng Yuan, Hadi Aggoune, Harald Haas, Sam Fletcher, and Erol Hepsaydir. Cellular architecture and key technologies for 5G wireless communication networks. *Communications Magazine, IEEE*, 52(2):122–130, 2014.

[40] Fourat Haider, Haiming Wang, Harald Haas, Dongfeng Yuan, Haiming Wang, Xiqi Gao, Xiao-Hu You, and Erol Hepsaydir. Spectral efficiency analysis of mobile femtocell based cellular systems. In *Communication Technology (ICCT), 2011 IEEE 13th International Conference on*, pages 347–351. IEEE, 2011.

[41] S. Jangsher and V.O.K. Li. Resource allocation in cellular networks with moving small cells with probabilistic mobility. In *Personal, Indoor, and Mobile Radio Communication (PIMRC), 2014 IEEE 25th Annual International Symposium on*, pages 1701–1705, Sept 2014.

[42] Wei Ni, Iain B Collings, and Ren Ping Liu. Decentralized user-centric scheduling with low rate feedback for mobile small cells. *Wireless Communications, IEEE Transactions on*, 12(12):6106–6120, 2013.

[43] Antonio Mastrosimone and Daniela Panno. A comparative analysis of mmWave vs LTE technology for 5G moving networks. In *Wireless and Mobile Computing, Networking and Communications (WiMob), 2015 IEEE 11th International Conference on*, pages 422–429. IEEE, 2015.

[44] Antonio Mastrosimone and Daniela Panno. New challenge: Moving network based on mmwave technology for 5g era. In *Computer, Information and Telecommunication Systems (CITS), 2015 International Conference on*, pages 1–5. IEEE, 2015.

[45] Mahmoud H Qutqut, Fadi M Al-Turjman, and Hossam S Hassanein. Hof: a history-based offloading framework for LTE networks using mobile small cells and Wi-Fi. In *Local Computer Networks Workshops (LCN Workshops), 2013 IEEE 38th Conference on*, pages 77–83. IEEE, 2013.

[46] S Mohammad Razavizadeh, Minki Ahn, and Inkyu Lee. Three-dimensional beamforming: A new enabling technology for 5G wireless networks. *Signal Processing Magazine, IEEE*, 31(6):94–101, 2014.

[47] Aymen Jaziri, Ridha Nasri, and Tijani Chahed. Offloading traffic hotspots using moving small cells. *In IEEE ICC, Wireless Networks Symposium*, 2016.

[48] Yanru Zhang, Erte Pan, Lingyang Song, Walid Saad, Zaher Dawy, and Zhu Han. Social network enhanced device-to-device communication underlaying cellular networks. In *IEEE Computer Society*, 2013.

[49] Omid Semiari, Walid Saad, Zaher Dawy, and Mehdi Bennis. Matching theory for backhaul management in small cell networks with mmWave capabilities. In *Communications (ICC), 2015 IEEE International Conference on*, pages 3460–3465. IEEE, 2015.

[50] Insoo Hwang, Bongyong Song, and Samy S Soliman. A holistic view on hyper-dense heterogeneous and small cell networks. *Communications Magazine, IEEE*, 51(6):20–27, 2013.

[51] Tony QS Quek, Guillaume de la Roche, İsmail Güvenç, and Marios Kountouris. *Small cell networks: Deployment, PHY techniques, and resource management*. Cambridge University Press, 2013.

[52] Mehdi Bennis, Samir M Perlaza, Pol Blasco, Zhu Han, and H Vincent Poor. Self-organization in small cell networks: A reinforcement learning approach. *Wireless Communications, IEEE Transactions on*, 12(7):3202–3212, 2013.

[53] Shanzhi Chen and Jian Zhao. The requirements, challenges, and technologies for 5G of terrestrial mobile telecommunication. *Communications Magazine, IEEE*, 52 (5):36–43, 2014.

[54] Mohammad Mozaffari, Walid Saad, Mehdi Bennis, and Merouane Debbah. Drone small cells in the clouds: Design, deployment and performance analysis. In *2015 IEEE Global Communications Conference (GLOBECOM)*, pages 1–6. IEEE, 2015.

[55] Sebastian Rohde and Christian Wietfeld. Interference aware positioning of aerial relays for cell overload and outage compensation. In *Vehicular Technology Conference (VTC Fall), IEEE*, pages 1–5. IEEE, 2012.

[56] Aymen Jaziri, Ridha Nasri, and Tijani Chahed. Congestion mitigation in 5G networks using drone relays. *in International Wireless Communications and Mobile Computing Conference (IWCMC), Wireless Networks symposium*, 2016.

[57] Aymen Jaziri, Ridha Nasri, and Tijani Chahed. Offloading moving traffic hotspots with drone cells in future wireless networks. *submitted to IEEE Transactions on Vehicular Technology*, 2016.

[58] Johan Johansson, Wuri A Hapsari, Sean Kelley, and Gyula Bodog. Minimization of drive tests in 3GPP release 11. *Communications Magazine, IEEE*, 50(11):36–43, 2012.

[59] Evolved universal terrestrial radio access (e-utra); mobility enhancements in heterogeneous networks, September 2012.

[60] Evolved universal terrestrial radio access (e-utra); physical layer procedures, March 2009.

[61] Evolved universal terrestrial radio access (e-utra); physical layer; measurements, April 2011.

[62] Sesia Stefania, Toufik Issam, and Baker Matthew. LTE-the UMTS long term evolution: From theory to practice. *A John Wiley and Sons, Ltd*, 19.4.3:432, 2011.

[63] Parveen Singla and Dr Jyoti Saxena. Beam forming algorithm for smart antenna in WCDMA network. *International Journal of Engineering and Innovative Technology (IJEIT) Volume*, 3, 2013.

[64] Lars Zimmermann, Alexander Goetz, Georg Fischer, and Robert Weigel. Gsm mobile phone localization using time difference of arrival and angle of arrival estimation. In *Systems, Signals and Devices (SSD), 2012 9th International Multi-Conference on*, pages 1–7. IEEE, 2012.

[65] Sébastien Reynaud, Moctar Mouhamadou, K Fakih, O Akhdar, Cyril Decroze, David Carsenat, E Douzon, and Thierry Monediere. Outdoor to indoor channel characterization by simulations and measurements for optimising WiMAX relay network deployment. In *VTC Spring 2009-IEEE 69th Vehicular Technology Conference*, 2009.

[66] Ari Kangas and Torbjörn Wigren. Angle of arrival localization in LTE using MIMO pre-coder index feedback. *Communications Letters, IEEE*, 17(8):1584–1587, 2013.

[67] Ridha Nasri and Zwi Altman. Handover adaptation for dynamic load balancing in 3GPP long term evolution systems. *International Conference on Advancnes in Mobile Computing and Multimedia (MoMM)*, 2007.

[68] Qiaoyang Ye, Beiyu Rong, Yudong Chen, Mazin Al-Shalash, Constantine Caramanis, and Jeffrey G Andrews. User association for load balancing in heterogeneous cellular networks. *Wireless Communications, IEEE Transactions on*, 12(6):2706–2716, 2013.

[69] Matt P Wand and M Chris Jones. *Kernel smoothing*. Crc Press, 1994.

[70] Stephen Boyd and Lieven Vandenberghe. *Convex optimization*. Cambridge university press, 2004.

[71] Preben Mogensen, Wei Na, István Z Kovács, Frank Frederiksen, Akhilesh Pokhariyal, Klaus Pedersen, Troels Kolding, Klaus Hugl, Markku Kuusela, et al. LTE capacity compared to the Shannon bound. In *Vehicular Technology Conference, 2007. VTC2007-Spring. IEEE 65th*, pages 1234–1238. IEEE, 2007.

[72] Alan Jeffrey and Daniel Zwillinger. *Table of integrals, series, and products*. Elsevier Academic Press publications, 7 edition, 2007.

[73] George Neville Watson. *A treatise on the theory of Bessel functions*. Cambridge university press, 1995.

[74] Thomas Bonald and Mathieu Feuillet. *Network performance analysis*. John Wiley & Sons, 2013.

[75] 3GPP TR 36.839 V11.0.0 (2012-09). *Evolved Universal Terrestrial Radio Access (E-UTRA); Mobility enhancements in heterogeneous networks*. 2012.

[76] Nivine Abbas, Thomas Bonald, and Berna Sayrac. Opportunistic gains of mobility in cellular data networks. In *Modeling and Optimization in Mobile, Ad Hoc, and Wireless Networks (WiOpt), 2015 13th International Symposium on*, pages 315–322. IEEE, 2015.

[77] Mugen Peng, Dong Liang, Yao Wei, Jian Li, and Hsiao-Hwa Chen. Self-configuration and self-optimization in LTE-advanced heterogeneous networks. *IEEE Communications Magazine*, 51(5):36–45, 2013.

[78] Noman Shabbir, Muhammad T Sadiq, Hasnain Kashif, and Rizwan Ullah. Comparison of radio propagation models for LTE network. *International Journal of Next-Generation Networks*, 3(3):27, 2011.

[79] Physical Channels. Modulation (Release 8), 3GPP TS 36.211. *V1. 0.0, Mar*, 2007.

[80] Joan Olmos, Albert Serra, Silvia Ruiz, Mario García-Lozano, and David Gonzalez. Exponential effective sir metric for LTE downlink. In *2009 IEEE 20th International Symposium on Personal, Indoor and Mobile Radio Communications*, pages 900–904. IEEE, 2009.